Review

Triboelectric Charging of Powders: A review

S. Matsusaka[a,*], H. Maruyama[a], T. Matsuyama[b], M. Ghadiri[c]

[a] *Department of Chemical Engineering, Kyoto University, Kyoto 615-8510, Japan*

[b] *Department of Environmental Engineering, Soka University, Tokyo 192-8577, Japan*

[c] *Institute of Particle Science and Engineering, University of Leeds, Leeds LS2 9JT, UK*

* corresponding author.

E-mail address: matsu@cheme.kyoto-u.ac.jp (S. Matsusaka).

Abstract

Particles are often electrostatically charged by frictional contact during powder-handling operations. This phenomenon is called ‘triboelectric charging’ or ‘contact electrification’. The charged particles cause problems such as particle deposition and adhesion. In addition, if particles are excessively charged, an electrostatic discharge may occur, which can pose a risk of fire and explosion hazards; thus, to mitigate the adverse effects, it is important to elucidate the underlying triboelectric charging mechanisms. The electrostatics is, on the other hand, very useful in a number of applications that have been developed using the principles. In this review, the basic concepts and theories of charge transfer between solid surfaces are summarized, and chemical factors depending on materials and environmental effects are described. To theoretically analyze the process of particle charging, relevant models are discussed. Using the models, particle charging by repeated impacts on a wall is formulated. To experimentally evaluate particle charging, measurement and characterization methods are outlined. Furthermore, important applications and computer simulations are described.

Keywords: Powder technology; Particulate processes; Triboelectric charging; Charge transfer; Characterization; Electrostatic application

Contents

1. Introduction

In industry, powders and particulate solids are widely used as raw materials, intermediates, or final products. When handled in air, the surfaces become triboelectrically charged and various phenomena occur; for instance, the charged particles in pneumatic transport lines or in fluidized beds experience electrostatic forces, and tend to adhere to the walls (Joseph and Klinzing, 1983; Nifuku et al., 1989; Adhiwidjaja et al., 2000; Guardiola et al., 1996; Yao et al., 2004). If the particles are excessively charged, an electrostatic discharge will occur, which can pose a risk of fire and explosion hazards (Jones and King, 1991; Ohsawa, 2003; Nifuku and Katoh, 2003). On the other hand, electrostatic forces can control the motion of charged particles; thus, many applications have been developed (Mazumder, 1999), e.g. electrophotography (Schein, 1992/1996, 1999), electrostatic powder coating (Hughes, 1984; Bailey, 1998; Kleber and Makin, 1998), electrostatic precipitation (Lawless, 1999), particle separation (Gupta et al., 1993; Yanar and Kwetkus, 1995), and electromechanical valve for solids (Ghadiri et al., 1992; Balachandran et al., 1997). In addition, the charge on the particles can provide useful information on the state of the process, e.g. powder flow rate (O'Neill and Willis, 1987; Matsusaka and Masuda, 2006; Gajewski, 2006, 2008), concentration distribution (Machida and Scarlett, 2005) and others (Matsusaka et al, 2008a).

Contact charging and electromechanics of particles have been studied for many years (Schnurmann, 1941; Harper 1951, 1967; Lowell and Rose-Innes, 1980; Jones, 1995); however, there are still many unknowns, and in some cases, inconsistent results have been reported. This is because there are many factors, such as chemical, physical and electrical properties and environmental conditions, which affect the process. Moreover, the amount of charge on particles is distributed, which makes the estimation of the electrostatic charge and the control of the process more difficult. To analyze and control particle charging, the measurement of electrostatic charge and the evaluation of electrostatic characteristics are important (Matsusaka and Masuda, 2003, 2006). Also, to improve existing processes and to develop new applications, it is necessary to obtain an in-depth understanding based on theoretical analyses.

In the present review, the basic concepts and theories of charge transfer between solid surfaces are summarized and the particle charging caused by repeated impacts on a wall is formulated, which is expanded to analyze the charge distribution of particles. Also, measurement of particle charge and characterization of electrostatic properties are outlined. Furthermore, important applications and computer simulations are described.

2. Basic concepts of contact charging and charge transfer

When two different materials are brought into contact and separated, an electric charge is transferred from one to the other. This phenomenon is often called ‘contact electrification’ or ‘contact charging’. When they are rubbed against each other, it can be called ‘frictional electrification’, ‘triboelectric charging’, or simply ‘tribo-charging’; as for short contact during collision, it can be called ‘impact charging’ (Matsusaka and Masuda. 2003). In practice, it is not easy to classify the contacting process for charge transfer purposes into groups, such as sliding, rolling, and impact, and thus the term ‘triboelectric charging’ is used in such a broad sense.

2.1 Electron transfer

2.1.1 Work function

We start with the well-established concept of electron transfer based on the contact potential difference (CPD) due to a difference of work functions for metal-to-metal contact. The triboelectric charging of metals is usually unnoticeable since the charge transferred moves away from the contact point due to its conductivity. However, when the metals are isolated electrically after the contact, the transferred charge can be measured. The charge transfer is explained in terms of ‘electron transfer’ arising from the difference in work function between the surfaces. Two metals with different work functions ϕ_1 and ϕ_2 in contact are schematically shown in Fig. 1. Assuming that electron transfer takes place by tunneling so that thermodynamic equilibrium prevails, the contact potential difference V_c is given by (Harper, 1951):

$$V_c = V_{1/2} = -\frac{(\phi_1 - \phi_2)}{e}, \tag{1}$$

where $V_{1/2}$ is the contact potential difference of metal 1 against metal 2 (Matsusaka and Masuda. 2003), e is the elementary charge. The amount of the transferred charge is equal to the product of the contact potential difference and the capacitance between the two bodies. The capacitance depends on the state of the contacting surfaces. Although the position of the electrons can vary after the metals are separated, the net charge transferred Δq_c is approximated by the following equation:

$$\Delta q_c = C_0 V_c, \tag{2}$$

where C_0 is the capacitance between the bodies at the critical separation distance where the charge transfer is cut off. The theoretical and experimental results for the charge after contact and

separation are shown in Fig. 2 (Harper, 1951). Although the experimental results are somewhat less than the theoretical ones, the tendencies are in reasonable agreement. The difference is probably caused by uncertain factors, such as surface roughness, impurities, oxidized layer, separation speed, and others.

2.1.2 Effective work function

The charge transfer for insulator-metal contact can be explained by a simulated concept of the metal-to-metal electron transfer. This assumes an apparent or effective work function to be assigned to the insulator. The amount of the transferred charge is determined so as to equalize the energy levels of the two materials, and the following relationship is applicable to the electrostatic characterization:

$$\Delta q_c = C_0 \frac{-(\phi_I - \phi_M)}{e}, \tag{3}$$

where ϕ_I is the effective work function of insulator and ϕ_M is the work function of metal. The effective capacitance C_0 depends on the characteristics of the insulator. A linear relationship obtained experimentally is shown in Fig. 3 (Davies, 1969). Murata and Kittaka (1979), also, produced the evidence of the electron transfer by comparing contact charging and photoelectric emission experiments.

2.1.3 Surface state model

The main criticism of the 'effective work function' model is that there is no available 'free electron' in an insulator. To cover this point and to explain the charge transfer for insulator-insulator contacts, several modified models have been presented (Lowell and Rose-Innes, 1980; Lee, 1994; Bailey, 2001). Some of them are similar to those for insulator-metal contact, but the movement of electrons in the body is more restricted. In one of the models it is assumed that available energy levels of electron are only on surface, not in bulk, and the available level is called 'surface state' (Fig. 4). (Gutman and Hartmann, 1992; Anderson, 1994; Cotler et al., 1995). When the insulators come to contact, electrons move from the filled surface states of insulator 1 to the empty surface states of insulator 2. The driving force for the charge transfer between the surfaces is the difference in the effective work functions of the two surfaces. The charge transfer will cease when the Fermi levels of the two materials coincide with each other. The charge transfer causes the Fermi energy of the insulator 1 and insulator 2 to change with Δ_1 and Δ_2, respectively. The charge transfer also produces a potential difference between the surfaces E_f z_0. The net effect is that the Fermi levels of the surfaces are the same at contact and the expression for the energy level is given

as

$$\phi_1 + \Delta_1 + eE_f z_0 = \phi_2 - \Delta_2 \quad (4)$$

For the charging of toner particles used in electrophotography, it was reported that the data agree with the high density limit of the surface state density (Cotler et al., 1995), which directly corresponds to the effective work function model. However, there are cases where the high density limit does not stand (Ikezaki et al., 2005).

2.1.4 Molecular-ion-state model

Since the physicochemical structure of the surface states was difficult to strictly define, Fabish and Duke (1977) proposed the molecular-ion-state model assuming that polymers have donor and acceptor states and charge is carried by electrons. Thus, despite the inclusion of ion in the name of the model, this is actually one of the electron transfer models.

A schematic illustration of a metal-insulator contact for electron injection into the acceptor of the polymer insulator is shown in Fig. 5. In this model, electrons can only tunnel into the polymer whose energy is in a narrow range, so-called 'window', around the Fermi level of the metal. The density of the charge acquired from the metal of a given Fermi level E_F is therefore supposed to be the density of the insulator states at energy E_F. The general equation for the charge transfer q_{IM} is expressed as

$$q_{IM} = \int_{E_F}^{E_F+\Delta E} \rho_D(E)\, f(E)\, dE - \int_{E_F-\Delta E}^{E_F} \rho_A(E)\{1 - f(E)\}\, dE, \quad (5)$$

where ΔE is the window ($\approx$ 0.4 eV) for the charge transfer, $\rho_D(E)$ and $\rho_A(E)$ are the density of the insulator states for the donor and acceptor, respectively, $f(E)$ is the probability of the charge states occupied by electrons, and 1-$f(E)$ is the probability of the charge states unoccupied. As shown in Fig. 5, for $f(E_F)$=0 in Eq. (5), the charge density q_{IM} is approximately equal to $-\rho_A(E_F)\,\Delta E$.

A schematic illustration of the states for an insulator-insulator contact is shown in Fig. 6 (Duke and Fabish, 1978). Donor states of insulator 1 align in energy with acceptor states of insulator 2 within the energy interval between the distribution centroids $\langle E_1 \rangle$ and $\langle E_2 \rangle$. Hence, the charge transfer can take place to an extent limited by the smaller state distribution within this energy interval. The charge transfer $q_{2,1}$, i.e. the variation of the charge density of the insulator 2 is obtained by summing up the number of aligned donor-acceptor charge states. The general equation is expressed as

$$q_{2,1} = \int_{<E_1>}^{<E2>} \min[\rho_{D2}(E), \rho_{A1}(E)]\, f_2(E)\{1 - f_1(E)\}\,dE - \int_{<E_1>}^{<E2>} \min[\rho_{D1}(E), \rho_{A2}(E)]\, f_1(E)\{1 - f_2(E)\}\,dE, \quad (6)$$

in which, min ($\rho_{Di}(E)$, $\rho_{Aj}(E)$) is the smaller state density of the donor and acceptor. The polarity of the insulators after contact depends on the values of the centroid energies.

2.1.5 Quantum chemical calculation

Instead of using the assumed Gaussian distribution of the 'molecular-ion-state,' an evaluation of the electronic state of polymer was tried by computational molecular orbital calculation. Yanagida et al. (1993) calculated the level of the highest occupied molecular orbital (HOMO) of an oligomer, using a semi-empirical molecular orbital method. The calculated values were almost proportional to the measured values of the threshold energy of photoemission, which corresponded to the effective work function of polymers. This result showed that quantum chemical calculations are applicable to the evaluation of the triboelectric charging of polymers.

Yoshida et al. (2006) and Shirakawa et al. (2008) studied the charge transfers for a polymer–metal contact system using another molecular orbital method, paying attention to surface defects. When an atom is missing a neighbor to which it would be able to bind, a dangling bond occurs. Such defects can be made during frictional contact. A model of surface contact used for the calculations is shown in Fig. 7. The molecular chains of polytetrafluoroethylene (PTFE), are arranged perpendicular to the surface of aluminum Al, and dangling bonds are placed at the interface. The densities of the states (DOS) of the PTFE with the dangling bond obtained by the quantum chemical calculation are shown in Fig. 8 (Shirakawa et al., 2008). A zero value of the vertical-axis is equal to the HOMO level of the PTFE. Compared with the work function of metal, the charging tendency of the PTFE–metal contact can be analyzed. The electron distribution of the interface of the PTFE obtained by the calculation is shown in Fig. 9 (a) and the variation of the distribution by contact charging is shown in (b). The solid and broken lines mean, respectively, increase and decrease of electrons. This figure indicates that the electrons of the carbon atom (C) increase. In general, it is believed that PTFE easily accepts negative charge because of the high electronegativity of fluorine atom (F); however, this result shows that the C atom with dangling bond is more effective to transfer electrons than the fluorine atom. Although the quantitative analysis is still limited, it is expected that the quantum chemical calculation can be used to understand the charge transfer between surfaces.

2.2 Ion transfer

In the early 1960s, ion transfer caused by the adsorption of water on a solid surface was believed to be the major mechanism of charge transfer. However, water vapor affects other surface properties, e.g. increasing the surface conductivity and lowering the electrical breakdown strength of air. Therefore, the charge transfer and the maximum potential are lowered in moist atmospheres (Lee, 1994).

The mechanism of ion transfer has regained attention in recent years. In the electrophotographic industry, the external addition of ionic charge control agents (CCAs) is widely used to accelerate and control the charging process. These additives generally consist of a mobile ion and an immobile ion. For example, substances with cationic group have a positive charging property, while ones with anionic groups have a negative charging property. The performance of these additives has been examined (see §3.3); however, their roles in triboelectric charging remain obscure. As an experimental approach to observe ion transfer, secondary ion mass spectrometry (SIMS) was used (Mizes et al., 1990). Also, the scanning probe microscopy (SPM) was applied to study triboelectric charging, showing that the ionic species in the insulators can influence the charging (Saurenbach et al., 1992). To make clear the mechanism of the ion transfer, further experimental studies should be conducted.

2.3 Material transfer

The impact and friction between two bodies can result in a transfer of materials from one to the other, which can be fragments of the bodies as well as contaminated small dusts or impurities on the surfaces. For instance, when a metal object slides over a polymer surface, a certain amount of polymer will transfer to the metal surface and the metal can also transfer to the polymer. If the transferred material carries charge, charge transfer will occur (Lowell and Rose-Innes, 1980). When brittle particles impact on a metal wall, elements of particles are easily transferred on the metal (Tanoue et al., 1999). However, there is currently no theoretical model of charge transfer and its equilibrium state with such mass transfer mechanism.

3. Chemical concept and environmental conditions

3.1 Inorganic compounds

The work function or energy band concept has been widely applied to explain the contact charging between metals (Harper, 1967). For insulators, it is, however, difficult to predict the charging tendency from this concept because of the lack of the data for band structures. For a practical approach to predict the charging tendency of insulators, several methods have been developed (Oguchi and Tamatani, 1986, 1993). The amount of charge on particles after contact with other kinds of particles was measured using a blow-off method (see §5.2). The results for metal oxidized particles are shown in Fig. 10. The specific charge, i.e. charge to mass ratio of particles, shifts linearly to a negative direction with an increase in the generalized electronegativity χ_i for constituent metal ions, which is defined as

$$\chi_i = (1+2Z)\,\chi_0\,, \tag{7}$$

where Z is the valency of the metal ion and χ_0 is the Pauling's electronegativity for the metal element. The same tendency is observed for metal fluorides and metal sulfides.

3.2 Organic compounds

Shinohara et al., (1976) approximated the electronic states of polymer with the chemical constants such as e value in copolymerization,[1] Hammett substituent constant,[2] and the ionization potential, and investigated the relationship between the triboelectric charging and the electronic state. Gibson (1975, 1984) investigated the substituent effect on triboelectric charging using a cascade method, where metal beads (steel or zinc) were fed at the top of an inclined plate coated with a film made of salicylaldehyde anils or substituted polystyrenes, and the specific charges of the metal beads were measured with a Faraday cage. The logarithms of the absolute values of the specific charge as a function of the Hammett substituent constant are shown in Fig. 11. Good linear correlations exist both for the anils and the polystyrenes; thus, the triboelectric charging is likely related to the molecular structure. The triboelectric charging is regarded as a solid state electrochemistry, where there is no transport medium (electrolyte) and also the reaction depends on physical contact. In both gas and liquid phases, molecular orbital energy levels can be correlated with Hammett substituent constants.

Gibson (1975, 1984) also explained the triboelectric charging by a model based on electron transfer. According to the model, when the energy level of the highest occupied molecular orbital (HOMO) of an organic solid is higher than the Fermi level of the metal, organic solid is positively

charged; while, when that of the lowest unoccupied molecular orbital (LUMO) is lower than the Fermi level of the metal, it is negatively charged. The direction of electron transfer for metal–organic contact is shown in Fig. 12 (Diaz, and Guay, 1993).).

---

[1] e values of the $Q-e$ concept of copolymerization proposed by Alfrey and Price (1947) represents the electron density on the double bond, and accounts for the polar effect of substituents in monomers; its value is negative when substituents are electron-repelling and positive when they are electron-attracting.

[2] σ values of Hammett's rule is called the substituent constant and is determined by the type and position (*m*- or *p*-) of the substituent regardless of the kind of reaction; its value tends to be negative for electron-repelling groups and positive for electron-attractive groups.

Substituent constants (σ values).

Substituent	para effect	meta effect
NH_2	–0.66	–0.16
OH	–0.37	0.12
CH_3	–0.17	–0.07
H	0	0
Cl	0.23	0.37
$COCH_3$	0.50	0.38
CN	0.66	0.56
NO_2	0.78	0.71

3.3 Surface treatment and charge control agents

Surface modification of particles is of great importance for industrial applications, since surfaces affect various properties such as triboelectric charging, adhesion, friction, and flowability. One of the simple and effective methods for the surface modification is to coat it with different materials. To investigate the effect of the coating materials and their contents on contact charging, titania particles of 0.15–0.3 μm in diameter coated with alumina and silica were brought into contact with iron. The experimental results are shown in Fig. 13 (Oguchi and Tamatani, 1993). The contact charge shifted toward the positive direction with an increase in the alumina content, while the silica contributed to a shift toward the negative direction.

For polymeric materials, the molecular structure affects the charging characteristics (Shinohara, et al., 1976; Lowell and Akande, 1988); thus, the contact charge can be controlled by changing the molecular structure of the surfaces. Irradiation with ultra violet rays (Uyama and Ikada, 1990) and plasma processing (Kodama et al., 1993) are useful methods to change the charging characteristics of polymers.

In electrophotography, pigmented polymer particles called toner are used to reproduce an image on paper. The toner particles are strongly required to have a definite amount and polarity of charge since the particles have to be properly moved by the electrostatic force. This can be achieved by adding charge control agents (CCAs) either on toner surfaces or to bulk. Examples of surface charge control agents are fumed silica and highly fluorinated polymeric material such as polyvinylidene fluoride. Bulk charge control agents are blended into the polymer. For positive bulk CCAs, amine and quaternary ammonium salts are used. The counterions can be halogens (Cl^-, Br^-, I^-), fluoroborates (BF_4^-), sulfates (RSO_4^-) or sulfonates (RSO_3^-). For negative bulk CCAs, metal complex dyes are used (Schein, 1992/1996; Mazumder 1999). Although little information appears available on how these charge control agents affect the triboelectric charging, the charging process can involve transfer of the counterion on the toner surface to the carrier surface upon contact. Some negative CCAs such as chromium or cobalt complex azo dyes have a tendency to remove a proton, depending on the molecular structure. Moreover, if they depend on the acidic nature and a water layer is present on the surface, H^+ can move in the aqueous layer between the contact surfaces (Schein, 1992/1996).

A class of compounds such as a polyester salt has the advantage to stabilize triboelectric charge. These agents are called ‘charge stabilizers’. In comparison with the charge control agents, the charge stabilizers show lower charging magnitude but long-term charge stability. When used in combination with a CCA, the controllability of the triboelectric charging is further improved (Michel et al., 2001).

3. 4 Moisture and temperature

Environmental conditions such as relative humidity and temperature affect triboelectric charging. Greason (2000) measured the charge on a metal sphere with a Faraday cage after contact with an insulating material under various conditions. The relationships between the charge and relative humidity for three temperatures are shown in Fig. 14. At a given temperature, the charge decreases with increasing relative humidity. This can be due to increased leakage caused by a decrease in the electric resistance on the surface. Also, it is true that the charge decreases more rapidly where the charged particles are kept at a high relative humidity (Nomura et al., 2003). The effects of temperature on the charge on the sphere are shown in Fig. 15. The charge tends to decrease with increasing temperature. This tendency is remarkable when the relative humidity is low (Greason, 2000).

4 Mechanism of particle charging

4.1 Condenser model

A schematic illustration of the condenser model of particle charging by contact is shown in Fig. 16. The contact region between a particle and a wall is regarded as a capacitor. When a particle impacts and rebounds on a wall, the contact time is short, but still long enough for the charge transfer; thus, the transferred charge Δq caused by impact can be represented by the condenser model, i.e. (Matsusaka et al., 2000):

$$\Delta q = k_c C V , \tag{8}$$

where k_c is the charging efficiency, C is the capacitance, and V is the total potential difference. The capacitance C is given by

$$C = \frac{\varepsilon_0 S}{z_0} , \tag{9}$$

where ε_0 is the absolute permittivity of gas, S is the contact area and z_0 is the critical gap including the geometrical factors between the contact bodies. The total potential difference V at the contact gap is given by

$$V = V_c - V_e - V_b + V_{ex} , \tag{10}$$

where V_c is the potential difference based on the surface work functions, V_e is that arising from the

image charge, which is given by

$$V_e = k_e q, \tag{11}$$

where q is the particle charge held on the particle before contact. V_b is that arising from the space charge caused by surrounding charged particles, which is given by

$$V_b = k_b q. \tag{12}$$

V_{ex} is the potential difference arising from other electric fields. For instance, an external electric field may be applied in this system. When the wall is insulator, the wall surface can have charge and form an electric field, which affects the total potential difference. If the charge is accumulated by contact charging, the total potential difference will decrease with increasing surface charge (Matsusaka et al. 2003 a).

4.2 Charge relaxation model

Matsuyama and Yamamoto (1995 a, b) proposed another charging model, named 'charge relaxation model'. The concept of the charge relaxation process is sequentially shown in Fig. 17; i.e. (a) there are two neutral bodies separated; (b) when the bodies are brought into contact with each other, charge is transferred through the contact gap; (c) the bodies are in separation; (d) relaxation of the transferred charge occurs due to gas discharge in the separation process (Matsusyama and Yamamoto, 2006 a).

A quantitative scheme of this model is indicated in Fig. 18. To determine the breakdown voltage in the gap, the Paschen curve is applied, which is widely used in the air insulating technology to give the gas breakdown limit voltage between two parallel electrodes as a function of pressure and gap distance (Paschen, 1889). Now, it is assumed that a particle with a small initial charge approaches a metal wall, and a charge is transferred by a contact with the wall. When the charge transferred on the particle is high enough to make the potential curve intersect the Paschen curve in the separation process, the charge relaxation occurs due to gas breakdown, and the potential curve with the residual charge leaves the Paschen curve downwards after the process. As a result, the total charge remaining on the particle becomes larger than the initial charge. This difference of the charge is the net transferred charge to be observed. On the other hand, when the particle approaching the wall has a large amount of charge which gives the potential curve exceeding the Paschen curve, the particle releases the surplus charge by the gas breakdown before impact. The charge remaining on the particle is kept after impact since the potential curve does not exceed the

Paschen curve. Therefore, the released charge is equivalent to the net transferred charge. The remaining charge depends on the dielectric constant and the diameter of the particle as well as the breakdown voltage of the gas.

4.3 Impact on a wall

In powder handling operations, individual particles acquire charge during collision with walls. An understanding of the charging process of a single particle is a basic requirement for the development of a theory of triboelectric charging of particles (Bailey, 1993). Several studies have been reported, in which a single particle of a few millimeters in diameter was made to collide with a metal target, and the transferred charge was measured (Masui and Y. Murata, 1983, 1984; Yamamoto and Scarlett, 1986; Matsuyama and Yamamoto, 1989, 1994, 1995a–c, 1997). Also, single-particle experiments with a larger sphere, 31 mm in diameter (Matsusaka et al., 2000) and with a particle as small as 100-300 μm (Matsuyama et al., 2003) were performed. These methods have several advantages, i.e. the contact state during the particle collision can be reproducible by controlling the impact velocity and angle. An example of the impact charging test rig for single particles is shown in Fig. 19 (Watanabe et al., 2006, 2007a, b). A particle is fed into the funnel at the top of the rig and is accelerated by air flowing through a glass tube. The particle then collides with a metal target in a collection chamber. To measure the particle charge before impact, an open ended (through-type) Faraday cage (FC1) is installed. The second Faraday cage (FC2) is installed in the collection chamber to measure the particle charge after impact. The amount of charge transferred during the impact, i.e. impact charge, is quantified by subtracting the initial charge (measured by FC1) from the particle charge after impact (FC2). The relationship between the impact charge and initial charge has a linear trend, as shown in Fig. 20. The impact charge at zero initial charge Δq_0 is a characteristic charge, and it increases with the impact velocity. The intercept on the horizontal axis is the equilibrium charge q_e, where there is no net charge transfer. Δq_0 and q_e are important characteristics of the charging tendency of particles. The characteristic line with these values is expressed as the following equation:

$$\Delta q = \Delta q_0 \left(1 - \frac{q_i}{q_e} \right). \tag{13}$$

The equilibrium charges of particles made of different materials as a function of impact velocity is shown in Fig. 21. Although there are some fluctuations in the data, the equilibrium charge is independent of the impact velocity but depends on the material.

The effect of impact angle on the triboelectric charging was investigated by Ema et al (2003). The particle impact tests using an inclined target and a rotating target are illustrated in Fig. 22. As

particles impact on the metal target in a stream, the value of electric current generated from the target is represented by the following equation:

$$I = -\frac{W}{m_p}\Delta q \quad , \tag{14}$$

where W is the mass flow rate, m_p is the mass of a particle, and Δq is the impact charge of a particle. The relationship between normalized current I/I_{max} and impact angle θ is shown in Fig. 23, in which I_{max} is the maximum current at a constant normal component of impact velocity. The electric current increases with the impact angle up to 60^o and then decreases. This charging tendency can be explained by a rolling–slipping model. For $\theta \leq 60^o$, the effective contact area increases with the angle because of the increase in the rotation of the particle on the target (Fig. 24 (a)). As for $\theta > 60^o$, the effect of the slip on the target increases with the angle; thus, the effective contact area decreases (Fig. 24 (b)).

4.4 Repeated impacts of a single particle

When particles repeatedly collide with a wall, the charge on the particles varies according to the electrostatic properties and the state of the collisions; thus, it is important to trace the variation of the charge on a particle. As a first step to analyze successive impact charging, single-particle experiments were carried out using two metal targets (Fig. 25) (Matsuyama and Yamamoto, 1995c**)**. The charge generated by the first impact affects the next impact charging. For polymer particles, the surface charge caused by impact is non-uniform, and the localization on the surface affects the successive particle charging**.**

The relationship between the impact charge and the initial charge of 200 μm polymer particles is shown in Fig. 26 (Matsuyama et al., 2003). The wide scatter on the data is thought to be caused by the non-uniform surface charge. The substantial effect of the localization of the surface charge on the impact charge can be explained (Fig. 27). If charged area contacts with a wall, the impact charge will strongly depend on the initial charge; however, the charged area is at the remote side, there is no effect.

Repeated impact tests to study the charge accumulation were carried out by Matsusaka et al. (2000) (Fig. 28). To control the contact area easily, a larger sphere (31 mm in diameter), made of synthetic rubber was used. The sphere was supported at its initial rest point using a fine string, and then was dropped onto a metal plate. After impact on the plate, the string was then pulled up to prevent the sphere from falling again. This impact test was repeated many times, and the initial charge on the sphere and the transferred charge were measured with a through-type Faraday cage.

The variation in the charge on the sphere is shown in Fig. 29. The transferred charge caused by

an impact decreases with the number of impacts and the accumulated charge approaches a limiting value, which tends to decrease as the time interval between impacts increases. This is because the leakage of the electrostatic charge increases with increasing elapsed time.

It is possible to formulate the particle charge generated by repeated impacts. First, the condenser model (see § 4.1) is applied to the formulation. In order to obtain the charge q_c as a function of the number of collisions n, a continuous quantity dq_c/dn is used, i.e.:

$$\frac{dq_c}{dn} = k_c C V \quad . \tag{15}$$

The leakage of electrostatic charge dq_r/dt is approximated by (Itakura et al., 1996)

$$\frac{dq_r}{dt} = -k_r q \quad , \tag{16}$$

where k_r is a constant. When the frequency of particle collisions is defined as f, Eq. (16) is rewritten as

$$\frac{dq_r}{dn} = -\frac{k_r}{f} q \quad . \tag{17}$$

For simple repeated impacts of a single particle, the values of V_b and V_{ex} in Eq. (10) are zero; therefore, from Eqs. (9)-(11), (15) and (17), the net charge transfer is derived as

$$\begin{aligned} \frac{dq}{dn} &= \frac{dq_c}{dn} + \frac{dq_r}{dn} \\ &= -\left\{ \frac{k_c k_e \varepsilon_0 S}{z_0} + \frac{k_r}{f} \right\} q + \frac{k_c \varepsilon_0 S V_c}{z_0} \quad . \end{aligned} \tag{18}$$

Solving Eq. (18) with the initial conditions, $n = 0$ and $q = q_0$, gives the following exponential equation:

$$q = q_0 \exp\left(-\frac{n}{n_0} \right) + q_\infty \left\{ 1 - \exp\left(-\frac{n}{n_0} \right) \right\} , \tag{19}$$

where

$$n_0 = \frac{1}{\dfrac{k_c k_e \varepsilon_0 S}{z_0} + \dfrac{k_r}{f}} \tag{20}$$

and

$$q_\infty = \frac{V_c}{k_e + \dfrac{k_r z_0}{k_c \varepsilon_0 S f}} . \tag{21}$$

It should be noted that the same form as Eq. (19) can also be derived from the charge relaxation model in a phenomenological level. By replacing q_e and q_i in Eq. (13) with q_∞ and q, respectively, the transferred charge per collision dq/dn is given by

$$\frac{\mathrm{d}q}{\mathrm{d}n} = -\frac{\Delta q_0}{q_\infty} q + \Delta q_0 \tag{22}$$

.

Solving Eq. (22) with the initial conditions, $n = 0$ and $q = q_0$ gives the same form as Eq. (19). Here, n_0 in Eq. (19) is given by

$$n_0 = \frac{q_\infty}{\Delta q_0} . \tag{23}$$

Comparing the charge relaxation model with the condenser model, one can notice a difference. For the condenser model, n_0 is independent of the contact potential difference V_c (see Eq. (20)), but q_∞ is proportional to V_c (see Eq. (21)). On the other hand, for the charge relaxation model, both n_0 and q_∞ are independent of V_c.

The exponential equation represented by Eq. (19) can be used for almost all the repeated impacts of a single particle. The effect of the differences in experimental conditions including particle diameter should be considered in the two terms, i.e. q_∞ and n_0.

4.5 Particle charging in gas–solids pipe flow

In gas–solids pipe flow, particles repeatedly collide with the inner wall, as a result of which charge transfer takes place. When a metal pipe is grounded, the charge transferred from the particles to the wall flows to earth, and can be detected as electric currents (Masuda et al. 1976, 1994; Cartwright et al. (1985); Nieh and Nguyen (1988); Gajewski (1989)). A system to analyze the particle charging in gas–solids pipe flow is shown in Fig. 30 (Matsusaka et al. 2008a). Particles that are continuously fed are dispersed into airflow through an ejector. To increase the efficiency of the particle charging, spiral pipes can be used instead of straight pipes. The electric currents flowing from the metal pipes to earth are measured with an electrometer. To confirm the validity of the charge balance in this system, the charge-to-mass ratio, i.e. specific charge, of particles at the inlet and outlet of the metal pipe must be measured by connecting them to a Faraday cage. Also, a digital oscilloscope can be used to analyze the pulsating electric signals of the charge transfer (see §6.5.2).

The electric currents generated from a metal pipe are shown in Fig. 31(a) (Masuda, et al. 1994; Matsusaka and Masuda, 2006). During the operation, the measured values are almost constant (I = 2.3 nA for $W_p = 7.0 \times 10^{-7}$ kg·s^{-1}). The amount of charge of the particles that is being collected in the Faraday cage under the same conditions as above is shown in Fig. 31(b). The values of the specific charge at the inlet and outlet of the detector are $q_{mIN} = 3.9\times10^{-3}$ and $q_{mOUT} = 0.6\times10^{-3}$ C·kg^{-1}, respectively. The difference between these values $q_{mIN} - q_{mOUT}$ is equal to the current generated per unit mass flow rate, $I/W_p = 3.3\times10^{-3}$ C·kg^{-1}. This means that the charge balance is satisfied and the system is working correctly.

When the effect of particle–particle interactions on the particle charging is negligible in dilute phase gas–solids pipe flow, each particle can freely collide with the inner wall. Under such conditions, the electric current is proportional to the mass flow rate of particles (Fig. 32) (Masuda et al. 1998a). For dense-phase gas–solids pipe flows, the surrounding particles prevent the free particle–wall contacts, and consequently the efficiency of the charge transfer is reduced. Also, for smaller particles, the efficiency decreases because of the agglomeration. In addition, the initial charge on particles affects the electric currents as shown in Fig. 33 (Masuda et al. 1994). In powder handling operations, particles will collide with different walls before arriving at the current detection pipe, e.g. hopper, feeder, chute, disperser, etc., and hence the polarity and amount of charge on particles vary according to the conditions. To estimate the charge transferred from the particles to the wall, the initial charge has to be known beforehand.

The particle charging in gas-solids pipe flow can be formulated. When a particle moves from x to $x+\Delta x$ along the pipe axis, the variation of the charge is derived from Eq. (19) as follows:

$$\Delta q = q(x+\Delta x) - q(x) = (q_\infty - q_0)\left\{\exp\left(-\frac{n(x)}{n_0}\right)\right\}\left\{1-\exp\left(-\frac{n(\Delta x)}{n_0}\right)\right\}. \tag{24}$$

The charges transferred from the particles to the pipe wall can be analyzed by the electric currents. When a length of Δx is isolated electrically and grounded, the electric current I flowing to earth is expressed as (Matsusaka and Masuda, 2006):

$$\frac{I}{W_p} = -\frac{\Delta q}{m_p} = (q_{m0} - q_{m\infty})\left\{\exp\left(-\frac{n(x)}{n_0}\right)\right\}\left\{1-\exp\left(-\frac{n(\Delta x)}{n_0}\right)\right\}, \tag{25}$$

where W_p is the mass flow rate of particles, m_p is the mass of the particle, q_{m0} and $q_{m\infty}$ are the specific charge at $x = 0$ and $x = \infty$, respectively. When the point of x at the inlet of the detection pipe is redefined as zero, Eq (25) becomes

$$\frac{I}{W_p} = (q_{m0} - q_{m\infty})\left\{1-\exp\left(-\frac{n(\Delta x)}{n_0}\right)\right\}. \tag{26}$$

When the value of Δx is quite small and $n(\Delta x) << n_0$, Eq. (26) is simplified as

$$\frac{I}{W_\mathrm{p}} = \left(q_{\mathrm{m}0} - q_{\mathrm{m}\infty}\right)\frac{n(\Delta x)}{n_0}, \tag{27}$$

where

$$q_{\mathrm{m}\infty} = \frac{6V_\mathrm{c}}{\pi\rho_\mathrm{p}D_\mathrm{p}^3\left\{\left(k_\mathrm{e}+k_\mathrm{b}\right)+\dfrac{k_\mathrm{r}z_0}{k_\mathrm{c}\varepsilon_0 S f}\right\}}, \tag{28}$$

where ρ_p is the particle density and D_p is the particle diameter. The constants of k_e regarding image charge and k_b regarding the space charge in Eq. (28) are, respectively, approximated by (Appendix A and B)

$$k_\mathrm{e} = \frac{2z_0}{\pi\varepsilon_0 D_\mathrm{p}^2} \tag{29}$$

and

$$k_\mathrm{b} = \frac{3z_0 m\rho_\mathrm{g}D_\mathrm{i}\bar{u}}{2\pi\varepsilon_0\rho_\mathrm{p}D_\mathrm{p}^3\bar{v}}, \tag{30}$$

where m is the mass flow ratio of particles to gas, ρ_g is the density of the gas, D_i is the inner diameter of the pipe, $\bar{u}$ is the average gas velocity and $\bar{v}$ is the average particle velocity. When the leakage of the electrostatic charge is sufficiently small compared to the particle charging, k_r can be neglected. Using Eqs. (29) and (30), n_0 and $q_{\mathrm{m}\infty}$ are expressed as

$$n_0 = \frac{\pi D_\mathrm{p}^2}{2k_\mathrm{c}S\left(1+\alpha\right)} \tag{31}$$

and

$$q_{\mathrm{m}\infty} = \frac{3\varepsilon_0 V_\mathrm{c}}{\rho_\mathrm{p}D_\mathrm{p}z_0\left(1+\alpha\right)}, \tag{32}$$

where α is the ratio of the space charge effect to the image charge effect, i.e.:

$$\alpha = \frac{3}{4}m\frac{\rho_\mathrm{g}D_\mathrm{i}\bar{u}}{\rho_\mathrm{p}D_\mathrm{p}\bar{v}}. \tag{33}$$

For dilute phase flow ($\alpha << 1$), Eq. (27) is rewritten as

$$\frac{I}{W_p} = aq_{m0} + b \quad , \tag{34}$$

where

$$a = \frac{2n(\Delta x)k_c S}{\pi D_p^2} \tag{35}$$

and

$$b = -\frac{6\varepsilon_0 V_c n(\Delta x)k_c S}{\pi D_p^3 \rho_p z_0} \quad . \tag{36}$$

From Eq. (34), it is found that the transferred charge is proportional to the initial charge of particles. This relationship was confirmed experimentally (see Fig. 33).

The above theoretical approach can be used for analyzing the charge distribution (Matsusaka et al., 2002). Although the particle charge distribution depends on various factors, the main factors are considered to be the number of particle collisions, initial charge on the particles, and the state of the impact. Introducing the probability density functions of these factors, one can obtain the equation of particle charge distribution (Appendix C).

Furthermore, the maximum (or the equilibrium) charge of particles in gas–solids pipe flow was studied by Matsuyama and Yamamoto (2008). They conducted a theoretical calculation based on the charge relaxation model, taking into account the space charge effect and compared with the experimental data cited from literature.

4.6 Control of triboelectric charging

In general, the reproducibility of the triboelectric charging of particles is poor; however, the control of the charge on particles is possible using the triboelectric charging principles. In this section, typical triboelectric characteristics in dilute phase gas–solids pipe flow is shown first and then useful methods to control triboelectric charging are explained.

Matsusaka et al. (2007) conducted experiments for triboelectric charging of micrometer-sized particles using five different kinds of pipes. The relationships between the specific charge of particles and the pipe length are shown in Fig. 34. The particles were charged positively by contact with the walls of the two kinds of stainless steel. As for aluminum, copper, and brass pipes, the particles were charged negatively. Among them, the charging level for the aluminum pipe was rather small. Although the absolute value of the specific charge increased with pipe length, the rate of increase gradually decreased and the specific charge approached an equilibrium value depending on the wall material. In order to apply the theoretical model to the experimental results, it can be

assumed that the frequency of the particle-wall impacts per unit pipe length is constant, and that the number of impacts n is proportional to the pipe length L; therefore, Eq. (19) is rewritten as

$$\bar{q}_{\mathrm{m}}(L) = \bar{q}_{\mathrm{m0}} \exp\left(-\frac{L}{L_0}\right) + \bar{q}_{\mathrm{m}\infty}\left\{1 - \exp\left(-\frac{L}{L_0}\right)\right\}, \tag{37}$$

where L_0 is the characteristic length of the particle charging. The experimental results were in good agreement with the calculated ones (Fig. 34). Also, Eq. (37) can be used to evaluate the particle charging efficiency γ_{q}, i.e.:

$$\gamma_{\mathrm{q}} = \frac{\bar{q}_{\mathrm{m}} - \bar{q}_{\mathrm{m0}}}{\bar{q}_{\mathrm{m}\infty} - \bar{q}_{\mathrm{m0}}} = 1 - \exp\left(-\frac{L}{L_0}\right). \tag{38}$$

The particle charging efficiency for 3-m pipe in this experiment is found to be in a range from 93% to 99%.

The effect of the initial charge on particle charging is shown in Fig. 35. The experimental results were obtained using two different pipes made of stainless steel and brass. Although the particle charging depends on the initial charge on particles and pipe materials, all the experimental results agree well with the results calculated using Eq. (37). These results imply that the triboelectric charging of particles can be controlled by arranging pipes made of different materials.

The experimental result for the specific charge obtained by connecting 1-m brass pipe and 1-m stainless steel (SUS316) pipe alternately is shown in Fig. 36(a). The particles are charged negatively in the brass pipes but positively in the stainless steel pipes. As a result, the values of the specific charge are within a certain range. The experimental results are in good agreement with the solid lines calculated using Eq. (37). The result obtained by 0.5-m pipes instead of 1-m pipes is shown in Fig. 36(b). It is clear that the specific charge in Fig. 36 (b) is within a narrower range compared with that in Fig. 36(a)

Examples of the general calculation to control the triboelectric charging in gas-solids pipe flow using two different pipe materials A and B are shown in Fig. 37. Although the charge is fluctuated positively and negatively, the fluctuation level decreases with decreasing each pipe length. The upper limit $\bar{q}_{\mathrm{mA}}{}^*$ for pipe A and the lower limit $\bar{q}_{\mathrm{mB}}{}^*$ for pipe B are given by

$$\bar{q}_{\mathrm{mA}}{}^* = \frac{\bar{q}_{\mathrm{mA}\infty}\left\{1 - \exp\left(-\frac{\Delta L_{\mathrm{A}}}{L_{\mathrm{A0}}}\right)\right\} + \bar{q}_{\mathrm{mB}\infty}\exp\left(-\frac{\Delta L_{\mathrm{A}}}{L_{\mathrm{A0}}}\right)\left\{1 - \exp\left(-\frac{\Delta L_{\mathrm{B}}}{L_{\mathrm{B0}}}\right)\right\}}{1 - \exp\left(-\frac{\Delta L_{\mathrm{A}}}{L_{\mathrm{A0}}} - \frac{\Delta L_{\mathrm{B}}}{L_{\mathrm{B0}}}\right)} \tag{39}$$

and

$$\bar{q}_{\mathrm{mB}}{}^{*}=\frac{\bar{q}_{\mathrm{mB}\infty}\left\{1-\exp\left(-\frac{\Delta L_{\mathrm{B}}}{L_{\mathrm{B0}}}\right)\right\}+\bar{q}_{\mathrm{mA}\infty}\exp\left(-\frac{\Delta L_{\mathrm{B}}}{L_{\mathrm{B0}}}\right)\left\{1-\exp\left(-\frac{\Delta L_{\mathrm{A}}}{L_{\mathrm{A0}}}\right)\right\}}{1-\exp\left(-\frac{\Delta L_{\mathrm{A}}}{L_{\mathrm{A0}}}-\frac{\Delta L_{\mathrm{B}}}{L_{\mathrm{B0}}}\right)}, \tag{40}$$

where ΔL_{A} and ΔL_{B} are the pipe lengths, L_{A0} and L_{B0} are the characteristic lengths, and the subscripts A and B denote the two different materials. Also, the polarity and amount of charge can be controlled by changing the pipe length ratio of A to B ($r = \Delta L_{\mathrm{A}}/\Delta L_{\mathrm{B}}$). As the pipe length ΔL_{A}, $\Delta L_{\mathrm{B}} \rightarrow 0$, the limiting values of the charge satisfy the relation of $\bar{q}_{\mathrm{m}}{}^{*} = \bar{q}_{\mathrm{mA}}{}^{*} = \bar{q}_{\mathrm{mB}}{}^{*}$. Substituting $\Delta L_{\mathrm{A}} = r\Delta L_{\mathrm{B}}$ into Eq. (39) and setting ΔL_{A}, $\Delta L_{\mathrm{B}} \rightarrow 0$, the limiting value $\bar{q}_{\mathrm{m}}{}^{*}$ is given by

$$\bar{q}_{\mathrm{m}}{}^{*}=\frac{\bar{q}_{\mathrm{mA}\infty}rL_{\mathrm{B0}}+\bar{q}_{\mathrm{mB}\infty}L_{\mathrm{A0}}}{L_{\mathrm{A0}}+rL_{\mathrm{B0}}}. \tag{41}$$

Therefore, the charge on particles can be controlled positively, negatively, or neutrally using two materials.

If two materials are arranged in parallel instead of in series, the charge on particles will approach the limiting value without the fluctuations mentioned above. In addition, various shapes and structures are available for a particle charging control device. Matsusaka et al. (2008b) developed a high-efficiency particle charger having an inverted truncated cone. Micrometer-sized particles are introduced into the charger from the tangential direction at the top, carried spirally downward, and discharged to the tangential direction at the bottom. The particles are triboelectrically charged by contact with the side wall of the charger due to the centrifugal force. Since two different metal sheets are attached in the side wall, particles can contact with these metals alternately.

5. Characterization of triboelectric charging

5.1 Work function and Contact potential difference

When materials are exposed to electromagnetic radiation, electrons are emitted (photoelectric effect). The number of the emitted electrons depends on the intensity of the radiation. Also, the kinetic energy of the electrons depends on the frequency or wave length of the radiation. The radiation is regarded as a stream of photons, each having an energy $h\nu$, where h is the Planck constant and ν is the frequency of the photon. If the photon energy exceeds the work function of the material ϕ, a photon can eject an electron out of the surface; thus, there is the minimum frequency, i.e. threshold frequency, at which ejection occurs. For many solid materials, the photoelectric effect occurs at ultraviolet frequencies or above, and for some materials having low work functions it occurs with light. The maximum kinetic energy of the photoelectron depends on

the energy of a photon and the work function. This is applied to a technique for determining the work function or analyzing the surface properties of various materials (Murata, 1979; Murata and Kittaka, 1979).

When two dissimilar electrically conductive materials are in contact, a potential difference is generated between them. This is called the contact potential difference (CPD). Its origin can be described in terms of the process necessary to bring the two materials into thermal equilibrium, and it is expected that electrons migrate through the surfaces when they make contact. If there is a net flow of electrons, they are electrostatically charged. Therefore, the measurement of CPD is important to evaluate the contact charging. In fact, the surface of materials is not pure and is usually covered with an oxide layer, and thus the CPD of the materials may significantly differ from the values shown in literature. To measure the CPD between a powder and a wall, a measuring system based on the Kelvin–Zisman method was developed (Fig. 38) (Yoshida et al., 1991, 1992; Itakura et al., 1996; Tanoue et al., 2001a). The CPD measurement system has an electric circuit consisting of a vibrating capacitor made up of two electrodes, a DC bias voltage supply, and an electrometer (Fig. 39). Powder is filled in the concavity of the lower electrode and the upper electrode made of gold oscillates vertically. When the voltage applied on the upper electrode is equal to the potential difference between the powder and the upper electrode, the induced currents detected by the electrometer become zero. The applied voltage is called zero-point potential V_0, which is expressed by the following equation:

$$V_0 = V_{\mathrm{P/Au}} + \frac{\rho_\mathrm{c} d_\mathrm{l}^{\,2}}{2\varepsilon_\mathrm{p}}, \tag{42}$$

where $V_{\mathrm{P/Au}}$ is the CPD between the powder and the gold reference, ρ_c, d_l, and ε_p are, respectively, the volume charge density, the thickness of the powder layer, and the absolute permittivity of the powder layer. When the charge of the powder layer is sufficiently small ($\rho_\mathrm{c} \approx 0$), V_0 is equal to $V_{\mathrm{P/Au}}$.

5.2 Specific Charge

In general, the charge on particles is measured with a Faraday cage (Fig. 40) because of the advantages of simplicity and reliability. When charged particles are put into a metal enclosure isolated electrically, charge is induced in the inner wall of the metal enclosure. The specific charge of particles is obtained by dividing the charge by the mass of particles. For dust in air or particles in gas–solids pipe flows, a Faraday cage with a filter is used to collect the particles (Fig. 41). Also, an open ended Faraday cage, so-called through-type Faraday cage is available (Matsuyama and Yamamoto, 1989, 1994; Matsusaka et al., 2000; Watanabe et al., 2006, 2007a, b). Since this type

of Faraday cage does not obstruct the particle movement, the charge can be measured in situ.

In electrophotography, to evaluate the triboelectric charging of a toner-carrier system called 'developer', the blow-off method is used (Fig. 42). In this system, the toner particles are charged by contact with a carrier (larger bead). In the Faraday cage, a mixed powder of the toner and the carrier is placed on a stainless steel filter whose mesh size is chosen to be between the sizes of the toner particles and carrier beads. Nitrogen gas spurts from the upper nozzle of the Faraday cage and separates the mixture into toner and carrier. Only the toner is blown off through the filter and the carrier with a charge equivalent but opposite in polarity to that of the blown-off toner is left in the cage. The variation of the charge in the cage is measured by an electrometer (Oguchi and Tamatani, 1993)

5.3 Charge distribution

An aerodynamic technology is widely used to measure particle charge distribution for fine particles. A typical example of the system is shown in Fig. 43. Particles are injected into a laminar flow, where a perpendicular electric field is applied, and deposit on the walls of the channel by the electrostatic force. From the position of the deposited particles, the amount of the charge can be determined. A filter placed at the end of the apparatus can be used to collect the particles with small or no charge. The drag force on small particles immediately becomes equal to the Coulomb force; thus the force balance is given by

$$qE = \frac{3\pi\mu v_{\mathrm{E}} D_{\mathrm{p}}}{C_{\mathrm{c}}}, \tag{43}$$

where q is the charge of the particle, E is the electric field strength, μ is the viscosity of air, v_{E} is the electrostatic terminal velocity of the particle, D_{p} is the particle diameter and C_{c} is the Cunningham correction factor. Therefore, the charge–to–diameter ratio q_{d} ($=q/D_{\mathrm{p}}$) is derived as

$$q_{\mathrm{d}} = \frac{3\pi\mu}{C_{\mathrm{c}}E} v_{\mathrm{E}} = \frac{3\pi\mu}{C_{\mathrm{c}}E} \frac{y_{\mathrm{d}}}{t}, \tag{44}$$

where y_{d} is the displacement and t is the time (Schein, 1992/1996).

Mazumder et al. (1991) developed a laser-based instrument called the electrical-single particle aerodynamic relaxation time (E-SPART) analyzer, which measures the aerodynamic diameter D_{p} and charge q of individual particles. In the measurement cell, electric field and acoustic field are formed horizontally (Fig. 44). When a charged particle passes vertically through an acoustic field, the particle oscillates with a phase lag depending on the particle diameter. Therefore, the particle diameter D_{p} is determined by measuring the phase lag θ, i.e.:

$$D_{\mathrm{p}} = \sqrt{\frac{18\,\mu \tan\theta}{C_{\mathrm{c}}\,\rho_{\mathrm{p}}\,\omega}}, \tag{45}$$

where ρ_{p} is the particle density and ω is the angular velocity of the acoustic wave. As a DC electric field is simultaneously superimposed in the cell, the charged particle experiences another velocity component. From the balance between the electrostatic force and aerodynamic drag, the charge–to–diameter ratio q_{d} is obtained using Eq. (44). The particle velocity v_{E} is measured by a laser Doppler method. This analyzer is available for analyzing bipolar charge distribution (Mazumder et al., 1991; Matsusaka et al., 2003 b).

For measuring particle charge, the particle motion analysis system (PMAS) is also used (Fig. 45). In the electrostatic separation chamber, there are two parallel electrodes and an electric field is applied horizontally. Particles that are injected into the chamber travel in the electric field. The PMAS, which consists of a short duration light source, a CCD camera with a zoom lens, and the data processor, captures pairs of multiple particle images using the double-spark light source with very short pulse interval. The particle velocity can be obtained from the tracking images. The amount of charge on particles can be calculated with both the velocity in the given electrical field and the diameter of particles in the images (Ahn et al., 2004).

As shown in Fig. 43, charge spectrometers for fine particles use a laminar flow to carry the particles; however, it is not easy to control the airflow and the injection of particles. The disturbance of the airflow causes a significant measurement error. To simplify the construction of the apparatus, and to increase the accuracy of the measurement, a free air beam is used for injecting particles in an electric field (Fig. 46). The air in the chamber is sucked to pull the aerosol particles from an activation cell. The charged particles in the measurement cell are deflected onto the electrodes according to the charge-to-diameter ratio. Both polarities can be determined by one measurement. However, the electric field caused by the inhomogeneous geometry leads to a more complex calculation to obtain the particle path through the measurement cell (Epping and Kuettner, 2002).

Fig. 47 shows a charge distribution measurement system consisting of dispersion feeder, sampling section, and measurement cell. The dispersion of particles is necessary to feed single particles into the measurement cell. However, highly charged aerosol particles readily deposit on the wall. To prevent the charged particles from depositing in the sampling section, an AC field called the ‘electric curtain’ (Masuda et al., 1972) can be used. In the measurement cell, the particles fall under gravity with moving horizontally by the electrostatic force. The horizontal and vertical velocities of the particles v_{x} and v_{y} in the cell are, respectively, given by (Masuda et al., 1993; Matsusaka et al., 2008c)

$$v_x = \frac{qEC_c}{3\pi\mu D_p} \tag{46}$$

and

$$v_y = \frac{m_p g C_c}{3\pi\mu D_p}, \tag{47}$$

where g is the gravitational acceleration. Therefore, the specific charge q/m_p is derived as

$$\frac{q}{m_p} = \frac{g}{E}\frac{v_x}{v_y} = \frac{g}{E}\frac{x_d}{y_d}, \tag{48}$$

where x_d and y_d are, respectively, the x-and y-components of the displacement. The particle diameter and the displacement can be measured with an automatic digital image processing system. An example of two-dimensional distribution of specific charge and particle diameter measured by this system is shown in Fig. 48. The cumulative distribution, dimensionless [0, 1] is given by the surface integral of the frequency distribution.

5.4 General techniques for characterization

Various techniques have been proposed to characterize the triboelectric charging of particles. Although these techniques were developed from practical needs, the high performance of the measurement methods made them the object of scientific interest. A representative method, namely the 'cascade method' is shown in Fig. 49 (Oguchi and Tamatani, 1993). Particles are fed from the top of the reference plate that is held at a certain angle. The triboelectric charging occurs while the particles cascade down the slope. The total amount of charge produced on the particles is measured with a Faraday cage. Although the polarity of the charge on the particles is opposite from that on the plate, the absolute values are the same as each other.

Another useful characterization method is shown in Fig. 50. The device consists of a vibrating feeder and a charging plate (Higashiyama et al., 1997). The particles move from one end toward the other while contacting with the plate. The charge of the particles falling from the edge is measured with a Faraday cage.

A fluidized bed can be used for a triboelectric charging device (Fig. 51) (Iuga et al, 2005). When different kinds of particles are mixed, the triboelectric charging is complicated, i.e. the charge transfer occurs during the collision with different type of particles, with the same type of particles, and with the inner wall, depending on the initial surface charge on the contact area. To measure the charge distribution of the particles, they are classified in a charge spectrometer, such as free fall separator with a horizontal electric field.

Fig. 52 shows a vertical array of Faraday cage sensors, which is combined with a fluidized bed (Zhao et al., 2002). This measurement system consists of special Faraday cages mounted vertically in cascade and a normal one located at the bottom. The series of Faraday cages have open holes on the upper and lower covers. The measurements are performed during the free falling of particles. Each particle experiences gravity and space charge repulsion; thus, large particles drop faster in the vertical direction and highly charged particles move faster in the radial direction. As a result, the particles are separated in the Faraday cages. The charge and mass of particles are measured with each Faraday cage. In addition, various analyses such as particle size distribution in the Faraday cages are useful for total evaluation of the particle charging.

The characteristics of the triboelectric charging can be evaluated by various methods; however, the particles may not be sufficiently charged. Kittaka and Murata (1976), Rowley (2001), and Matsusaka et al. (2008b) proposed a method using a cylinder in which particles can be charged by a circular airflow (Fig. 53). As strong centrifugal forces act on the particles in motion, the particles continue to rotate in the cylinder until the airflow is stopped. After rotation, the charged particles are taken out rapidly from the cylinder through a hole using a vacuum pump and are led into a Faraday cage.

5.5 Single particle impact test

Watanabe, et al. (2006, 2007a, b) developed an impact charging test rig, as mentioned in §4.3. The device consists of an impact target and two sets of Faraday cages. The device allows charge measurements of single particles as small as ~100 μm impacting on the target at different incident angles with a high velocity. The analysis of the charge transfer as a function of the initial charge of the particle determines an equilibrium charge, i.e. an initial charge for no net charge transfer (see Fig. 20).

5.6 Gas–solids pipe flow test

Charge transfer in dilute phase gas solids pipe flow can be analyzed from electric currents generated in a length of detection pipe, as mentioned in §4.5; i.e. the transferred charge per unit mass of particles in the pipe is obtained as the value of the electric current divided by the mass flow rate of the particles I/W_p. From the relationship between I/W_p and the specific charge q_{m0} at the inlet of the detection pipe, a characteristic of particle charging is obtained, and the equilibrium specific charge is determined (see Fig. 33). This method is available for micrometer-sized particles (Matsusaka and Masuda, 2006).

5.7 Atomic force microscopy

Force measurement with a micrometer-sized particle attached to the cantilever of atomic force microscope (AFM) has received increasing interest since 1991 (Ducker et al., 1991). One distinct advantage of the so-called 'colloid probe' technique is that a quantitative comparison between experimental force curves and theoretical expectations becomes possible using a probe of known geometry, while the disadvantage is that it is unsuitable for statistical analysis of a number of particles since the preparation of the colloid probes is not easy. In an attempt to better understand the origin of adhesion forces, quantitative studies of the surface force interaction as a function of the distance between particle and substrate have been carried out. The measurements have revealed two dominant forces, i.e. the electrostatic force due to localized contact charging on the particles and the van der Waals force. The sensitivity in the measurement of the charge transfer is ~10 electrons (Gady et al., 1998).

To study the contact charging of glass particles, Nishitani et al. (2000) used this method. Single particles attached to cantilevers were charged by repeated contact with a flat stainless steel. The charge accumulated on the particle was analyzed by considering a virtual point charge in the particle. Matsuyama et al. (2006) also performed similar measurements, and discussed how to determine the surface charge density and the contact area from the force curve. Furthermore, the consistency between the measured results and their charge relaxation model was discussed. Bunker et al. (2007) studied the charging of pharmaceutical particles. They performed two different experiments, i.e. the generation of charge by repeated contacts and by scanning across the surface of the substrate, showing that the particle charging by scanning was more effective than that by simple contacts.

6. Applications

6.1 Separation

The development of a process to separate solid materials can improve the possibilities for recycling wastes. If particles or small solids have largely different electrostatic properties, they can be separated. In this process, the particles are first triboelectrically charged and then fed into an electric field separator. The particle trajectories are deflected in the electric field according to the polarity and the amount of charge. Although the method to triboelectrically charge the particles is simple and easy, the charge transfer depends on the environmental conditions; thus temperature and humidity should be controlled in a certain range. A typical electrostatic separator is shown in Fig. 54 (Yanar and Kwetkus, (1995)). Particles that are triboelectrically charged in a cyclone separator

enter the electrostatic separator where a DC electric field is applied. The trajectory of the particles depends on the electrostatic charge and mass of particles. The inhomogeneous electric field is effective to achieve a large deflection of the charged particles in the upper part of the separator. The bottom of the separator consists of a series of collection trays.

Another electric separator is shown in Fig. 55 (Soong et al., 2007). Particles are charged in a venture by contact with the wall and other particles, and sent to an electric field between two series of louvered plates. The charged particles are collected on the louvered plates by adjusting the applied voltage according to the charge on particles.

Saeki (2006) proposed a different type of separator consisting of a vibratory conveyor equipped with two plate electrodes (Fig. 56). The advantage of the vibratory separator is to avoid the influence of the adhesion between oppositely charged particles and also particle-wall adhesion. The two electrodes are inclined toward the horizontal at an angle θ and are fixed to the vibrating plate. The upper electrode has negative polarity and the lower electrode is grounded. The separation unit vibrates in the direction of angle α to the x-axis. The charged particles are fed onto the lower electrode through a feeder. Positively charged particles are attracted toward the upper electrode by the electrostatic force and are repelled from the lower electrode, and thus the tangential vibration force acting on the particles is reduced. On the other hand, negatively charged particles are attracted toward the lower electrode and strongly experience the vibration force from the lower electrode and consequently conveyed on the x-direction. The difference in the particle trajectory enables the separation.

6.2 Powder coating

Electrostatic powder coating is a dry finishing process. The powder used in the process, which is a mixture of finely ground particles of pigment and resin, is electrostatically charged and sprayed onto an electrically conductive work piece to be coated. The main difference from a conventional liquid paint is that the powder coating does not require a solvent to keep the binder and filler parts in a liquid suspension form. Therefore, the powder coating offers several advantages. It does not use volatile organic compounds (VOCs), which are hazardous to human health, and over sprayed powder can be collected and recycled.

The general process is as follows; coating powder is fluidized by air and then blown through a pipe to a charging gun. Two types of guns are available, i.e. the triboelectric and corona guns. For the triboelectric gun, powder is charged by frictional contact with the walls in the gun. The sprayed, charged particles form a space-charge field, which is directed toward the grounded conductive workpiece. As a result, the charged particles drift toward the workpiece and deposit not only onto the surface of the workpiece facing the spray gun but also in hidden regions due to the

space-charge field. The particles that deposit onto the workpiece adhere by electrostatic image forces. After spraying, the workpiece is transferred to a high-temperature curing region in which the powder melts and flows to produce a smooth coating layer.

6.3 Electrophotography

Electrophotography is a photocopying technique developed by Chester Carlson in 1938. In this process, a visible image is created using electrostatic latent images in the form of surface charge patterns on a photoconductive surface. The visible images consist of fine particles called 'toner'. Toner is triboelectrically charged by mixing it with larger carrier beads. The mixture is called 'developer'. In some cases the toner is triboelectrically charged against walls without the use of carrier beads.

A typical process of the electrophotography consists of six steps: (i) the surface of photoreceptor, which is an insulator in the absence of light, is uniformly charged. (ii) Light reflected from the image discharges the normally insulating photoreceptor producing a latent image—a charge pattern on the photoreceptor that mirrors the information to be transformed into the real image. (iii) Toner particles charged spread over the surface adhere to the latent image, transforming it into a real image. (iv) The developed toner on the photoreceptor is transferred to paper charged on the backside. (v) The image is permanently fixed to the paper by melting the toner. (iv) The photoreceptor is discharged and cleaned of any excess toner (Schein, 1992/1996).

For black and white copiers, the photoreceptor can transfer the image directly to paper. However, for most color copiers the image is formed from four colors (cyan, magenta, yellow and black) of toner and the image is built up first on an intermediate surface; then, another transfer takes place where the full-color image is transferred to paper.

6.4 Self-assembly

Self-assembly of components is a useful method for preparing microstructured materials with interesting mechanical or optical properties. Although crystallization of particles with different sizes or shapes can be achieved, the methods to assemble binary lattices of particles of the same sizes but with different properties are limited. One of the available methods is the electrostatic self-assembly (ESA) of macroscopic components using interactions caused by triboelectric charging. The systems comprise two kinds of particles (usually spheres) that are charged oppositely when agitated on a flat, metallic surface. The interplay of repulsive interactions between like-charged particles and attractive interactions between unlike-charged ones results in the self-assembly of these particles into highly ordered arrays.

The type of the lattice formed by self-assembly depends on the number ratio of the two different particles. For example, when the number ratio, Nylon-6, 6 (N_{Nyl}) / Teflon (N_{Tef}), is close to unity, a square lattice array is formed (Fig. 57(a)). When particles of one kind are present in excess, they arrange themselves into either a pentagonal lattice array or a hexagonal lattice array. When N_{Nyl} / N_{Tef} >1, each Teflon particle is surrounded by five or six Nylon-6,6 particles (Fig. 57(b), (c)). Conversely, when N_{Nyl} / N_{Tef} <1, each Nylon-6,6 particle is surrounded by five or six Teflon particles. These observations suggest that the lattices are steady-state products of self-assembly (Grzybowski et al., 2003).

6.5 Measurements in pneumatic transport

6.5.1 Particle flow rate and specific charge

In gas-solids pipe flow, the charges transferred from the particles to the wall are detected as electric currents as mentioned in §4.5. For dilute phase flow, the electric current I generated from a pipe is formulated with the particle flow rate W_{p} and the specific charge of particles q_{m0} at the inlet of the pipe (see Eq. (34)). When two different detection pipes are connected in series with electrical isolation (Fig. 58), the following equations are held for the first and second pipes, respectively:

$$\frac{I_1}{W_{\mathrm{p}}} = a_1 q_{\mathrm{m0}} + b_1 \tag{49}$$

and

$$\frac{I_2}{W_{\mathrm{p}}} = a_2 q_{\mathrm{m1}} + b_2 \tag{50}$$

,

where subscripts 1 and 2 refer to the first and second detection pipes, respectively. Since the charge at the outlet of the first pipe is equal to that at the inlet of the second pipe, the charge balance is expressed as

$$q_{\mathrm{m0}} - q_{\mathrm{m1}} = \frac{I_1}{W_{\mathrm{p}}}, \tag{51}$$

From Eqs. (49)-(51), the particle flow rate W_{p} is expressed as

$$W_{\mathrm{p}} = c\, I_1 + d\, I_2, \tag{52}$$

here

$$c = \frac{(a_1 - 1)\, a_2}{a_1 b_2 - a_2 b_1} \tag{53}$$

and

$$d = \frac{a_1}{a_1 b_2 - a_2 b_1} . \tag{54}$$

The denominator of the right-hand side in Eqs. (53) and (54) must not be zero; this means that the electrostatic property of the first detection pipe must differ from that of the second one, i.e.

$$\frac{b_1}{a_1} \neq \frac{b_2}{a_2} . \tag{55}$$

Therefore, on-line measurement of particle flow rate is possible by measuring the two electric currents (Masuda et al., 1994, 1998b; Matsusaka and Masuda, 2006). In addition, from Eqs. (49)-(51), the following equation is derived:

$$q_{\mathrm{m0}} = \frac{\left(b_2 - a_2 b_1\right) I_1 - b_1 I_2}{a_2 \left(a_1 - 1\right) I_1 + a_1 I_2} . \tag{56}$$

The particle charge can also be calculated using Eq. (56).

6.5.2 Signal analysis

The current detected in gas–solids pipe flow consists of many pulsating electric signals, which vary in a wide range from positive to negative. In fact, these electric signals contain useful information on the state of particles flowing in the pipe. An example of the signals detected with a digital oscilloscope is shown in Fig. 59 (a). The variation of the signals on a magnified time scale is shown in (b). The pulsating signals are caused by the fluctuation of the particle flow rate. Even though particles continuously flow in the pipe, the particle concentration fluctuates on a time scale of milliseconds; as a result, a number of clouds of particles flow in the pipe.

For instance, when a cloud of negatively charged particles approaches the detection pipe, positive charge is induced on the inner surface of the detection pipe. This occurs by the fact that the electrons on the inner surface flow to earth, and consequently a negative peak is detected with the digital oscilloscope. If the particles impact on the wall of the detection pipe, charge transfer will occur. Since the transferred charges remain there while the particles are in the pipe, no electric signal is detected. When the particles pass out of the pipe, the whole charge held on the wall surface flows to earth, and a peak signal is detected.

The shape and intensity of the electric signals depend on the condition such as the polarity and amount of the charge of the cloud at the inlet and outlet of the detection pipe. Typical particle charging in gas–solids pipe flow and the shapes of the electric signals are illustrated in Fig. 60

(Matsusaka et al., 2008a). Here, it is supposed that the particle charging is represented by an exponential equation (Cole et al., 1969–1970; Masuda et al., 1976; Matsusaka et al., 2007) and that the detection pipe length is larger than the cloud; thus, the tails of the two peaks do not overlap with each other.

These electric signals can be applied to the correlation method for measuring particle velocity (Yan et al., 1995; Gajewski, 1996). Two detection pipes are used for the measurement system. Three sets of electric signals are shown in Fig. 61 (Matsusaka et al., 2008a). Since particles that are negatively charged obtain negative charge by contact with the wall of the first detection pipe, a larger positive signal is detected at the outlet. By passing through the intermediate pipe, the particles obtain positive charge by contact with the wall, material of which is different from that of the detection pipes, and the polarity of the particle changes from negative to positive. The polarity again changes to negative by passing through the second detection pipe. The time interval between the first and second detection pipes increases proportionally with the length of the intermediate pipe. The particle velocity can be calculated from the time interval.

7. Simulation

7.1 Triboelectric charging by repeated impacts

Matsuyama and Yamamoto (2006 b) proposed a Monte Carlo simulation for a charge accumulating process of a single particle during successive impacts. In the calculation, patch-like charges were localized randomly on the particle surface (Fig. 62(a)), and the charges were considered to work as the initial charge at the next impact. To reduce the load of the calculation, the patch-like charges were redistributed as an axisymmetric charge distribution as shown in Fig. 62(b). The charge transfer can be calculated based on the charge relaxation model (see § 4.2). The calculated results i.e. impact charge and the accumulated charge on the particle are shown as a function of the number of impacts (Fig. 63). Both the impact charge and the accumulated charge vary exponentially.

Yoshida et al., (2003) calculated multi-impact charging in a vibrating vessel using three-dimensional distinct element method (DEM). The surface of the particles is divided into many charging sites (Fig. 64). In this calculation, it is assumed that (i) particles are insulators, (ii) the charge transfer occurs by impact between particles as well as particle and wall, depending on the contact potential difference and the local electric field, and (iii) the charges transferred on the particle remain at the contact sites. The specific charge of the particles as a function of time elapsed is shown in Fig. 65. The particle charge approaches an equilibrium value, and the effect of

the number of the sites on the particle charge is not so significant if the number of the sites is sufficiently large.

Matsuyama et al. (2009) developed another DEM simulation to analyze the development of charge on particles in a shaker. In their analysis, particle charging model, space charge effect, electrical boundary condition of a container, and long range force were comprehensively involved.

In gas-solids pipe flow, particles are charged to an equilibrium value by collisions with the pipe wall and other particles. Tanoue et al. (2001b) carried out numerical simulations of particle charging based on the condenser model (see § 4.1). They used the standard k–ε model to express the turbulent flow in the pipe and determined the number of collisions of particles on the pipe wall by Lagrangian particle tracking, showing that the effect of the particle size, air velocity, and pipe diameter on the particle charging. Cangialosi et al. (2006) used a statistical model to determine the particle–wall collisions and used the charge relaxation model (see § 4.2) to predict the equilibrium charge and the impact charge caused by multiple impact events. Watano (2006) used three-dimensional discrete element method (DEM) to calculate the contact area for particle charging in pneumatic conveying systems.

7.2 Behavior of charged particles

Lim et al. (2006) studied the flow behaviors of charged particles in gas–solids pipe flow using DEM coupled with computational fluid dynamics (CFD), showing that the charged particles are spread by the electrostatic diffusion. Also, Mio et al (2006) simulated the developing behavior of toners in a two-component development system of electrophotography using the large-scale DEM (150,000 particles) and discussed the effect of the bias voltage and mechanical operation conditions on the behavior of toners.

8. Summary

The research on triboelectric charging of particles has been reviewed from theoretical and experimental viewpoints to evaluate the current state of understanding and applications. From this work, the following points are concluded:

(1) The triboelectric charging can be caused by electron transfer, ion transfer, and material transfer. Among them, the electron transfer is considered to be the base of the charge transfer. For metal–metal contacts, the difference in work function is used to explain the charge transfer. For inorganic compounds such as oxides, the charging tendency can be explained by the generalized electronegativity of metal ion. For organic compounds, the charging tendency depends on the

functional groups contained in them. For polymer–metal contacts, the electric polarity after charge transfer can be determined by the energy level of HOMO and LUMO of the organic solids and the Fermi level of the metal. In addition, environmental conditions such as temperature and humidity have to be taken into account.

(2) To analyze the particle charging, two basic models, i.e. the condenser model and the charge relaxation model exist. The former is based on the effective contact potential difference depending on the work functions and initial charge. The latter is based on the gas breakdown predicted by the Paschen curve. Irrespective of the difference in the concept of particle charging, these models derive the same type of exponential equations for the charge accumulation by repeated impacts. These equations enable us to analyze actual complicated particle charging processes.

(3) The values of work function or the contact potential difference characterizing the triboelectric charging can be obtained experimentally. For the measurement of the charge on particles, the Faraday cage method is available; in fact, there are several types of Faraday cages, which are used for each purpose. In recent years, there is increasing interest in the measurement of the charge distribution of particles to analyze processes in detail. To precisely measure the charge distributions, dispersion and sampling of the charged particles are important since positively and negatively charged particles agglomerate and highly charged particles easily deposit before measurement. To characterize the particle charging tendency, several practical methods are proposed. In particular, the single particle impact test and the gas–solids pipe flow test are useful to evaluate the equilibrium charge and transferred charge. The atomic force microscopy is also useful for analyzing the electrostatic force of a single particle in detail.

(4) Triboelectric charging of particles can be applied for various purposes, e.g. electrostatic separation, dry powder coating and electrophotography. The electrostatic self-assembly is expected as a technique to produce new functional materials. Also, the measurement techniques using triboelectric charging of particles are essential to evaluate and control particle handling processes.

(5) Numerical simulation is a powerful tool to analyze particle charging processes. Monte Carlo simulation is available to study the charge accumulation by repeated impacts. DEM simulation is also useful for the calculation since the information of all the particle collisions are taken into account for the charge transfer. In gas–solids pipe flow, Lagrangian particle tracking method is available to study the charge accumulation process. In recent years, the analysis of the behavior of charged particles in a complicated system such as two-component development system of electrophotography comes to attract attention.

Acknowledgements

The authors acknowledge financial support from the International Fine Particles Research Institute (IFPRI). This research was also supported by Core-to-Core Program for Advanced Particle Handling Science, JSPS, and a Grant no. S0901039 from MEXT, Japan.

Appendix A. Equations of image charge effect

An image charge is illustrated in Fig. A.1 (Matsusaka and Masuda, 2006). The potential difference V_e in the gap is represented by

$$V_e = k_e q, \tag{11}$$

where

$$k_e = \frac{1}{4\pi\varepsilon_0}\left(\frac{1}{r_1} - \frac{1}{r_2}\right), \tag{A.1}$$

in which

$$r_1 = \frac{D_p}{2} \tag{A.2}$$

and

$$r_2 = \frac{D_p}{2} + 2z_0. \tag{A.3}$$

Substituting Eqs. (A.2) and (A.3) into Eq. (A.1) gives

$$k_e = \frac{1}{2\pi\varepsilon_0}\left(\frac{1}{D_p} - \frac{1}{D_p + 4z_0}\right)$$

$$\approx \frac{2z_0}{\pi\varepsilon_0 D_p^2}. \tag{29}$$

Appendix B. Equations of space charge effect

Charged particles flowing through a vertical pipe are illustrated in Fig. B-1 (Matsusaka and Masuda, 2006). When the charged particles are dispersed uniformly, the electric field E is expressed as a function of radius r, i.e.

$$E(r) = \frac{n_p\, r\, q}{2\varepsilon_0}, \tag{B.1}$$

where n_p is the particle number concentration, which is given by

$$n_p = \frac{6m}{\pi D_p^3}\frac{\rho_g}{\rho_p}\frac{\bar{u}}{\bar{v}}, \tag{B.2}$$

where m is the mass flow ratio of particles to gas, ρ_g is the density of the gas, $\bar{u}$ is the average gas velocity, ρ_p is the particle density, and $\bar{v}$ is the average particle velocity.

The potential difference V_b in the gap z_0 close to the wall is represented by

$$V_b = \int_{\frac{D_i}{2}-z_0}^{\frac{D_i}{2}} E(r)\,dr$$

$$= \frac{3z_0 m\rho_g D_i \bar{u}}{2\pi\varepsilon_0\rho_p D_p^3 \bar{v}} q, \tag{B.3}$$

From Eq. (B. 3) and Eq. (12) in the text, the following equation is derived:

$$k_b = \frac{3z_0 m\rho_g D_i \bar{u}}{2\pi\varepsilon_0\rho_p D_p^3 \bar{v}}. \tag{30}$$

Appendix C. Equations of probability density function of specific charge

Assuming that the probability density function of particle collision is expressed as a normal distribution, which is derived from an binomial distribution, and also using the relationship between the number of particle collision and the particle charge, the probability density function of the specific charge $f_1(q_m)$ is represented by (Matsusaka et al., 2002)

$$f_1(q_m) = \frac{q_{m\infty}}{q_{m\infty}-q_m}\frac{1}{\sqrt{2\pi\bar{n}k}}\exp\left[-\frac{\left\{q_{m\infty}\ln\left(1+\frac{q_m-q_{m0}}{q_{m\infty}-q_m}\right)-\bar{n}k\right\}^2}{2\bar{n}k^2}\right], \tag{C-1}$$

where $\bar{n}$ is the mean number of particle collisions and k is the impact charging factor $(=q_{m\infty}/n_0)$.

Using a probability density function of initial charge $f_{ic}(q_{m0})$, the probability density function $f_2(q_m)$ after traveling through the pipe is represented by

$$f_2(q_m) = \int_{-\infty}^{q_{m\infty}} f_1(q_m) f_{ic}(q_{m0}) \mathrm{d}q_{m0} . \quad \text{(C-2)}$$

Furthermore, using a probability density function of the impact charging factor $f_k(k)$, the probability density function $f_3(q_m)$ after traveling through the pipe is represented by

$$f_3(q_m) = \int_{-\infty}^{\infty} f_2(q_m) f_k(k) \mathrm{d}k . \quad \text{(C-3)}$$

Substituting the probability density functions gives theoretical equations.

References

Adhiwidjaja, I., Matsusaka, S., Yabe, S., Masuda, H., 2000. Simultaneous phenomenon of particle deposition and reentrainment in charged aerosol flow—effects of particle charge and external electric field on the deposition layer. Advanced Powder Technology 11, 221-233.

Ahn, Y.C., Kim, D.H., Kim, S.C., Hwang, E.G., Lee, C.G., Kim, G.T., Shin, H.S., Lee, J.K., Lee, S.H., 2004. Measurement and control of triboelectrically charged silica and glassy carbon particles. Particulate Science and Technology 22, 305-320.

Alfrey, T., Price, C.C., 1947. Relative reactivities in vinyl copolymerization. Journal of Polymer Science 2, 101-106.

Anderson, J.H., 1994. A comparison of experimental data and model predictions for tribocharging of two-component electrophotographic developers. Journal of Imaging Science and Technology 38, 378-382.

Bailey, A.G., 1993. Charging of solids and powders. Journal of Electrostatics 30, 167-180.

Bailey, A.G., 1998. The science and technology of electrostatic powder spraying, transport and coating. Journal of Electrostatics 45, 85-120.

Bailey, A.G., 2001. The charging of insulator surfaces. Journal of Electrostatics 51/52, 82-90.

Balachandran, W., Hu, D., Ghadiri, M., Law, S. E., Thompson, S. A., 1997. The study of the performance of an electrostatic valve used for bulk transport of particulate materials. IEEE Transactions on Industry Applications 33, 871-878.

Bunker, M.J., Davies, M.C., James, M.B., Roberts, C.J., 2007. Direct observation of single particle electrostatic charging by atomic force microscopy. Pharmaceutical Research 24, 1165-1169.

Cangialosi, F., Liberti, L., Notarnicola, M., Stencel, J., 2006. Monte Carlo simulation of pneumatic tribocharging in two-phase flow for high-inertia particles. Powder Technology 165, 39-51.

Cartwright, P., Singh, S., Bailey, A.G., Rose, L.J., 1985. Electrostatic charging characteristics of polyethylene powder during pneumatic conveying. IEEE Transactions on Industry Applications IA-21, 541-546.

Cole, B.N., Baum, M.R., Mobbs, F.R., 1969–1970. An investigation of electrostatic charging effects in high-speed gas–solids pipe flows. Proceedings Institution of Mechanical Engineers, vol. 184, 77-83.

Cotler P., Castle, G.S.P., Schein, L.B., 1995. General model of sphere–sphere insulator contact electrification. Journal of Electrostatics 36, 165-173.

Davies, D.K., 1969. Charge generation on dielectric surfaces. British Journal of Applied Physics: Journal of Physics. D 2, 1533-1537.

Diaz, A.F., Guay, J., 1993. Contact charging of organic materials: ion vs. electron transfer. IBM Journal of Research Development 37, 249-259.

Duke, C. B., Fabish, T. J., 1978. Contact electrification of polymers: a quantitative model. Journal of Applied Physics 49, 315-321.

Ducker, W.A., Senden, T.J., Pashley, R.M., 1991. Direct measurement of colloidal forces using an atomic force microscope. Nature 353, 239-241.

Ema, A. Yasuda, D., Tanoue, K., Masuda, H., 2003. Tribo-charge and rebound characteristics of particles impact on inclined or rotating metal target. Powder Technology 135/136, 2-13.

Epping, R.H., Kuettner, A., 2002. Free air beam in an electric field for determination of the electrostatic charge of powders between 1 and 200 μm. Journal of Electrostatics 55, 279-288.

Fabish, T.J., Duke, C.B., 1977. Molecular charge states and contact charge exchange in polymers. Journal of Applied Physics 48, 4256-4266.

Gady, B., Reifenberger, R., Rimai, D.S., 1998. Contact electrification studies using atomic force microscope techniques. Journal of Applied Physics 84, 319-322.

Gajewski, A. 1989. Measuring the charging tendency of polystyrene particles in pneumatic conveyance. Journal of Electrostatics 23, 55-66.

Gajewski, J. B., 1996. Monitoring electrostatic flow noise for mass flow and mean velocity measurement in pneumatic transport. Journal of Electrostatics, 37, 261-276.

Gajewski, J. B., 2006. Non-contact electrostatic flow probes for measuring the flow rate and charge in the two-phase gas–solids flows. Chemical Engineering Science 61, 2262-2270.

Gajewski, J. B., 2008. Electrostatic nonintrusive method for measuring the electric charge, mass flow rate, and velocity of particulates in the two-phase gas–solid pipe flows—its only or as many as 50 years of historical evolution. IEEE Transactions on Industry Applications 44, 1418-1430.

Ghadiri, M., Martin, C. M., Morgan, J. E. P., Clift, R., 1992. An electromechanical valve for solids. Powder Technology 73, 21-35.

Gibson, H. W., 1975. Linear free energy relationships—triboelectric charging of organic solids. Journal of the American Chemical Society 97, 3832-3833.

Gibson, H. W., Control of electrical properties of polymers by chemical modification. Polymer, 25, 3-27 (1984).

Grzybowski, B. A., Winkleman, A., Wiles, J. A., Brumer, Y., Whitesides, G. M., 2003. Electrostatic self-assembly of macroscopic crystals using contact electrification. Nature Materials 2, 241- 245.

Greason, W. D., 2000. Investigation of a test methodology for Triboelectrification. Journal of Electrostatics 49, 245-256.

Guardiola, J., Rojo, V., Ramos, G., 1996. Influence of particle size, fluidization velocity and relative humidity on fluidized bed electrostatics. Journal of Electrostatics 37, 1-20.

Gupta, R., Gidaspow, D., Wasan, D. T., 1993. Electrostatic separation of powder mixtures based on the work functions of its constituents. Powder Technology, 75, 79-87.

Gutman, E. J., Hartmann, G. C., 1992. Triboelectric properties of two-component developers for

xerography. Journal of Imaging Science and Technology 36, 335-349.

Harper, W. R., 1951. The Volta effect as a cause of static electrification. Proceedings of the Royal Society of London Series A 205, 83-103.

Harper, W. R., 1967. Contact and Frictional Electrification, Clarendon Press, Oxford.

Higashiyama, Y., Ujiie, Y., Asano, K., 1997. Triboelectrification of plastic particles on a vibrating feeder laminated with a plastic film. Journal of Electrostatics, 42, 63-68.

Hughes, J. F., 1984. Electrostatic Powder Coating, Research Studies Press, Wiley, New York.

Ikezaki, K., Teraoka, S., Namekawa, M., 2005. Ultrasound aided tribocharging of polymeric powders. Journal of the Institute of Electrostatics Japan 29, 173-178.

Itakura, T., Masuda, H., Ohtsuka, C., Matsusaka, S., 1996. The contact potential difference of powder and the tribo-charge. Journal of Electrostatics 38, 213-226.

Iuga, A., Calin, L., Neamtu, V., Mihalcioiu, A., Dascalescu, L., 2005. Tribocharging of plastics granulates in a fluidized bed device. Journal of Electrostatics, 63, 937-942.

Jones, T. B., 1995. Electromechanics of Particles. Cambridge University Press, Cambridge.

Jones, T. B., King, J. L., 1991. Powder Handling and Electrostatics: Understanding and Preventing Hazards. Lewis, Chelsea.

Joseph, S., Klinzing, G. E., 1983. Vertical gas–solid transition flow with electrostatics. Powder Technology 36, 79-87.

Kittaka, S., Murata, Y., 1976. A new system for measuring the charging tendency of solid particles. Journal of Electrostatics 2, 111-119.

Kleber, W., Makin, B., 1998. Triboelectric powder coating: a practical approach for industrial use. Particulate Science and Technology 16, 43-53.

Kodama, J., Foerch, R., McIntyre, N.S., Castle, G.S.P., 1993. Effect of plasma treatment on the triboelectric properties of polymer powders. Journal of Applied Physics 74, 4026-4033.

Lawless, P.A., 1999. Electrostatic precipitators. In: Webster, J. (Ed.), Wiley Encyclopedia of Electrical and Electronics Engineering. John Wiley & Sons, Inc. vol. 7, pp.1- 15.

Lee, L.-H., 1994. Dual mechanism for metal–polymer contact electrification. Journal of Electrostatics 32 1-29.

Lim, E.W.C., Zhang, Y., Wang, C.-H., 2006. Effects of an electrostatic field in pneumatic conveying of granular materials through inclined and vertical pipes. Chemical Engineering Science 61, 7889-7908.

Lowell, J., Rose-Innes, A.C., 1980. Contact electrification. Advances in Physics 29, 947-1023.

Lowell, J., Akande, A.R., 1988. Contact electrification—why is it variable?. Journal of Physics D: Applied Physics 21, 125-137.

Machida, M., Scarlett, B., 2005. Process tomography system by electrostatic charge carried by particles. IEEE Sensors Journal 5, 251-259.

Masui, N., Murata, Y., 1983. Electrification of polymer particles by impact on a metal plate. Japanese Journal of Applied Physics 22, 1057-1062.

Masui, N., Murata, Y., 1984. Mechanisms of charge build-up on a polymer particle by repeated impact. Japanese Journal of Applied Physics 23, 550-555.

Masuda, S., Fujibayashi, K., Ishida, K., Inaba, H., 1972. Confinement and transportation of charged aerosol clouds via electric curtain, Electrical Engineering in Japan, 92, 43-52.

Masuda, H., Komatsu, T., Iinoya, K., 1976. The static electrification of particles in gas–solids pipe flow. AIChE Journal 22 558-564.

Masuda, H., Gotoh, K., Orita, N., 1993. Charge distribution measurement of aerosol particles. Journal of Aerosol Research, Japan 8, 325-332.

Masuda, H., Matsusaka, S., Nagatani, S., 1994. Measurements of powder flow rate in gas–solids pipe flow based on the static electrification of particles. Advanced Powder Technology 5, 241-254.

Masuda, H., Matsusaka, S., Akiba, S., Shimomura, H., 1998a, Electrification of fine particles in gas–solids pipe flow. KONA Powder and Particle 16, 216-222.

Masuda, H., Matsusaka, S., Shimomura, H., 1998b. Measurement of mass flow rate of polymer powder based on static electrification of particles. Advanced Powder Technology, 9, 169-179.

Matsusaka, S., Masuda, H., 2003. Electrostatics of particles. Advanced Powder Technology 14, 143-166.

Matsusaka, S., Masuda, H., 2006. Simultaneous measurement of mass flow rate and charge-to-mass ratio of particles in gas–solids pipe flow. Chemical Engineering Science 61, 2254-2261.

Matsusaka, S., Ghadiri, M, Masuda, H., 2000. Electrification of an elastic sphere by repeated impacts on a metal plate. Journal of Physics D: Applied Physics 33, 2311-2319.

Matsusaka, S., Umemoto, H., Nishitani, M., Masuda, H., 2002. Electrostatic charge distribution of particles in gascsolids pipe flow. Journal of Electrostatics 55, 81-96.

Matsusaka, S., Nishida, T., Gotoh, Y., Masuda, H., 2003a. Electrification of fine particles by impact on a polymer film target. Advanced Powder Technology 14, 127-138.

Matsusaka, S., Oki, M., Masuda, H., 2003b. Bipolar charge distribution of a mixture of particles with different electrostatic characteristics in gas–solids pipe flow. Powder Technology 135/136, 150-155.

Matsusaka, S., Oki, M., Masuda, H., 2007. Control of electrostatic charge on particles by impact charging. Advanced Powder Technology 18, 229-244.

Matsusaka, S., Fukuda, H., Sakura, Y., Masuda, H., Ghadiri, M., 2008a. Analysis of pulsating electric signals generated in gas–solids pipe flow. Chemical Engineering Science 63, 1353-1360.

Matsusaka, S., Ando, K., Tanaka, Y., 2008b. Development of electrostatic charge controller for particles in gases using centrifugal contact. Journal of the Society of Powder Technology, Japan

45, 380-386.

Matsusaka, S., Yoshitani, K., Tago, H., Nii, T., Masuda, H., Iwamatsu, T., 2008c. Sampling of charged fine particles by motion control under ac field. Journal of the Society of Powder Technology, Japan 45, 387-394.

Matsuyama, T., Yamamoto, H., 1989. Charge transfer between a single polymer particle and a metal plate due to impact. KONA Powder and Particle 7, 15-21.

Matsuyama, T., Yamamoto, H., 1994. Charge transfer between a polymer particle and a metal plate due to impact. IEEE Transactions on Industry Applications 30, 602-607.

Matsuyama, T., Yamamoto, H., 1995a. Charge relaxation process dominates contact charging of a particle in atmospheric conditions. Journal of Physics D: Applied Physics 28, 2418-2423.

Matsuyama, T., Yamamoto, H., 1995b. Characterizing the electrostatic charging of polymer particles by impact charging experiments. Advanced Powder Technology 6, 211-220.

Matsuyama, T., Yamamoto, H., 1995c. Electrification of single polymer particles by successive impacts with metal targets. IEEE Transactions on Industry Applications 31, 1441-1445.

Matsuyama, T., Yamamoto, H., 1997. Charge-relaxation process dominates contact charging of a particle in atmospheric condition: II. The general model. Journal of Physics D: Applied Physics 30, 2170-2175.

Matsusyama, T., Yamamoto, H., 2006 a. Impact charging of particulate materials. Chemical Engineering Science 61, 2230-2238.

Matsuyama, T., Yamamoto, H., 2006 b. Montecarlo simulation of charge accumulating process of a single particle due to successive impacts. Journal of the Society of Powder Technology, Japan 43, 169-173.

Matsuyama, T. Yamamoto, H., 2008. Maximum electrostatic charge of powder in pipe flow. Journal of the Society of Powder Technology, Japan 45, 373-379.

Matsuyama, T., Ogu, M., Yamamoto, H., Marijnissen, J. C. M., Scarlett, B., 2003. Impact charging experiments with single particles of hundred micrometre size. Powder Technology 135/136, 14-22.

Matsuyama, T., Ohtsuka, M., Yamamoto, H., 2006. Measurement of force curve due to electrostatic charge on a single particle using atomic force microscope. Journal of the Society of Powder Technology, Japan 43, 174-180.

Matsuyama, T., Šupuk, E., Ahmadian, H., Hassanpour, A., Ghadiri, M., 2009. Analysis of tribo-electric charging of spherical beads using distinct element method. Powders and Grains 2009. AIP, New York, pp. 127-130.

Mazumder, M. K., Ware, R. E., Yokoyama, T., Rubin, B. J., Kamp, D., 1991. Measurement of particle size and electrostatic charge distributions on toners using E-SPART analyzer. IEEE Transactions on Industry Applications 27, 611-619.

Mazumder, M. K., 1999. Electrostatic processes. In: Webster, J. (Ed.), Wiley Encyclopedia of Electrical and Electronics Engineering. John Wiley & Sons, Inc. vol. 7, pp.15- 39.

Michel, E., Baur, R., Macholdt, H.-T., 2001. Charge stabilizers: properties and applications. Journal of Electrostatics 51/52, 91-96.

Mio, H., Matsuoka, Y., Shimosaka, A., Shirakawa, Y., Hidaka, J., 2006. Analysis of developing behavior in two-component development system by large-scale discrete element method. Journal of Chemical Engineering of Japan 39, 1137-1144.

Mizes, H. A., Conwell, E. M., Salamida, D. P., 1990. Direct observation of ion transfer in contact charging between a metal and a polymer. Applied Physics Letters 56, 1597-1599.

Murata, Y., 1979. Photoelectric emission and contact charging of some synthetic high polymers. Japanese Journal of Applied Physics 18, 1-8.

Murata, Y., Kittaka, S., 1979. Evidence of electron transfer as the mechanism of static charge generation by contact of polymers with metals. Japanese Journal of Applied Physics 18, 421.

Nieh, S., Nguyen, T., 1988. Effects of humidity, conveying velocity, and particle size on electrostatic charges of glass beads in a gaseous suspension flow. Journal of Electrostatics, 21, 99-114.

Nifuku, M., Katoh, H., 2003. A study on the static electrification of powders during pneumatic transportation and the ignition of dust cloud. Powder Technology 135/136 234-242.

Nifuku, M., Ishikawa, T., Sasaki, T., 1989. Static electrification phenomena in pneumatic transportation of coal. Journal of Electrostatics 23, 45-54.

Nishitani, Y., Muramatsu, H., Maruyama, H., Tanoue, K., Matsusaka, S., Masuda, H., 2000. Measurement of interaction forces between particle and surface in air using AFM. In: Proceedings of Annual Meeting of Journal of the Society of Powder Technology, Japan, May, pp. 67-69.

Nomura, T., Satoh, T., Masuda, H., 2003. The environment humidity effect on the tribo-charge of powder. Powder Technology 135/136, 43-49.

Oguchi, T., Tamatani, M., 1986. Contact electrification in inorganic binary compounds. Journal of the Electrochemical Society 133, 841-847.

Oguchi, T., Tamatani, M., 1993. Contact electrification phenomena and powder surface treatments. Wear 168, 91-98.

Ohsawa, A., 2003. Computer simulation for assessment of electrostatic hazards in filling operations with powder. Powder Technology 135/136, 216-222.

O'Neill, B.C., Willis, C.A., 1987. An electrostatic method for the measurement of powder flow rates in pipes, Electrostatics '87, IOP Publishing, Oxford, pp. 303-306.

Paschen, F., 1889. Ueber die zum Funkenübergang in Luft, Wasserstoff und Kohlensäure bei verschiedenen Drucken erforderliche Potentialdifferenz. Annalen der Physik 273, 69-96.

Rowley, G., 2001. Quantifying electrostatic interactions in pharmaceutical solid systems. International Journal of Pharmaceutics 227, 47-55.

Saeki, M., 2006. Vibratory separation of plastic mixtures using triboelectric charging. Particulate Science and Technology 24, 153-164.

Saurenbach, F., Wollmann, D., Terris, B.D., Diaz, A. F., 1992. Force microscopy of ion-containing polymer surfaces: morphology and charge structure. Langmuir 8, 1199-1203.

Schein, L. B., 1992/1996. Electrophotography and Development Physics, 2nd ed. Springer-Verlag, Berlin/ Laplacian Press.

Schein, L. B., 1999. Recent advances in our understanding of toner charging. Journal of Electrostatics 46, 29-36.

Schnurmann, R., 1941. Contact electrification of solid particles. Proceedings of the Physical Society 53 547-553.

Shinohara, I., Yamamoto, F., Anzai, H., Endo, S., 1976. Chemical structure and electrostatic properties of polymers. Journal of Electrostatics, 2, 99-110.

Shirakawa, Y., Ii, N., Yoshida, M., Takashima, R., Shimosaka, A. Hidaka, J., 2008. Quantum chemical calculation of electron transfer at metal/polymer interfaces. Journal of the Society of Powder Technology, Japan 45, 366-372.

Soong, Y., Irdi, G.A., McLendon, T.R., Hedges, S.W., Dilmore, R.M., Griffith, C., Romanov, V., Haljasmaa, I., 2007. Triboelectrostatic separation of fly ash with different charging materials. Chemical Engineering & Technology 30, 214-219.

Tanoue, K., Ema, A., Masuda, H., 1999. Effect of material transfer and work hardening of metal surface on the current generated by impact of particles. Journal of Chemical Engineering of Japan 32, 544-548.

Tanoue, K., Morita, K., Maruyama, H., Masuda, H., 2001a. Influence of functional group on the electrification of organic pigments. AIChE Journal, 47, 2419-2424.

Tanoue, K., Tanaka, H., Kitano, H., Masuda, H., 2001b. Numerical simulation of tribo-electrification of particles in a gas–solids two-phase flow. Powder Technology 118, 121-129.

Uyama, Y., Ikada, Y., 1990. Electrostatic properties of UV-irradiated and surface-grafted polymers. Journal of Applied Polymer Science 41, 619-629.

Watanabe, H., Samimi, A., Ding, Y. L., Ghadiri, M., Matsuyama, T., Pitt, K. G., 2006. Measurement of charge transfer due to single particle impact. Particle & Particle Systems Characterization 23, 133-137.

Watanabe, H., Ghadiri, M., Matsuyama, T., Ding, Y.L., Pitt, K.G., Maruyama, H., Matsusaka, S., Masuda, H., 2007a. Triboelectrification of pharmaceutical powders by particle impact. International Journal of Pharmaceutics 334 149-155.

Watanabe, H., Ghadiri, M., Matsuyama, T., Ding, Y. L., Pitt, K. G., 2007b. New instrument for

tribocharge measurement due to single particle impacts. Review of Scientific Instruments 78, 024706.

Watano, S., 2006. Mechanism and control of electrification in pneumatic conveying of powders. Chemical Engineering Science 61, 2271-2278.

Yamamoto, H., Scarlett, B., 1986. Triboelectric charging of polymer particles by impact. Particle Characterization 3, 117-121.

Yan, Y., Byrne, B., Woodhead, S. Coulthard, J., 1995. Velocity measurement of pneumatically conveyed solids using electrodynamic sensors. Measurement Science and Technology 6, 515-537.

Yanagida, K., Okada, O., Oka, K., 1993. Low-energy electronic states related to contact electrification of pendant-group polymers: photoemission and contact potential difference measurement. Japanese Journal of Applied Physics 32, 5603-5610.

Yanar, D. K., Kwetkus, B. A., 1995. Electrostatic separation of polymer powders. Journal of Electrostatics, 35, 257-266.

Yao, J., Zhang, Y., Wang, C.-H., Matsusaka, S., Masuda, H., 2004. Electrostatics of the granular flow in a pneumatic conveying system. Industrial & Engineering Chemistry Research 43, 7181-7199.

Yoshida, H., Fukuzono, T., Masuda, H., 1991. Measurement of contact potential difference between a powder bed and a metal. Journal of the Society of Powder Technology, Japan 28, 226-231.

Yoshida, H., Fukuzono, T., Ami, H., Iguchi, Y., Masuda, H., 1992. The effect of the surface modification of particles on the contact potential difference between a powder bed and metal. Journal of the Society of Powder Technology, Japan 29, 504-510.

Yoshida, M., Shimosaka, A., Shirakawa, Y., Hidaka, J., Matsuyama, T., Yamamoto, H., 2003. Estimation of electrostatic charge distribution of flowing toner particles in contact with metals. Powder Technology 135/136, 23- 34.

Yoshida, M., Ii, N. Shimosaka, A., Shirakawa, Y., Hidaka, J., 2006. Experimental and theoretical approaches to charging behavior of polymer particles. Chemical Engineering Science 61, 2239-2248.

Zhao, H., Castle, G.S.P., Inculet, I.I., 2002. The measurement of bipolar charge in polydisperse powders using a vertical array of Faraday pail sensors. Journal of Electrostatics 55, 261-278.

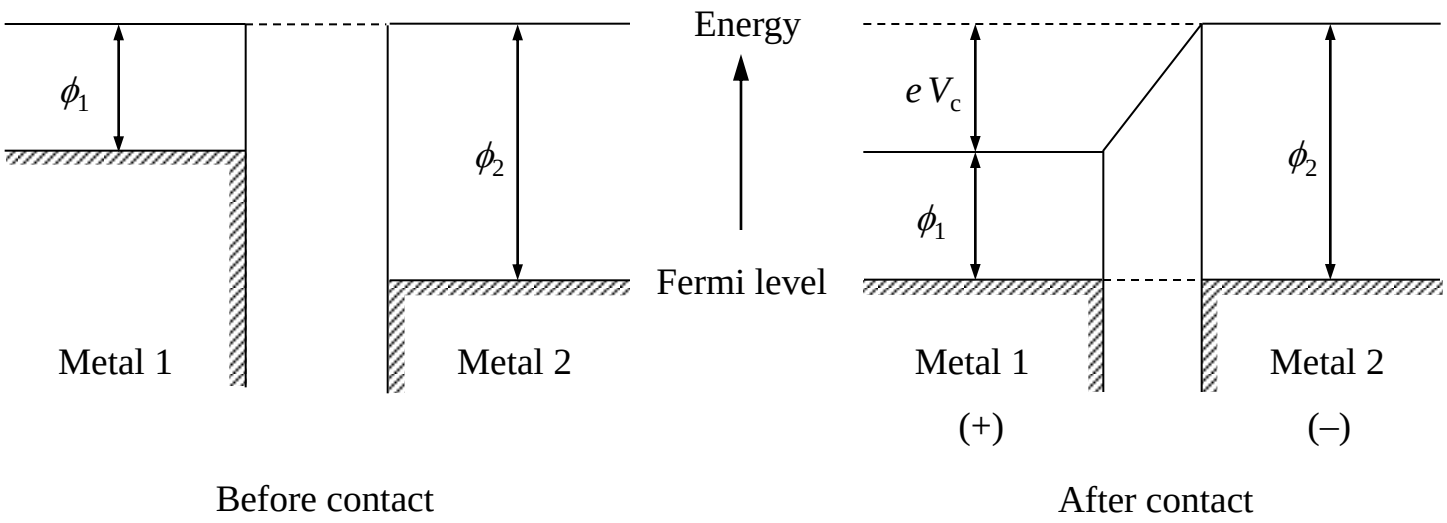

Fig. 1. Electron potential energy for metal–metal contact.

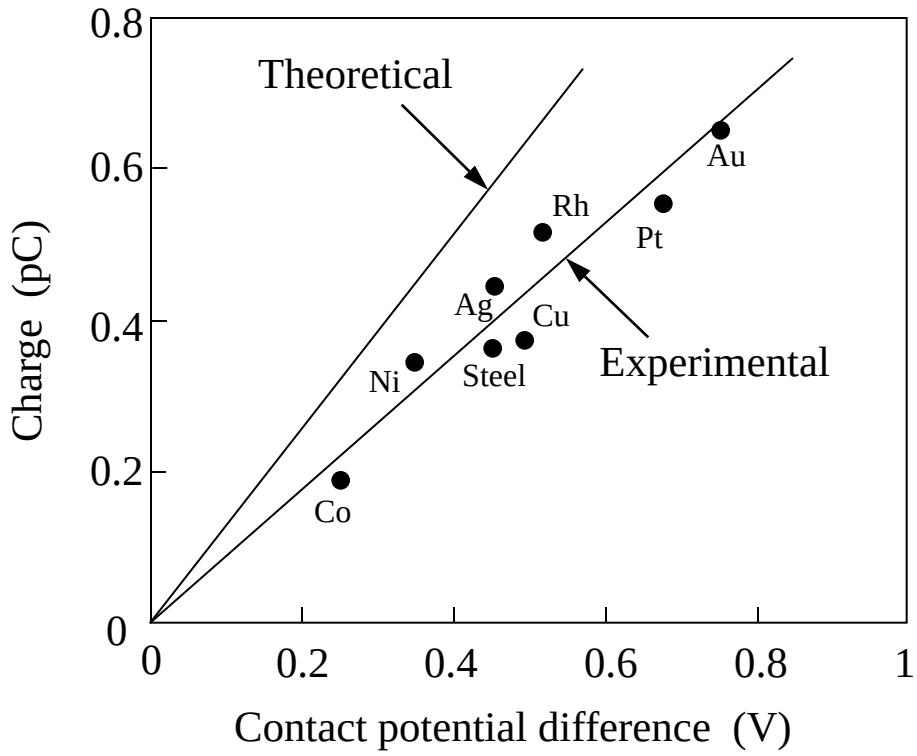

Fig. 2. Charge on a chromium sphere, 4 mm in diameter, in contact with another metal sphere, 13 mm in diameter, as a function of the CPD of chromium against each metal (Harper, 1951).

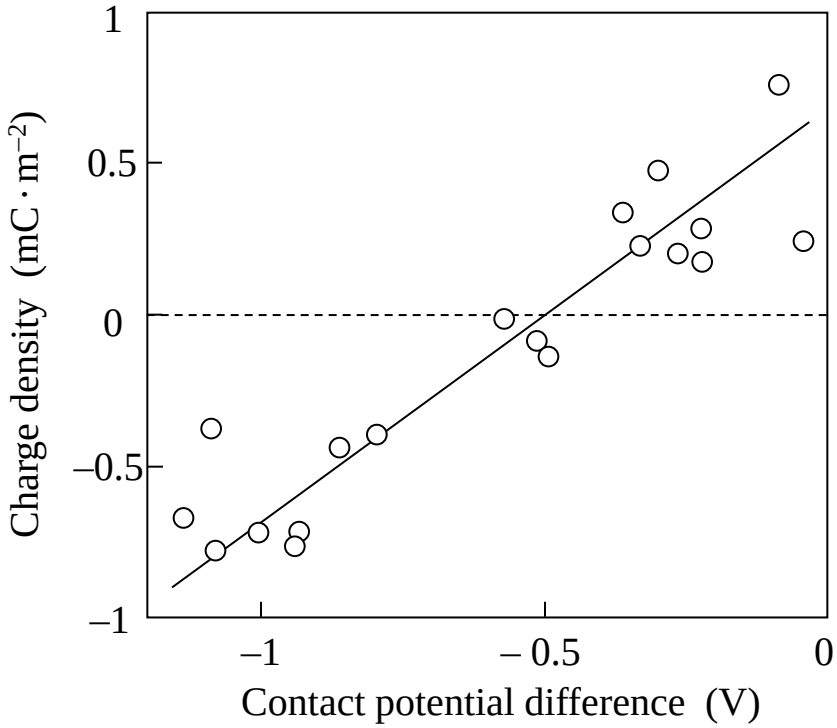

Fig. 3. Charge density of Nylon 66 by contact with various metals. The horizontal axis is the CPD of gold against each metal $V_{Au/M}$ (Davies, 1969).

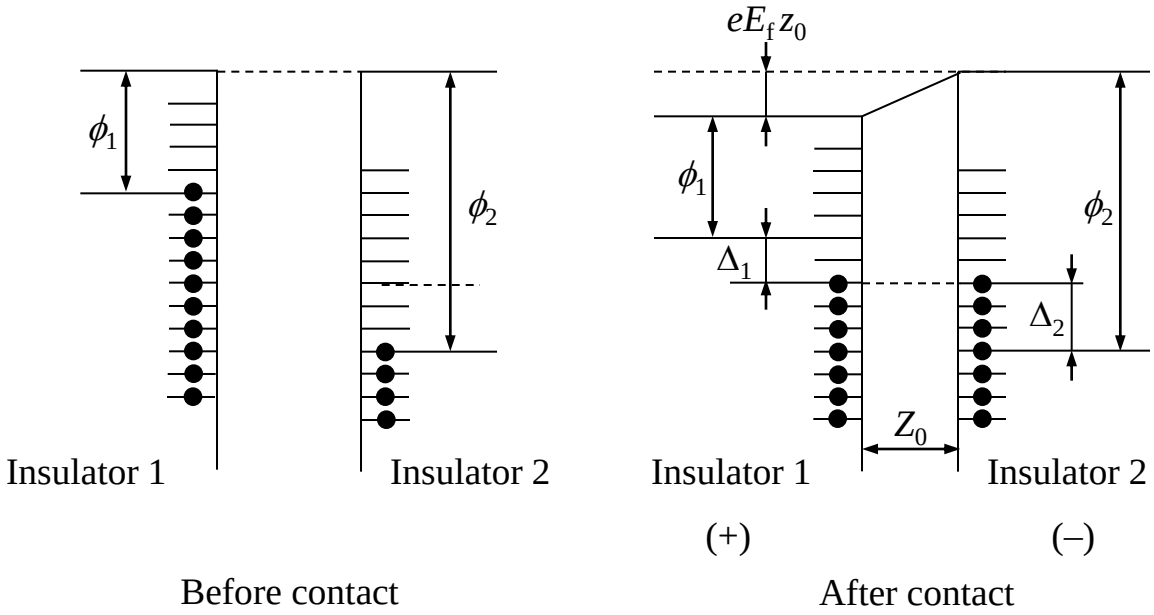

Fig. 4. Energy level diagram for insulator–insulator contact.

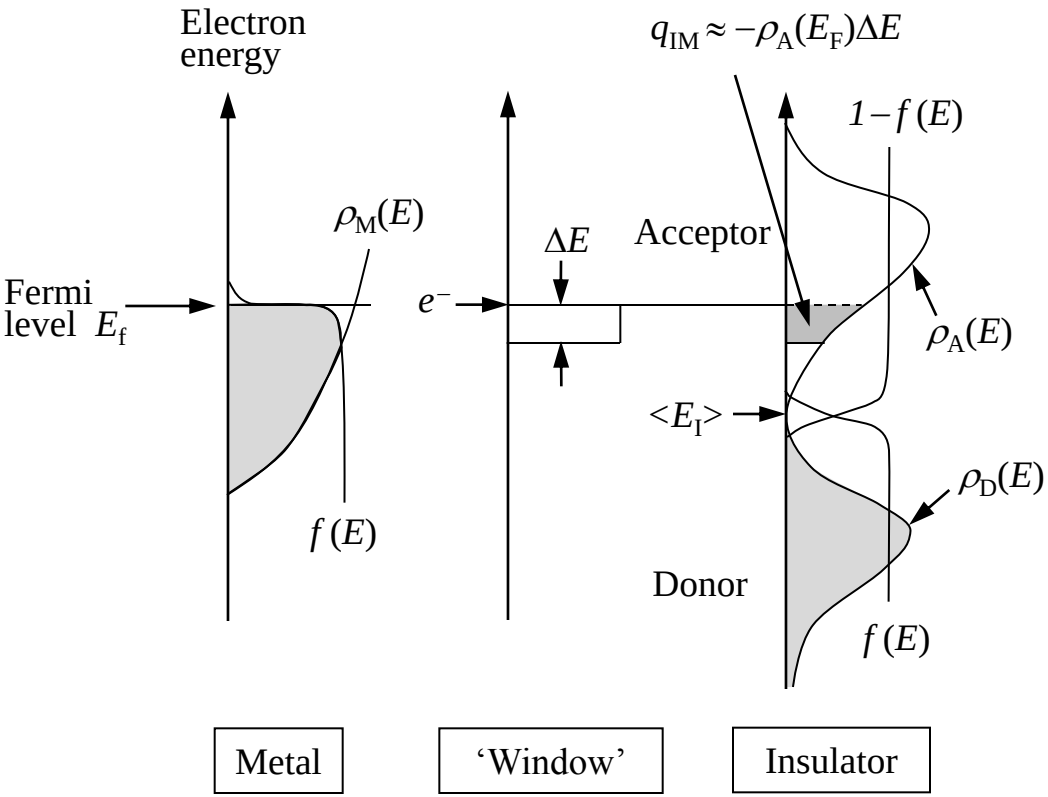

Fig. 5. Molecular-ion-state model for a metal–insulator contact (electron injection into acceptor states of polymer).

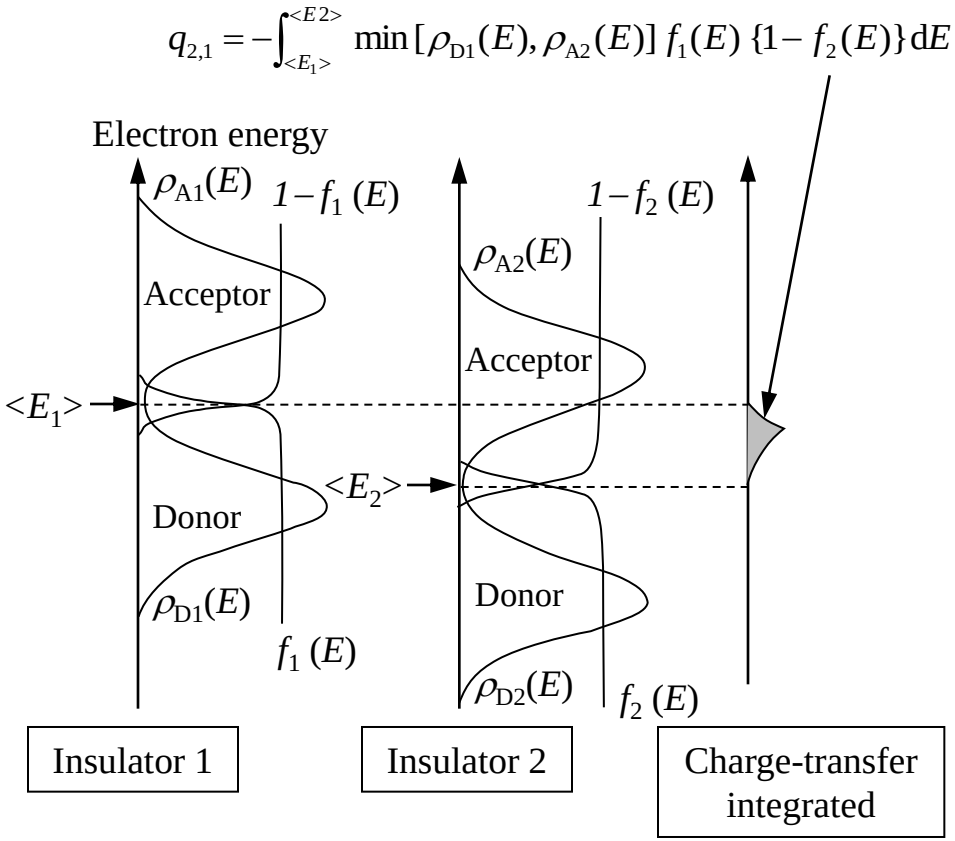

Fig. 6. Molecular-ion-state model for an insulator–insulator contact.

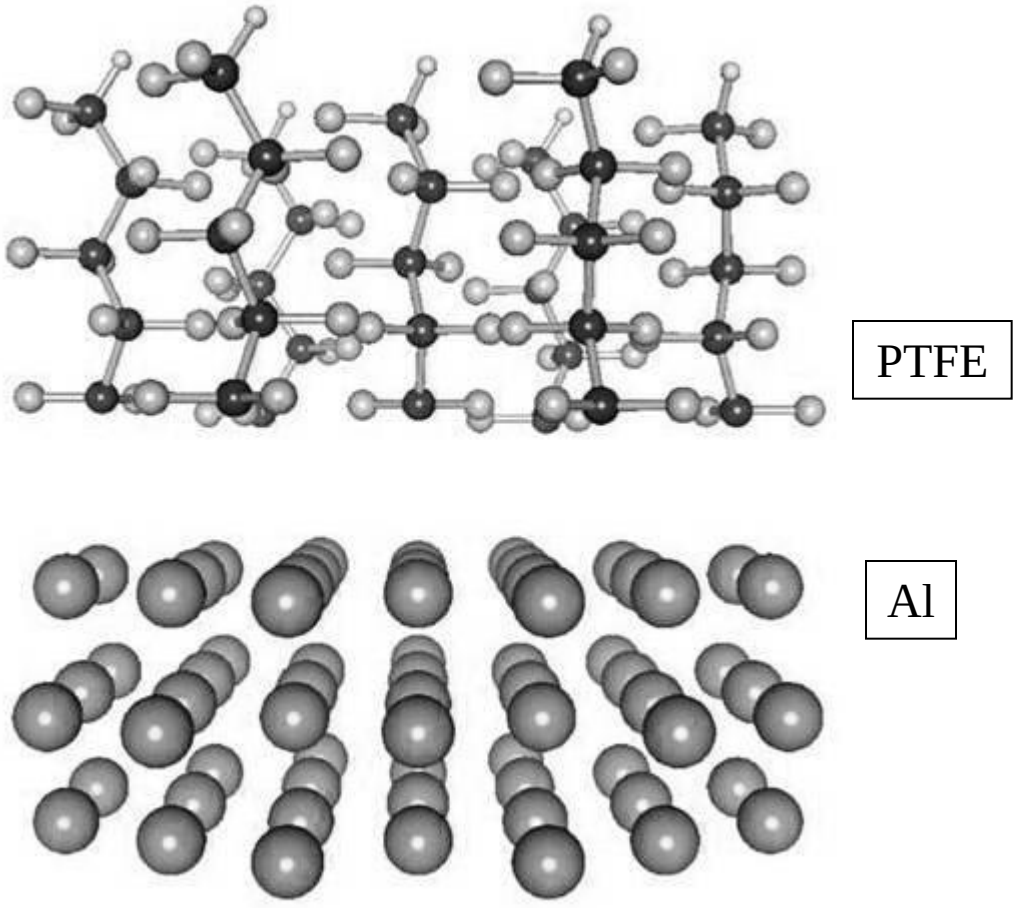

Fig. 7. Model of interface between polytetrafluoroethylene (PTFE) and aluminum (Al) for quantum chemical calculation (Yoshida et al, 2006).

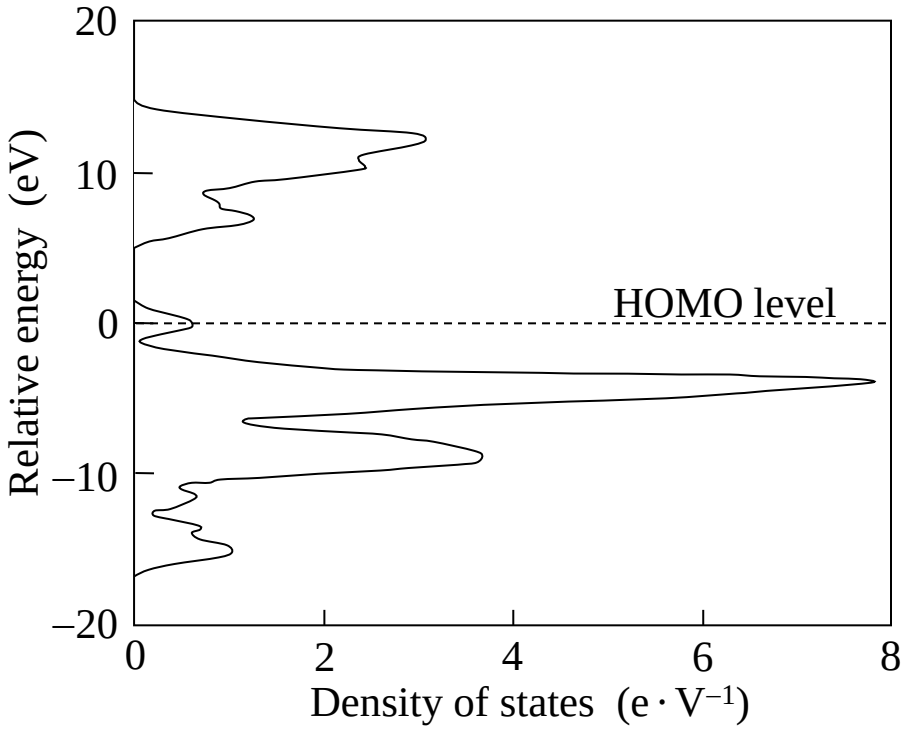

Fig. 8. Electron density of surface states of PTFE contacting with aluminum (Shirakawa et al., 2008).

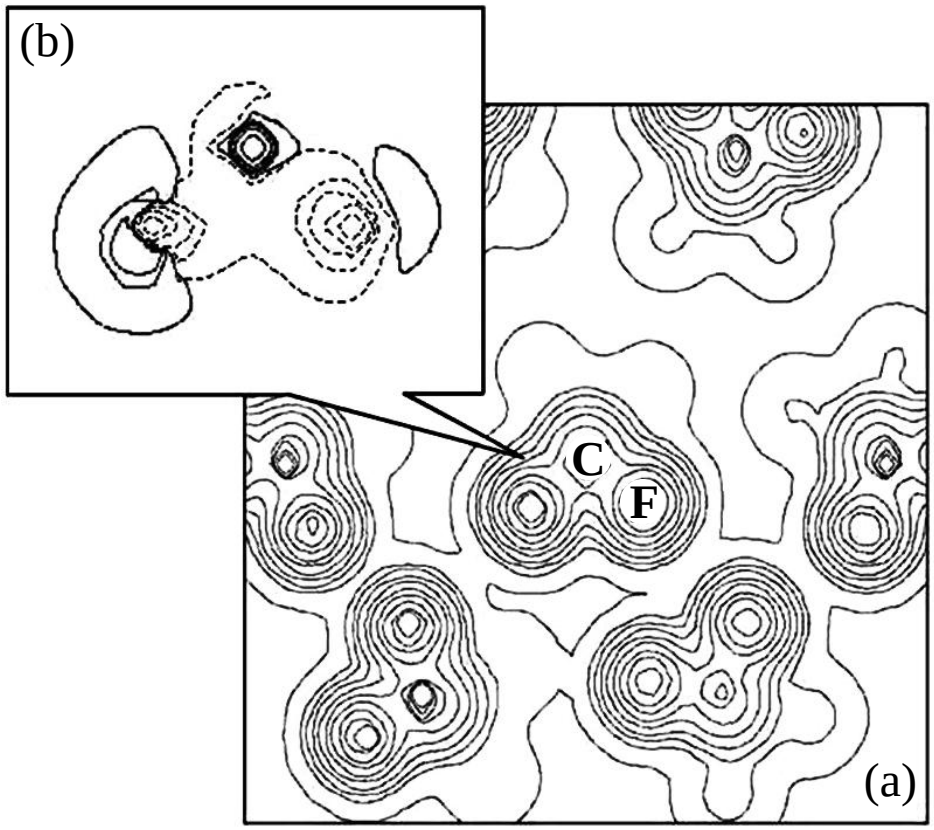

Fig. 9. (a) Electron distribution and (b) variation of the distribution (the solid and broken lines mean, respectively, increase and decrease of electrons by contact charging) (Yoshida et al., 2006).

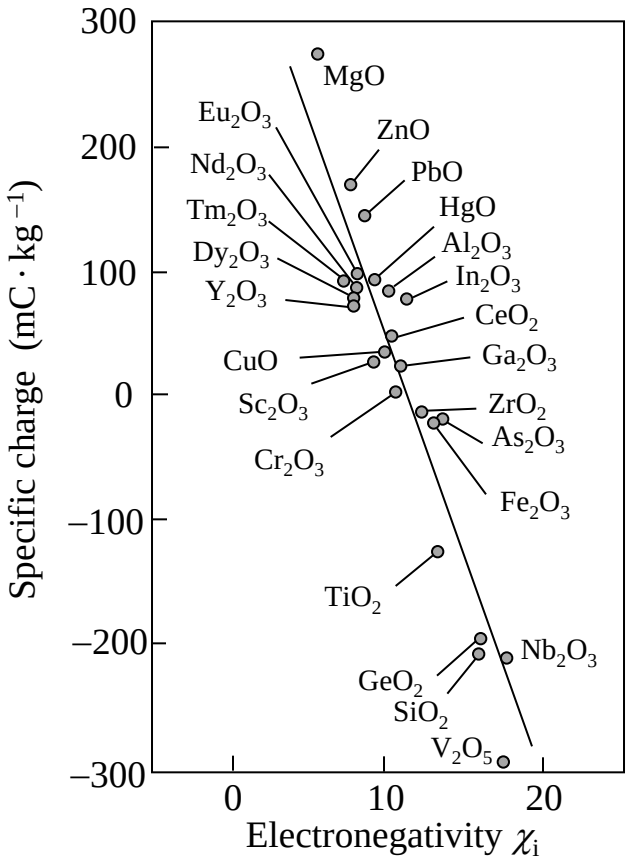

Fig. 10 Relationship between specific charge obtained by blow-off method and generalized electronegativity χi for metal ions (oxidized fine particles: 0.3–0.5 μm in diameter; reference particles for contact charging: surface oxidized iron, 44–74 μm in sieve diameter) (Oguchi and Tamatani, 1986).

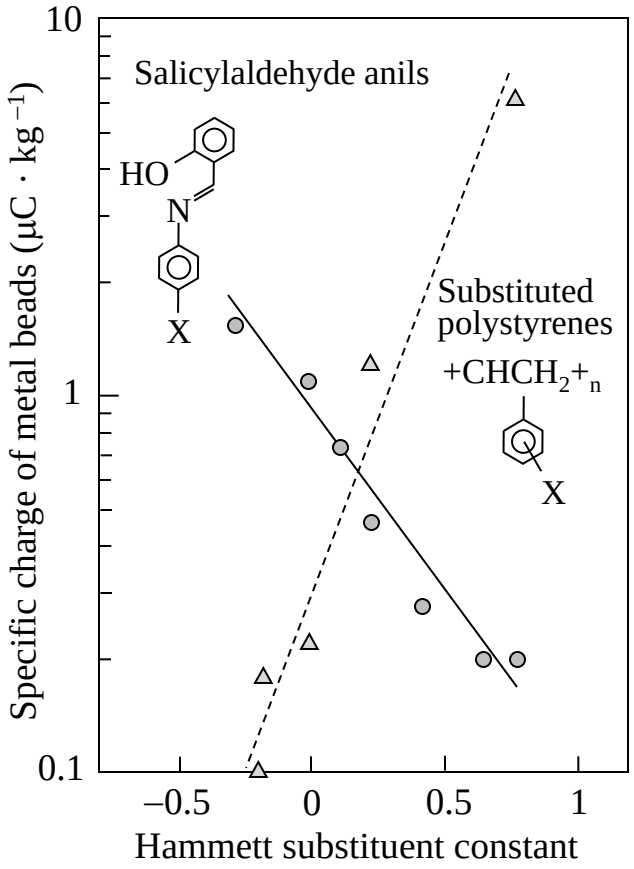

Fig. 11. Triboelectric charging as a function of substituent constant for salicylaldehyde anils (1) using 250 μm steel beads at 0% relative humidity, organic films were positively charged, and for substituted polystyrenes (2) using zinc powder at 56% relative humidity, organic films were negatively charged. X is a substituent (Gibson, 1975).

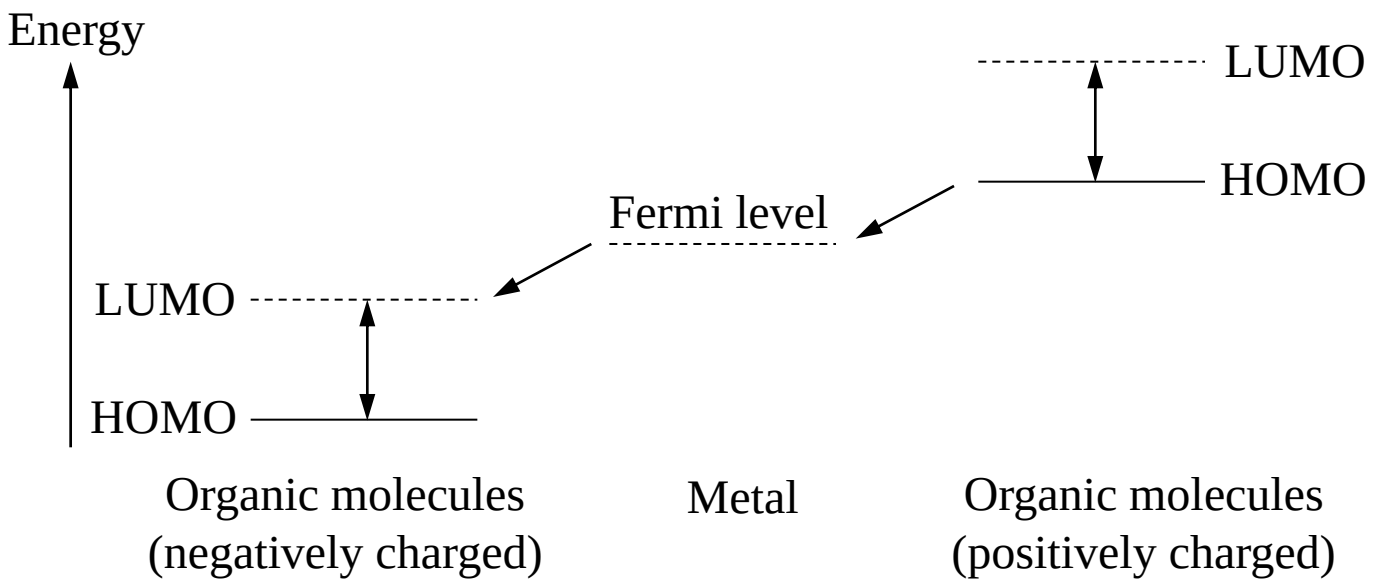

Fig. 12. Direction of electron transfer for metal–organic contact.

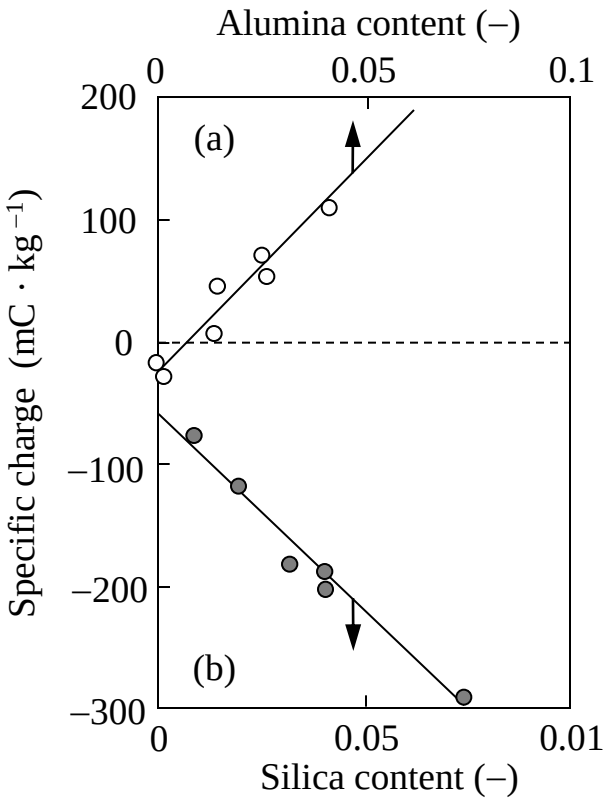

Fig. 13 (a) Charge as a function of alumina content for alumina-coated titania and (b) contribution of silica for alumina–silica-coated titania (Oguchi and Tamatani, 1993).

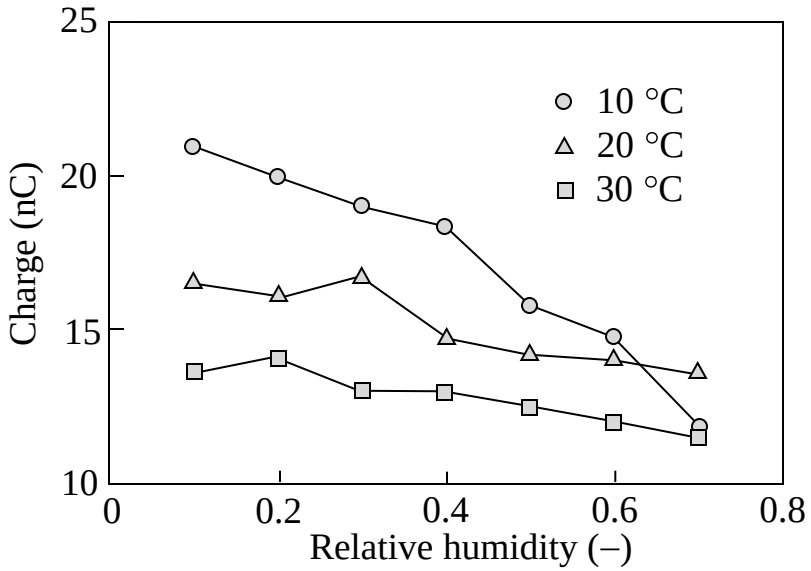

Fig. 14. Triboelectric charge of a metal sphere,12.7 mm in diameter, as a function of relative humidity (Greason, 2000)

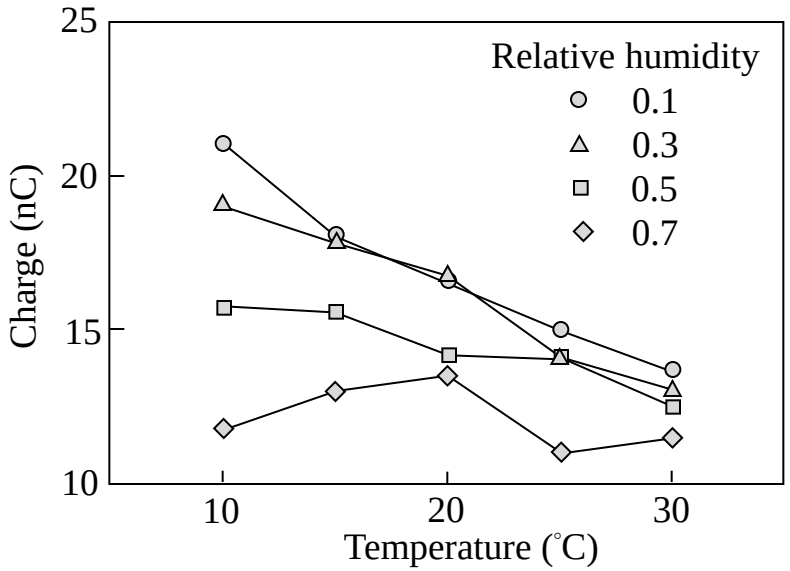

Fig. 15. Triboelectric charge of a metal sphere, 12.7 mm in diameter, as a function of temperature (Greason, 2000).

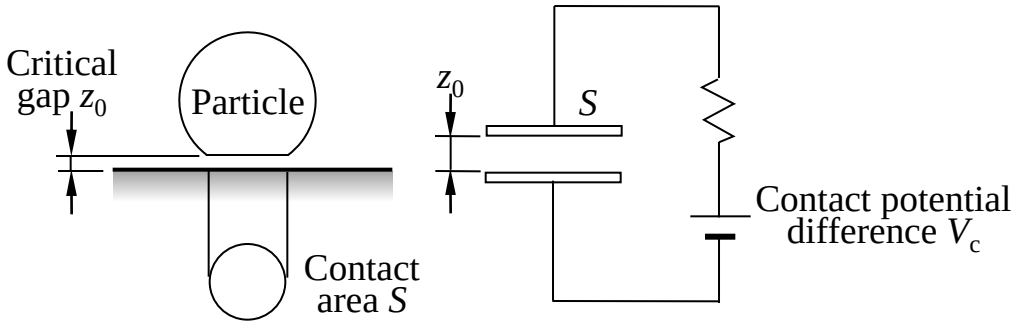

Fig. 16. Condenser model.

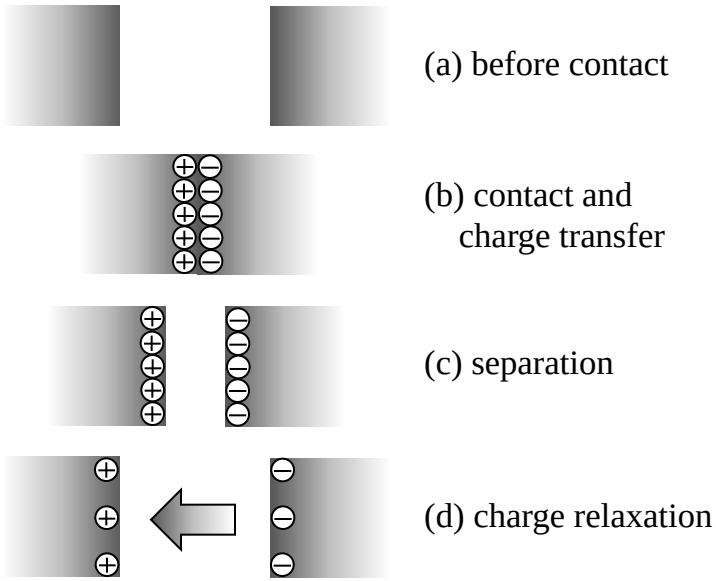

Fig. 17. Schematic illustration of contact process with charge relaxation.

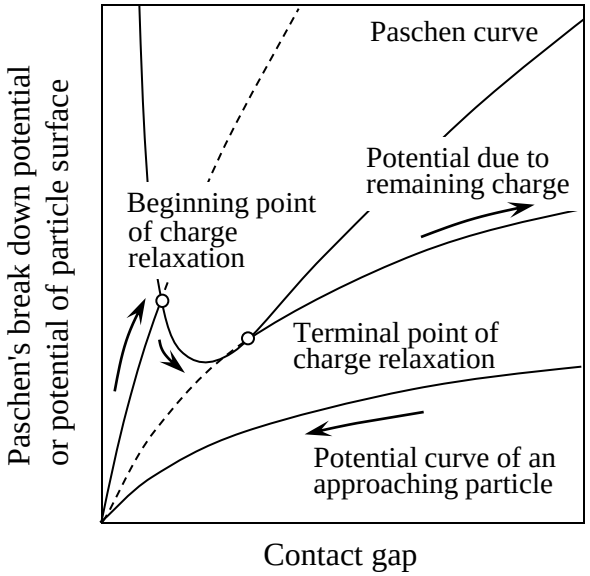

Fig. 18. Schematic illustration of the charge relaxation model.

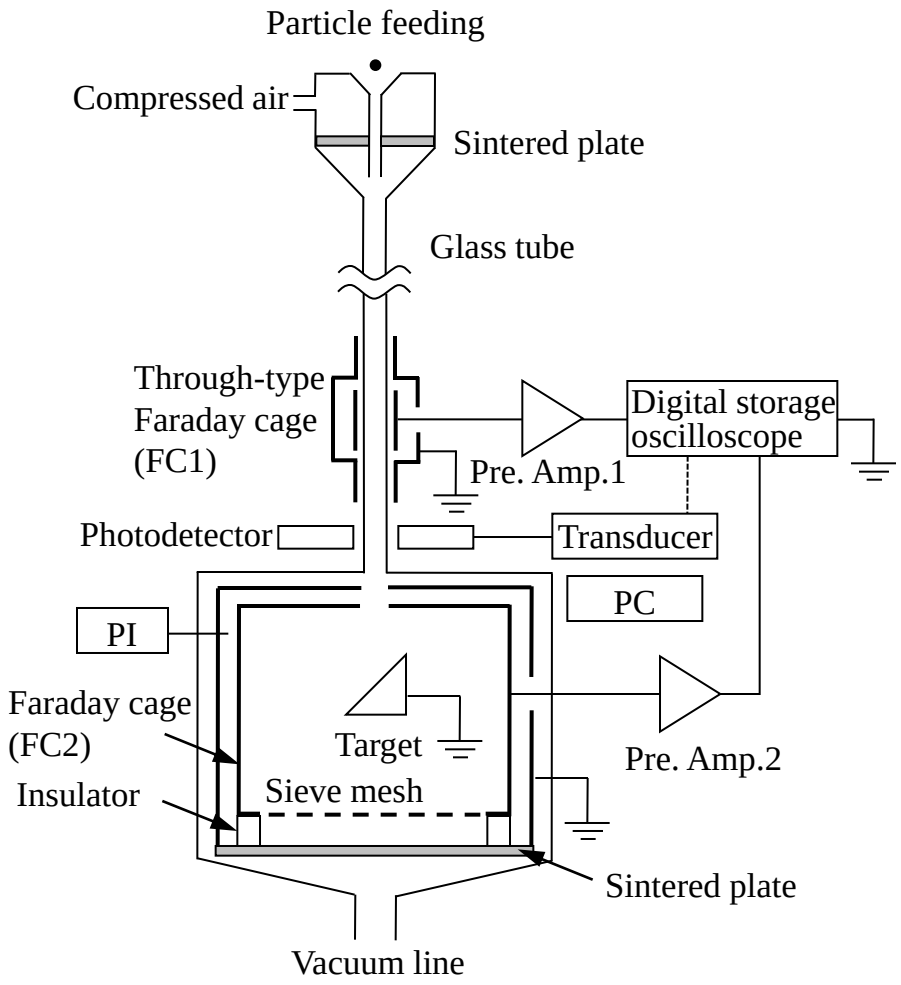

Fig. 19. Impact charging test rig for single particles.

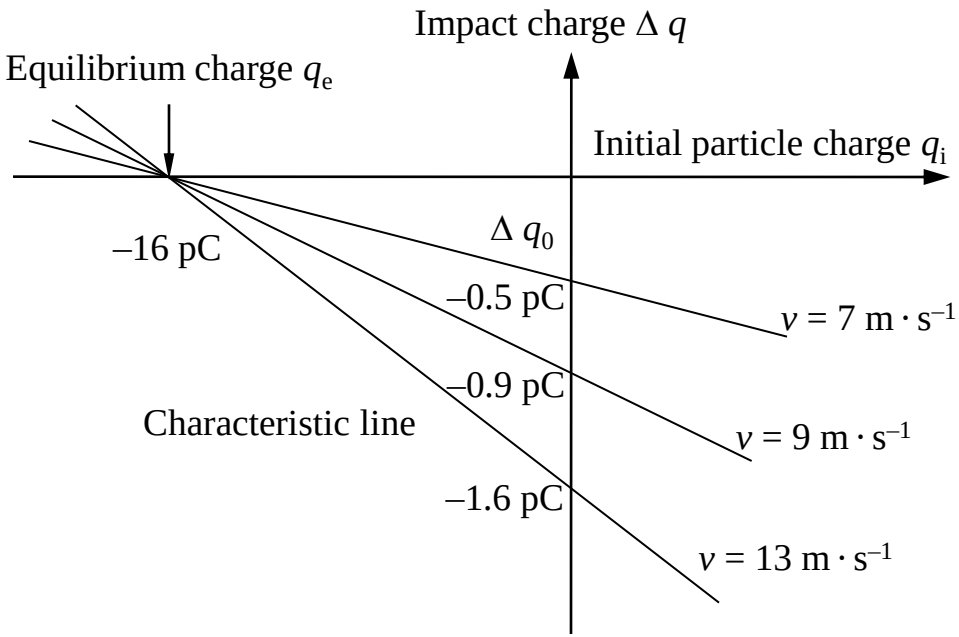

Fig. 20. Linear relationships between impact charge and initial charge (spherical sugar granules, 500–600 μm in sieve diameter) (Watanabe et al., 2006).

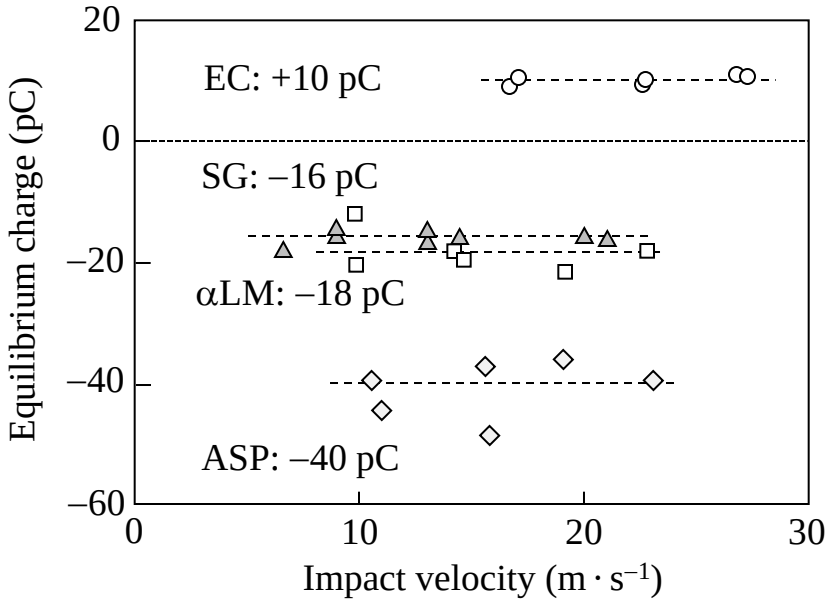

Fig. 21. Equilibrium charge as a function of impact velocity (EC: ethylcellulose granules, SG: sugar granules, αLM: α-lactose monohydrate, ASP: aspirin) (Watanabe et al., 2006).

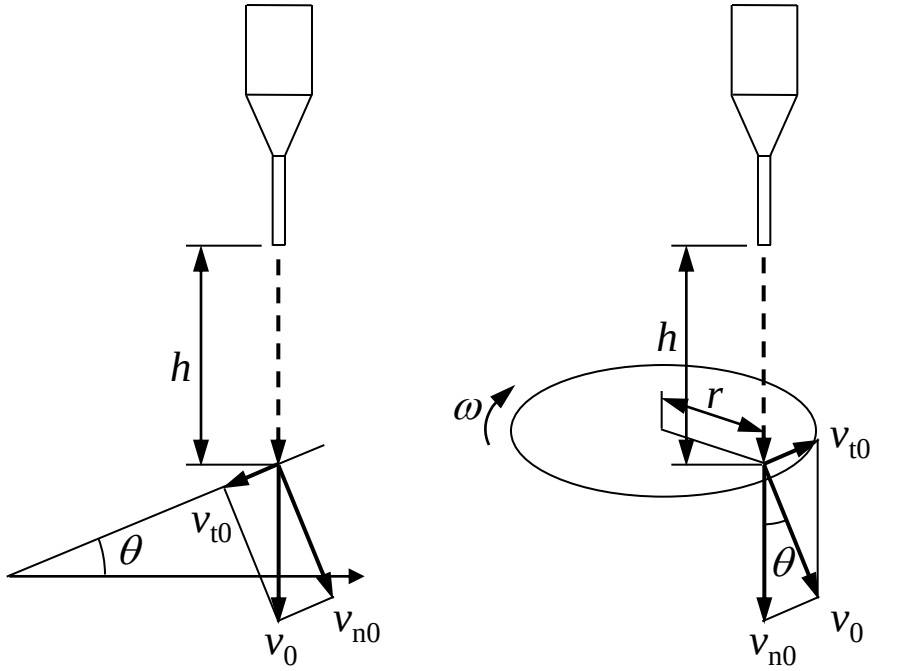

(a) Inclined target system (b) Rotating target system

Fig. 22. Particle impact tests.

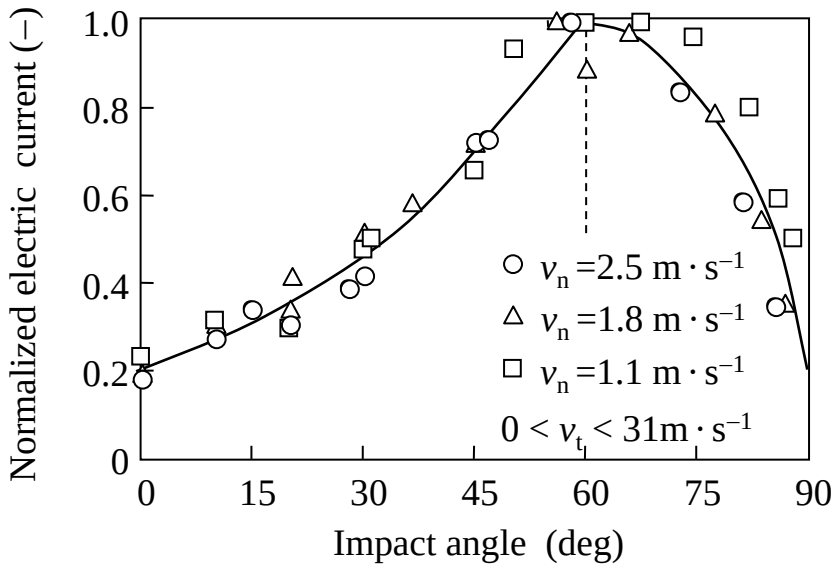

Fig. 23. Relationship between normalized electric current I/I_{max} and impact angle θ (v_n and v_t : normal and tangential component of impact velocity) (Ema et al., 2003).

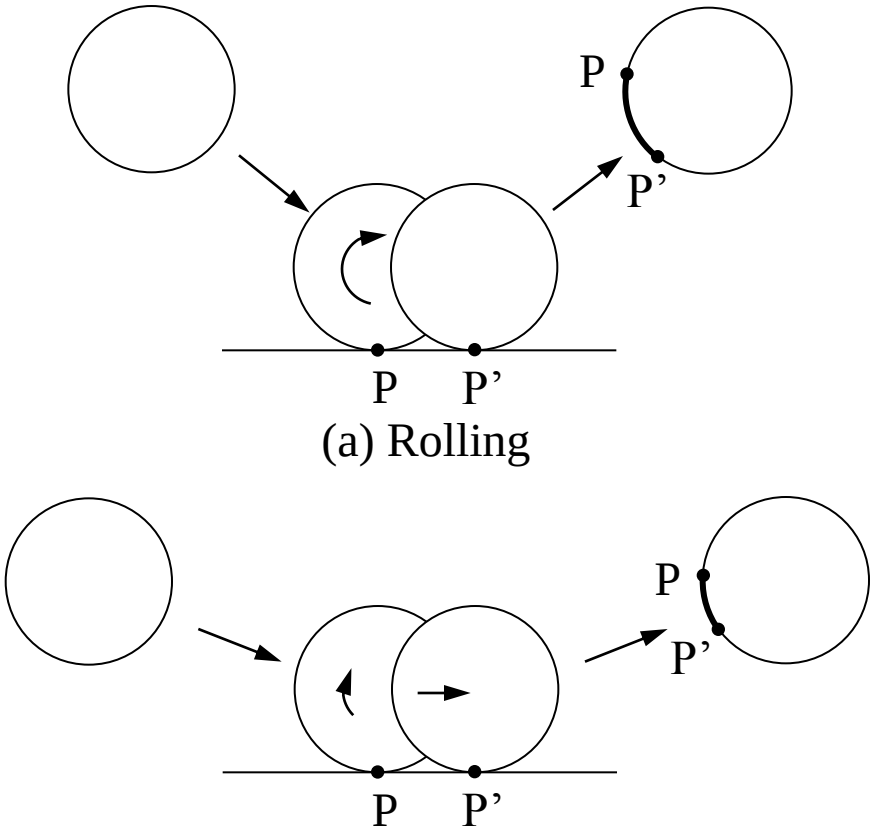

Fig. 24. Effective contact area.

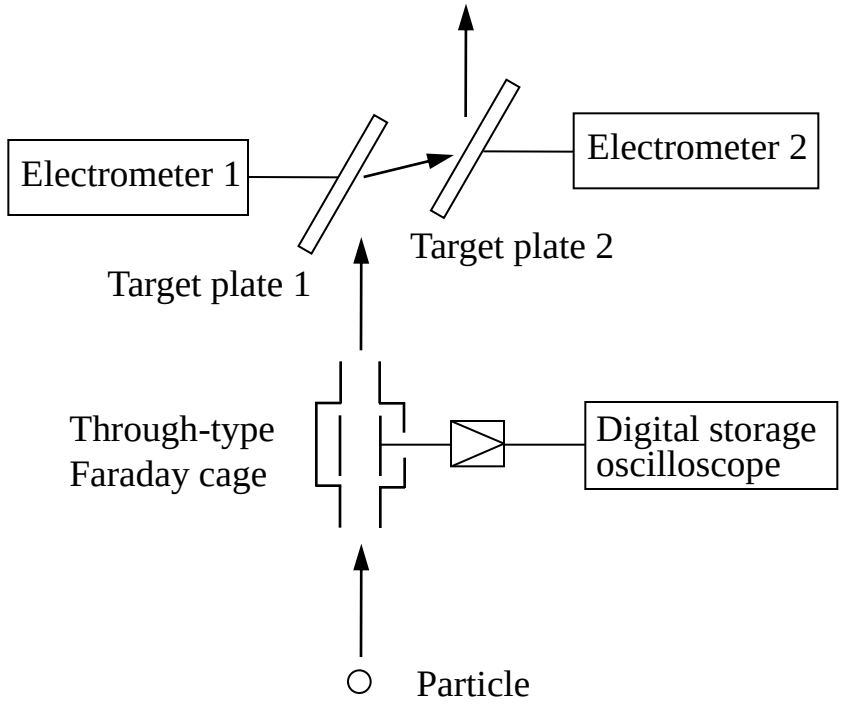

Fig. 25. Electrostatic charging test for successive particle impacts.

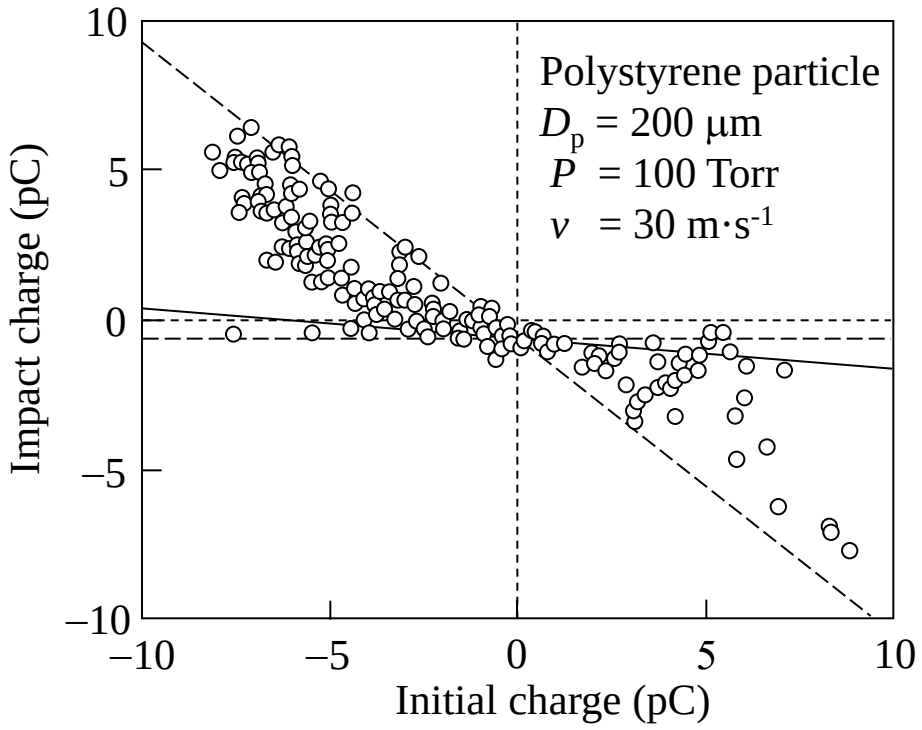

Fig. 26. Impact charging with 200 μm polymer particles (Matsuyama et al., 2003).

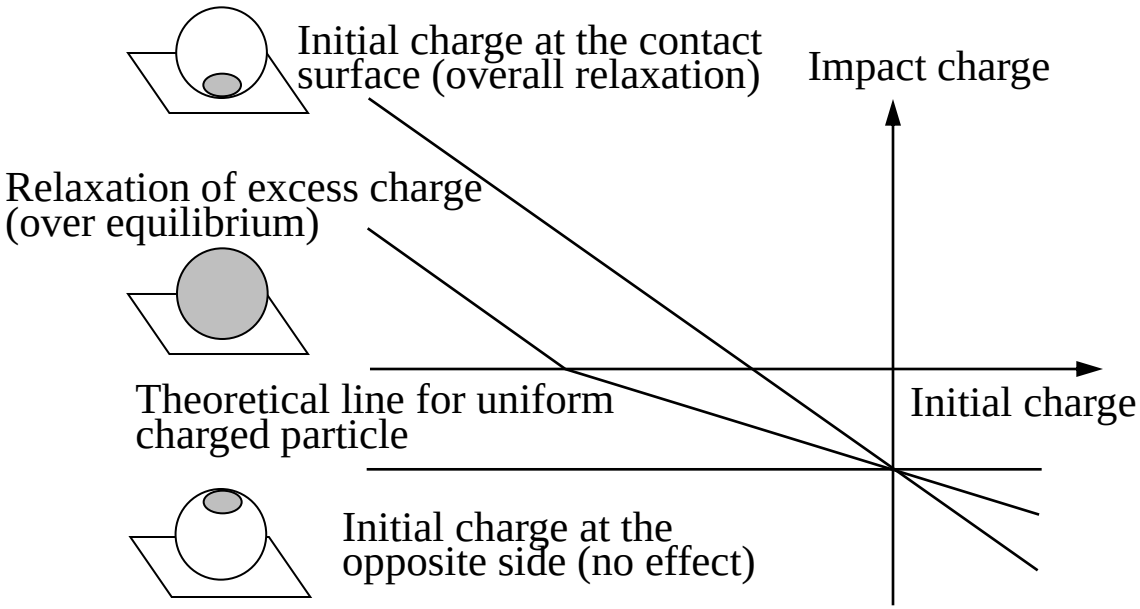

Fig. 27. Concept of localization of initial charge on a particle.

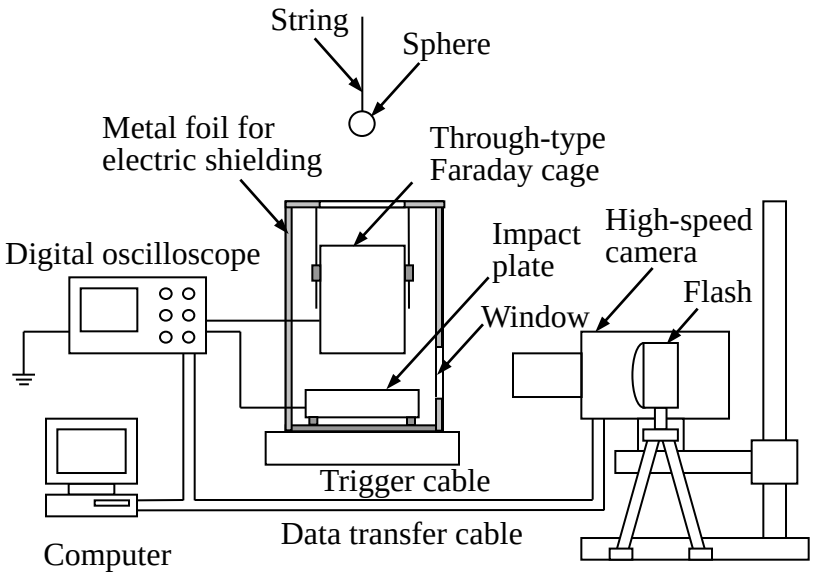

Fig. 28. Test to investigate the charge accumulation process by repeated impacts of an elastic sphere.

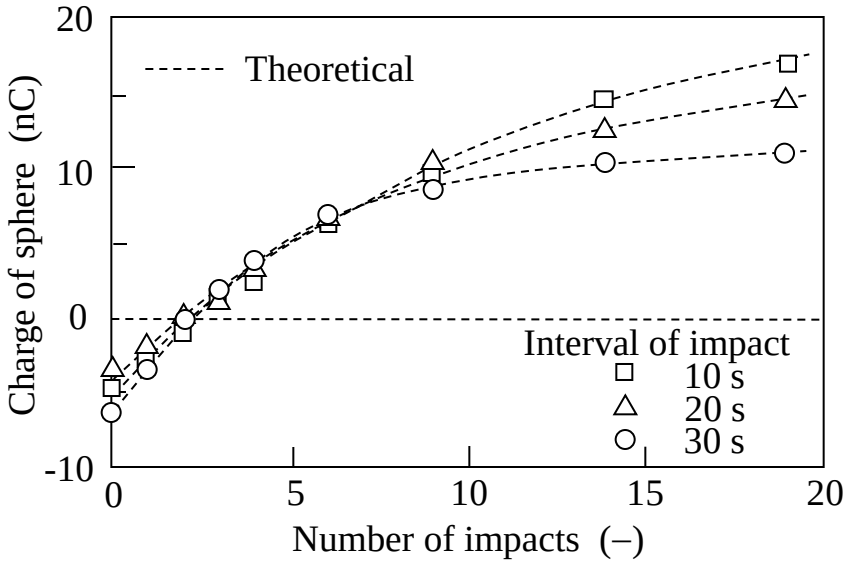

Fig. 29. Charge of synthetic rubber sphere by repeated impacts (Matsusaka et al., 2000).

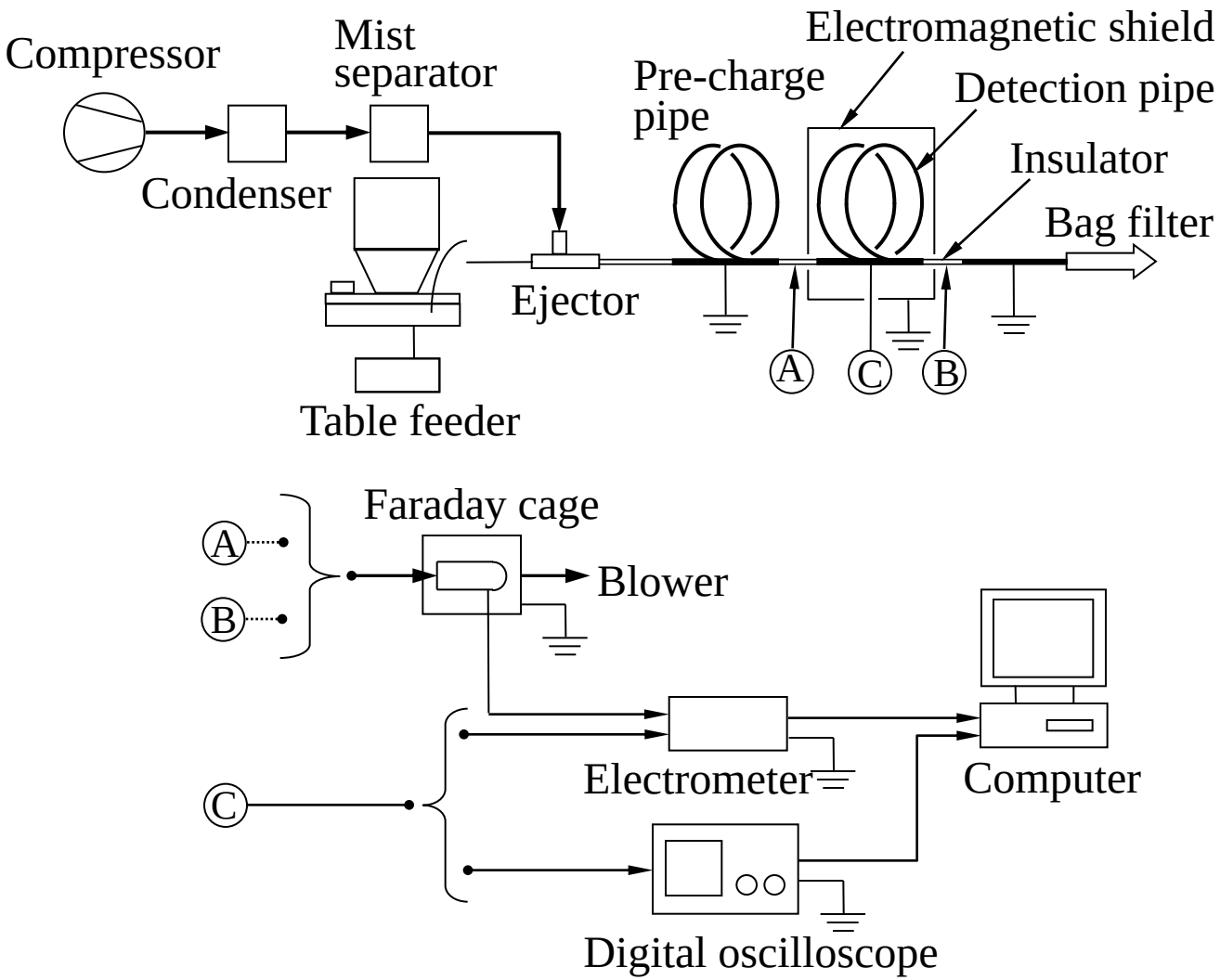

Fig. 30. System to analyze particle charging in gas–solids pipe flow.

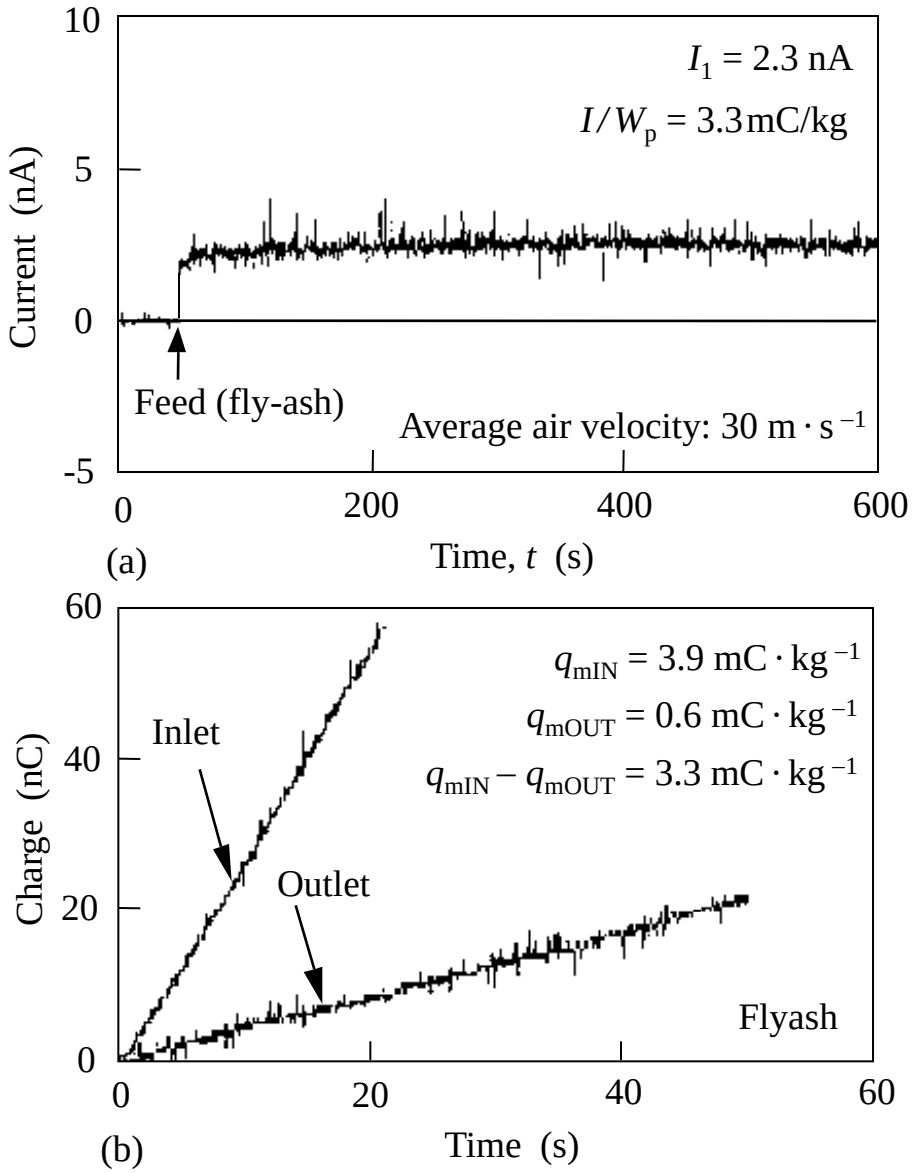

Fig. 31. (a) Electric currents generated from a stainless steel detector and (b) charges on particles at the inlet and outlet of the detector, which were measured with a Faraday cage (Matsusaka and Masuda, 2006).

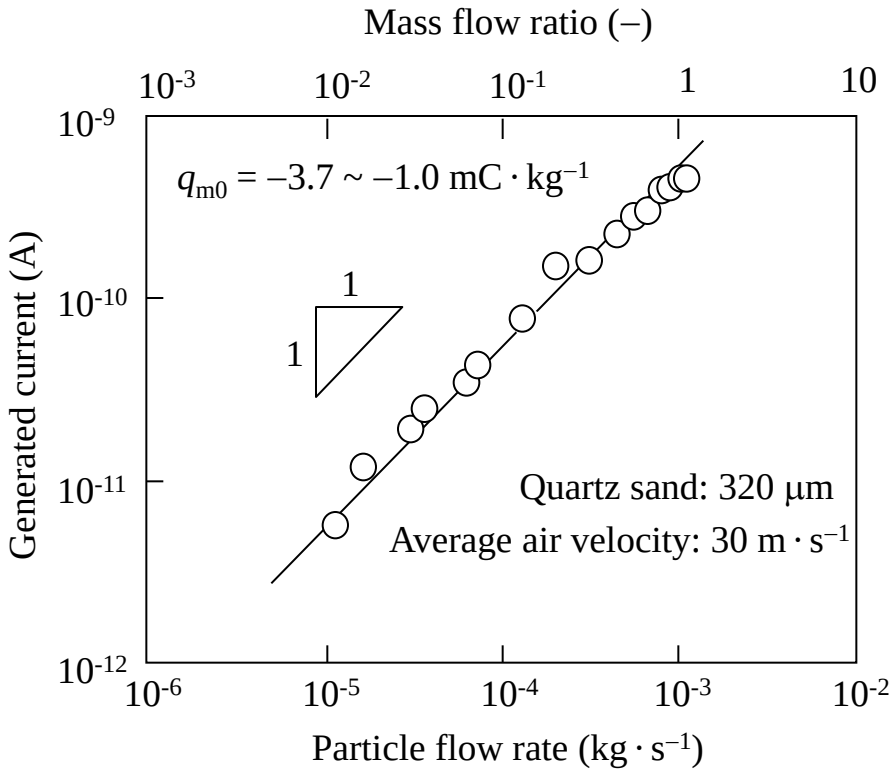

Fig. 32. Relationship between generated current and particle flow rate (Masuda et al., 1998 a).

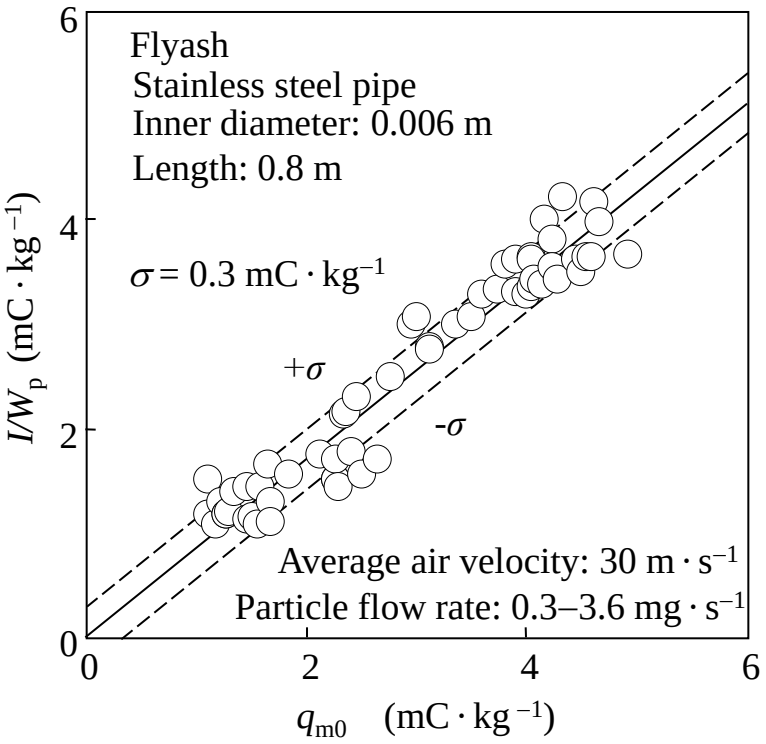

Fig. 33. Effect of the initial charge per unit mass of particles $(q/m_p)_0$ on the current generated per unit mass flow rate of particles I/W_p (Masuda et al., 1994).

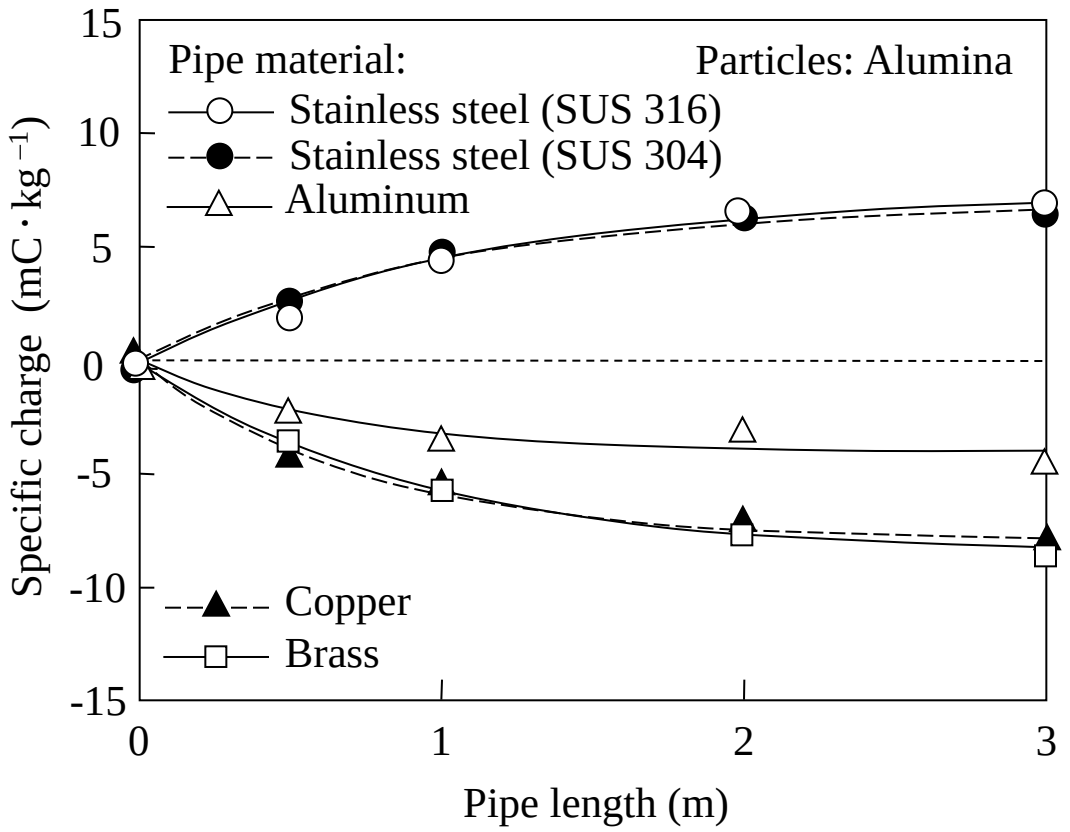

Fig. 34. Relationships between specific charge of micrometer-sized particles and pipe length (dilute phase gas–solids pipe flow systems, average air velocity: 40 m s^{-1}; solids lines: using Eq. (37)) (Matsusaka et al., 2007).

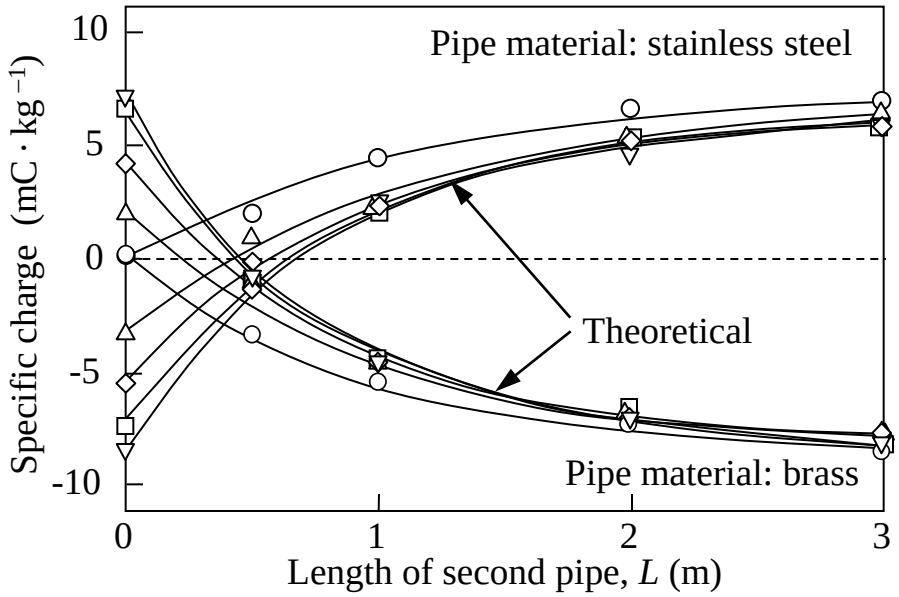

Fig. 35. Effect of initial charge on particle charging (Matsusaka et al., 2007).

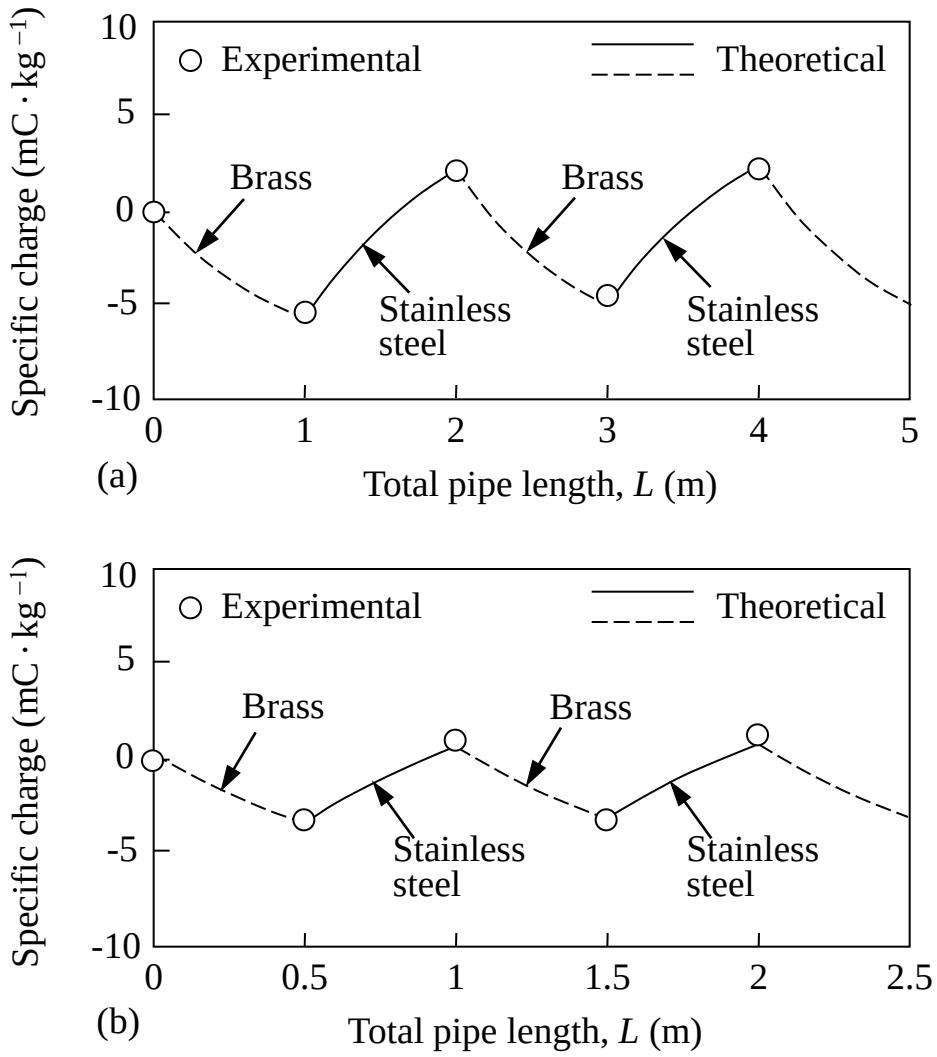

Fig. 36. Control of particle charging by a system combining two different pipe materials (Matsusaka et al., 2007).

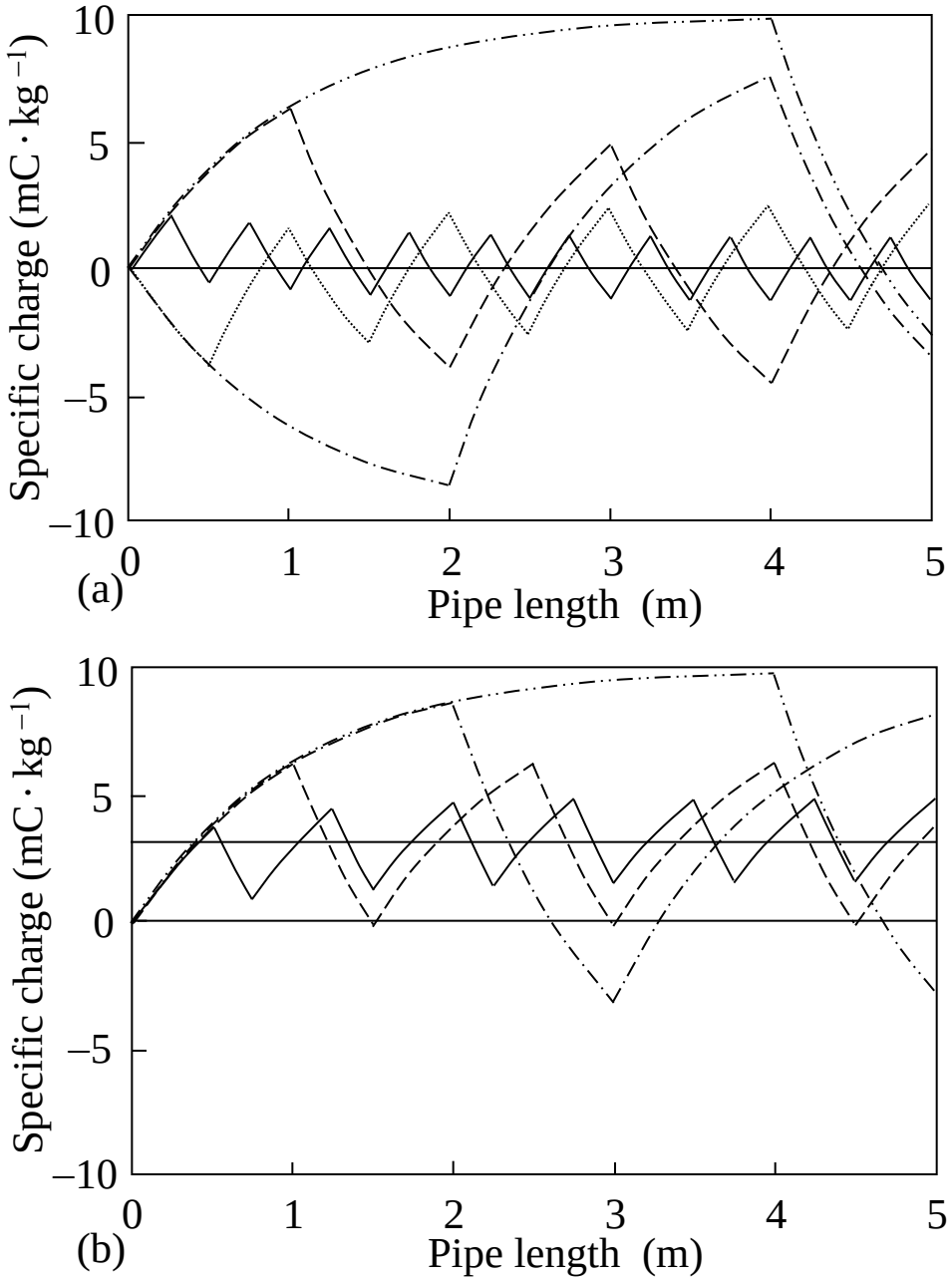

Fig. 37. General calculations of the triboelectric charging in gas–solids pipe flow using two different pipe materials.

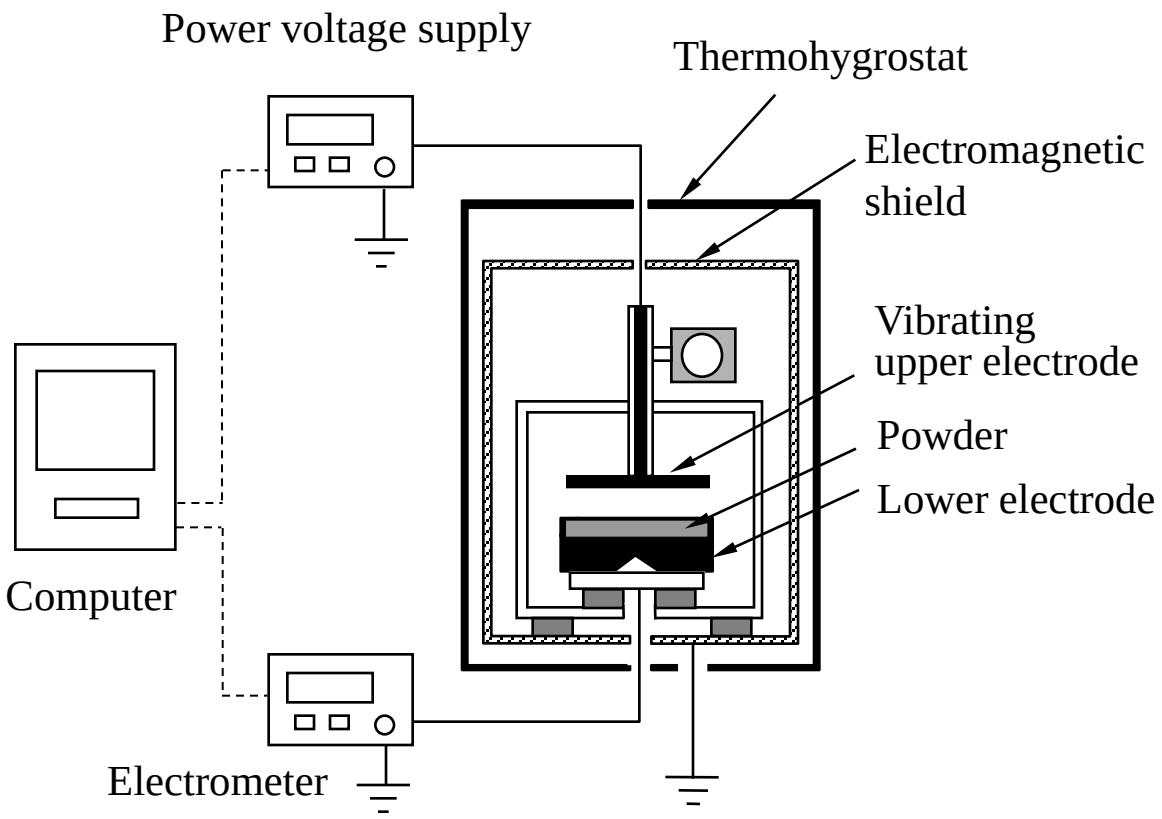

Fig. 38. Measurement of contact potential difference based on the Kelvin–Zisman method.

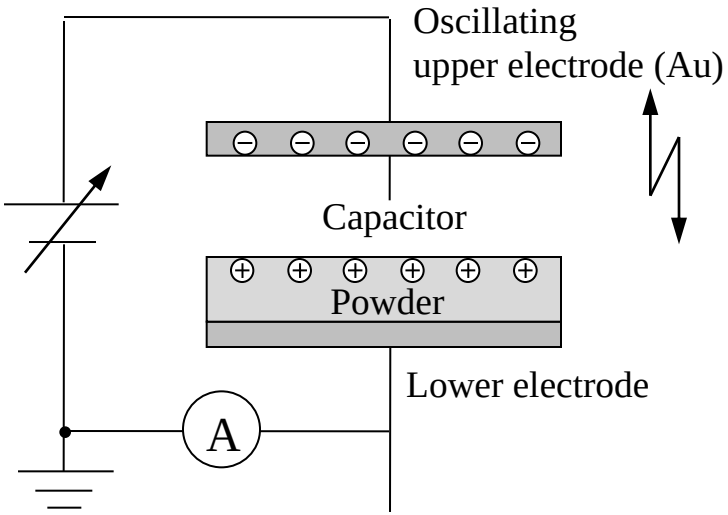

Fig. 39. Equivalent electric circuit of the Kelvin–Zisman method.

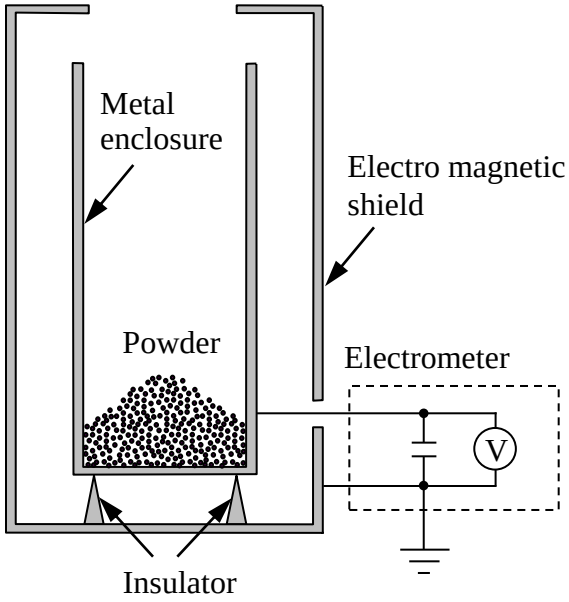

Fig. 40. Faraday cage.

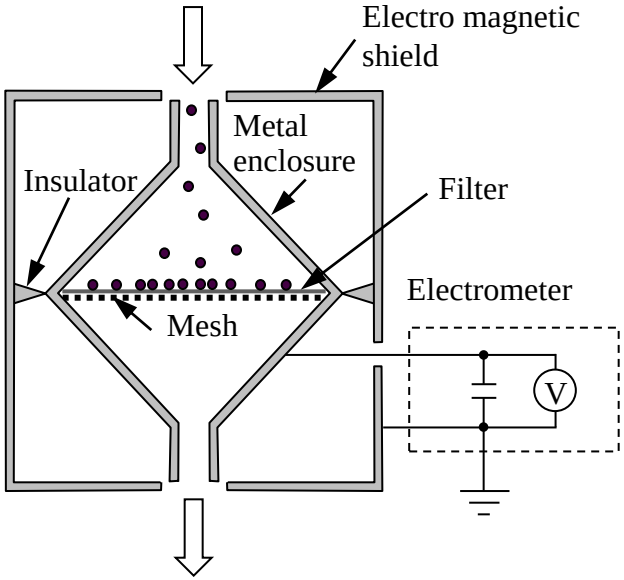

Fig. 41. Faraday cage to measure charge on aerosol particles.

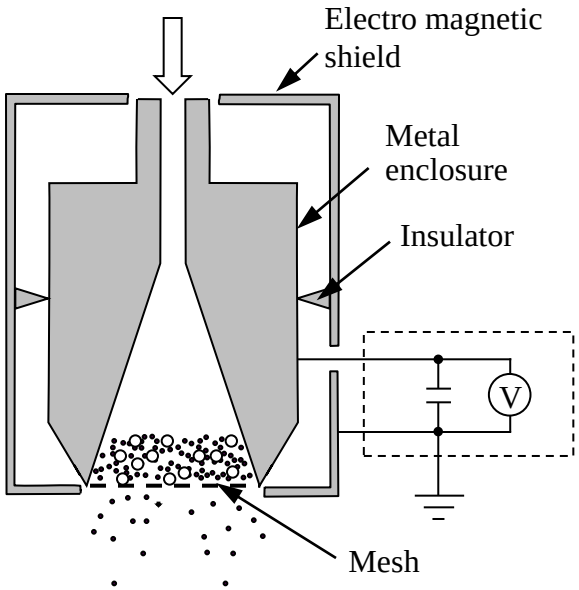

Fig. 42. Blow-off method.

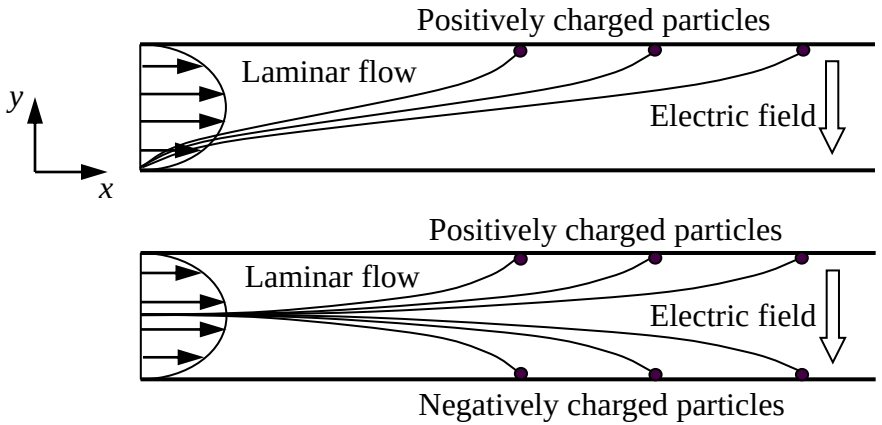

Fig. 43. Measurement of electrostatic charge distribution.

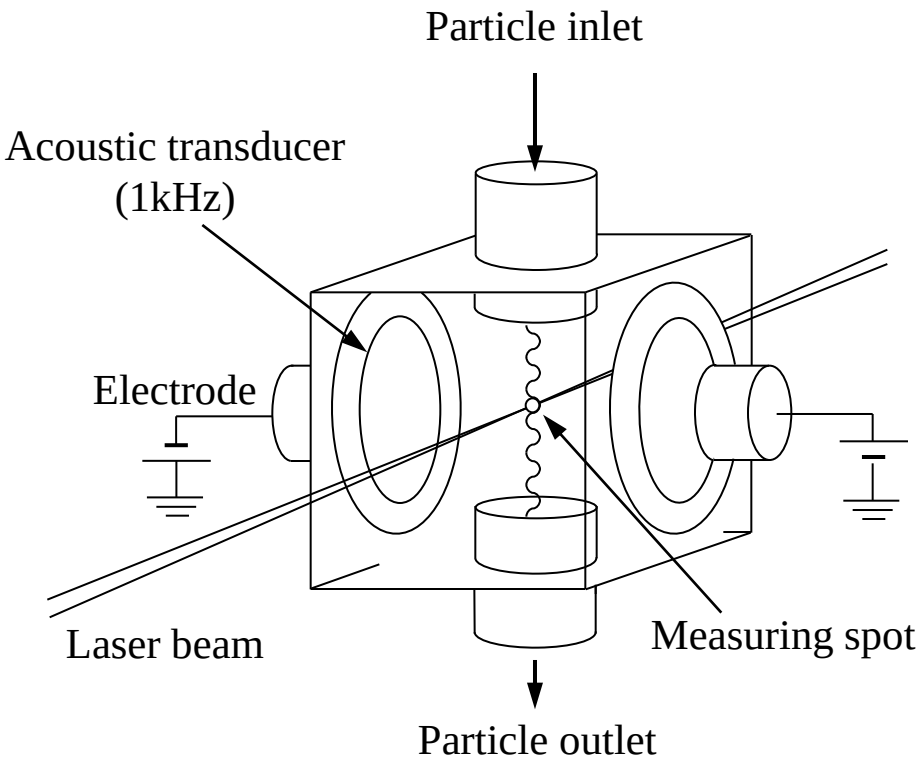

Fig. 44. Electrical-single particle aerodynamic relaxation time (E-SPART) analyzer.

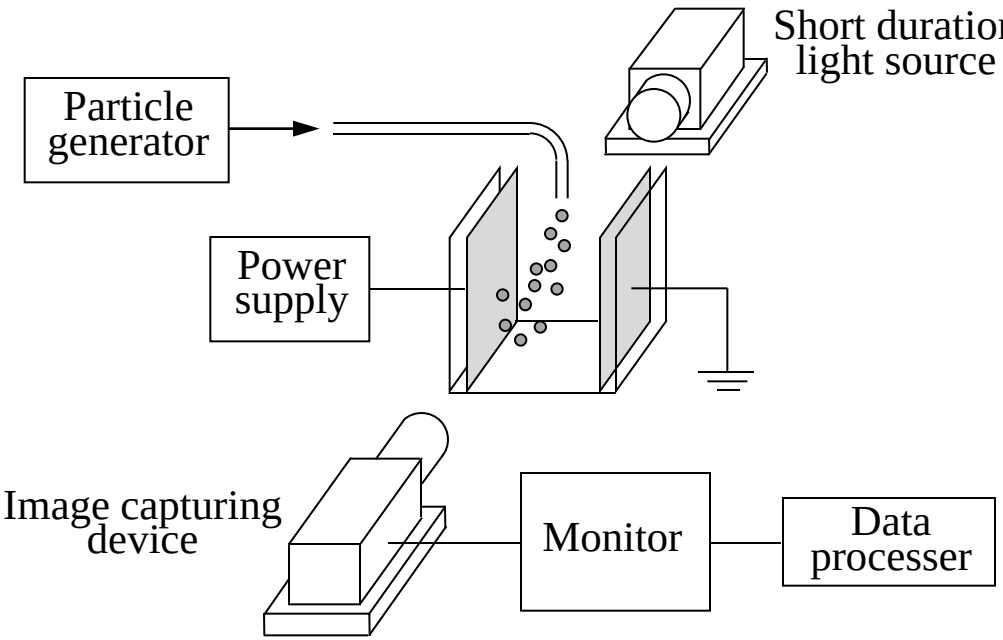

Fig. 45. Particle motion analysis system (PMAS).

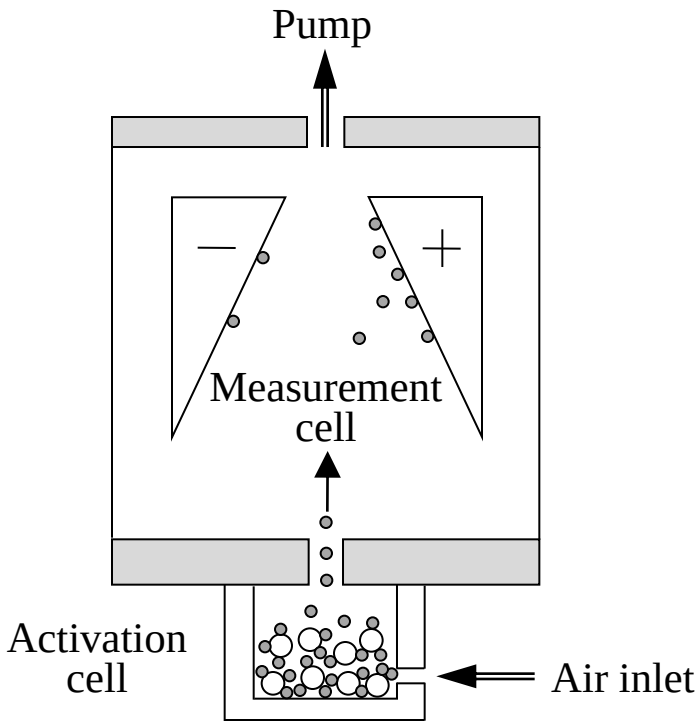

Fig. 46. The *q*-test device for two-component toners.

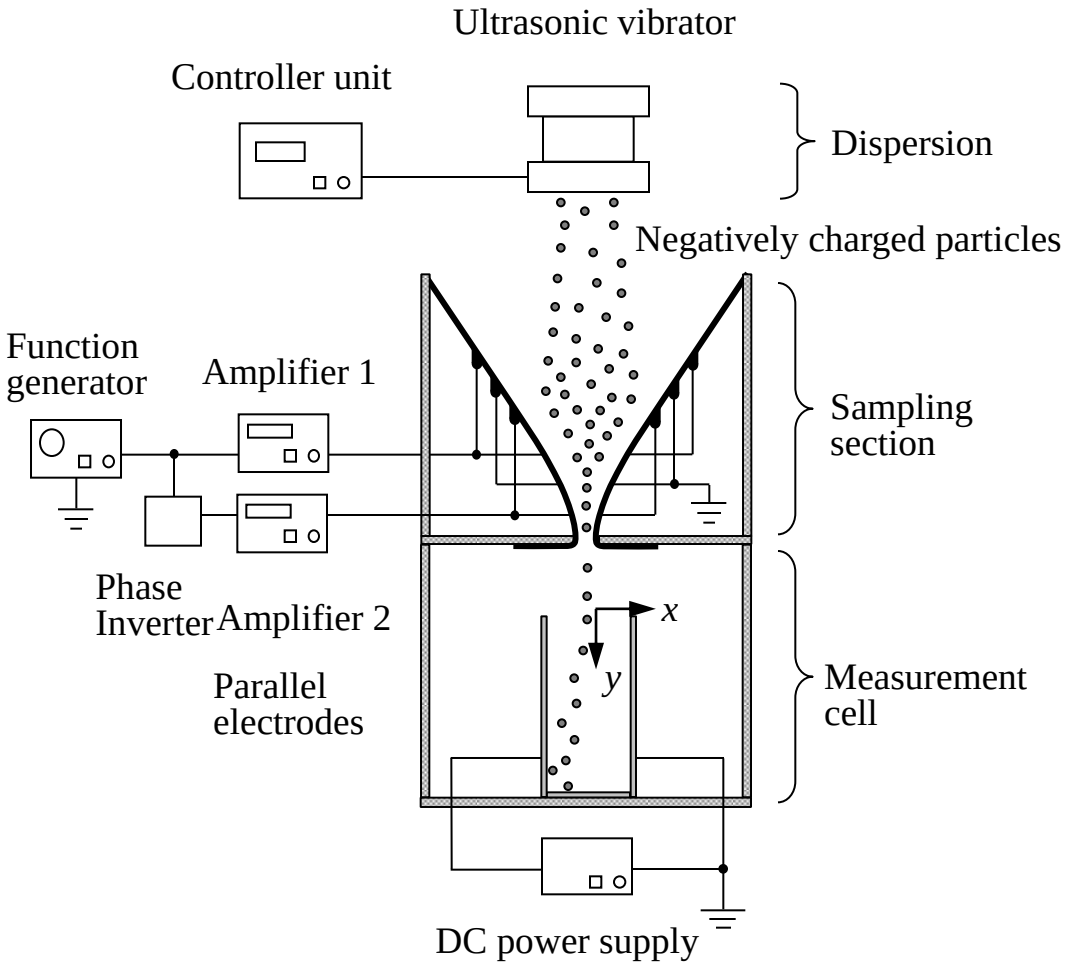

Fig. 47. Charge distribution measurement system consisting of dispersion feeder, sampling section, and measurement cell.

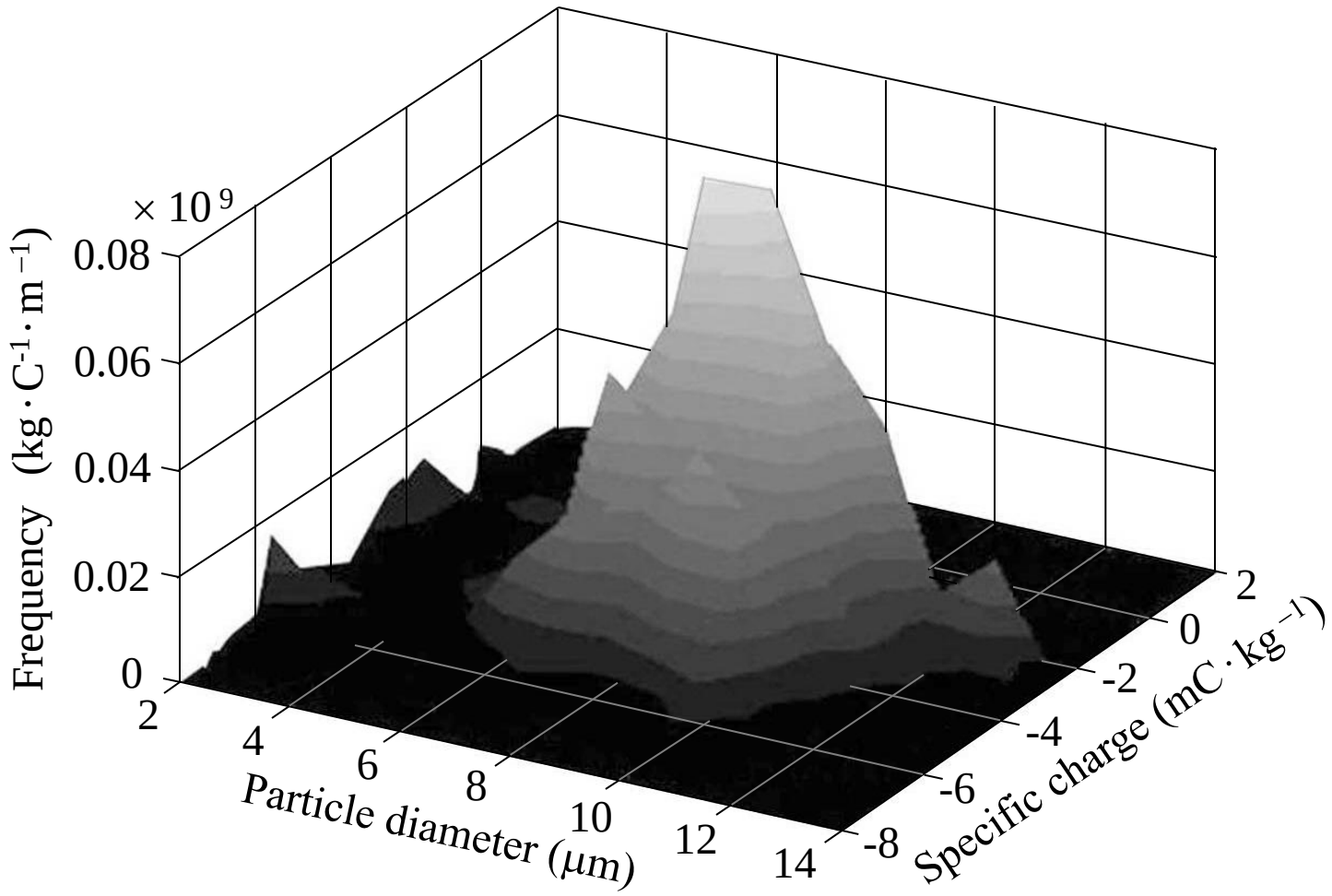

Fig. 48. Two-dimensional distribution of specific charge and particle diameter.

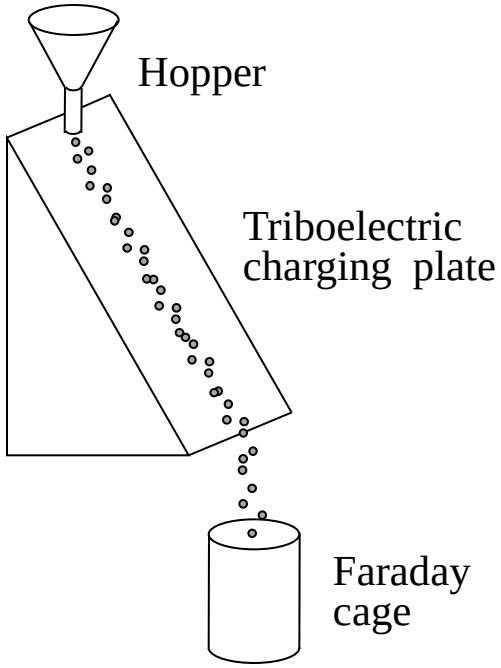

Fig. 49. Cascade method.

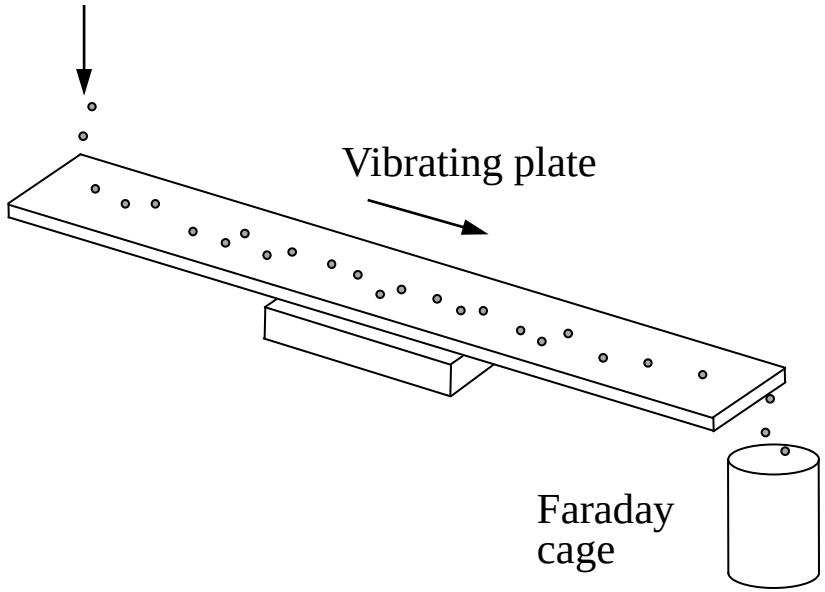

Fig. 50. Vibration method.

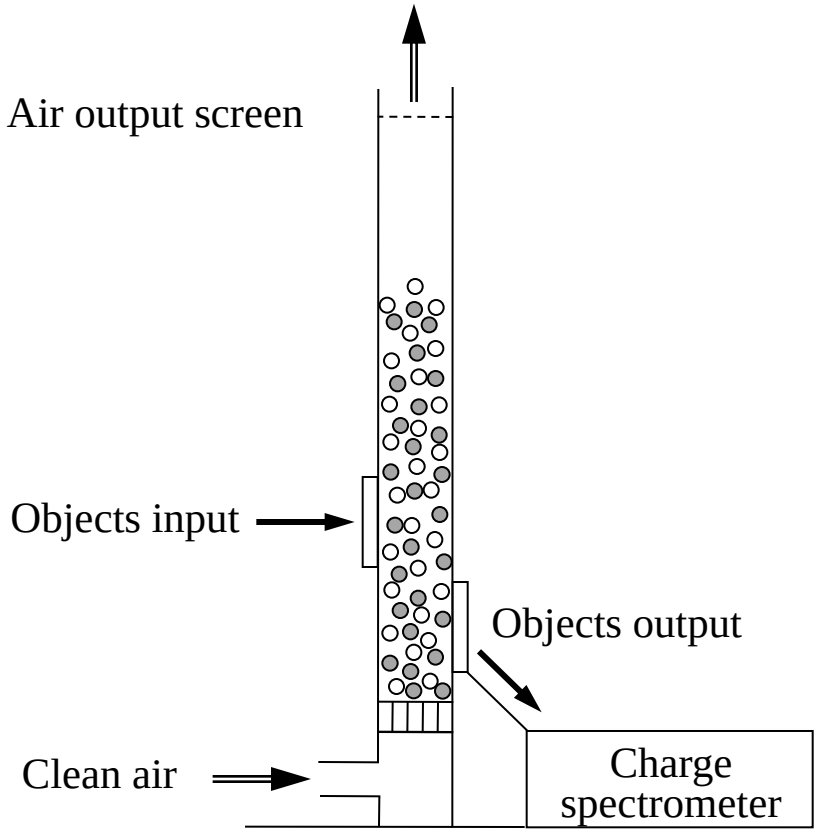

Fig. 51. Fluidization method.

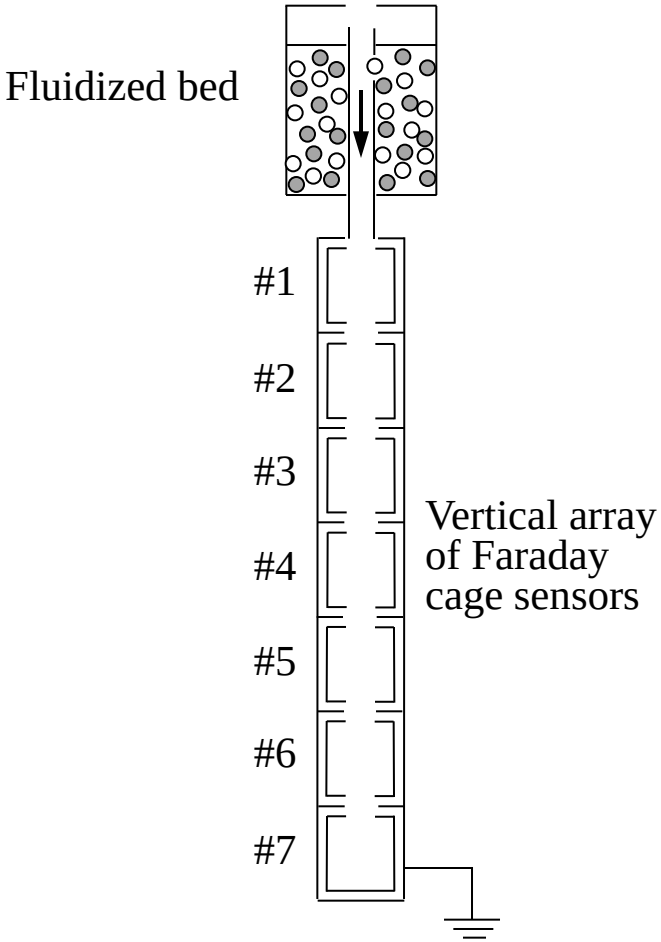

Fig. 52. Vertical array of Faraday cage sensors combined with a fluidized bed.

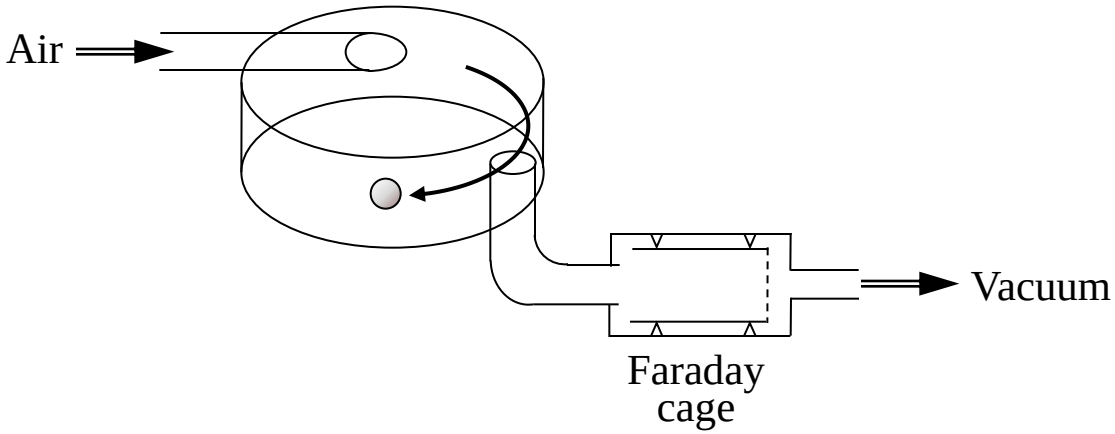

Fig. 53. Centrifugal method for measuring maximum triboelectric charge of particles.

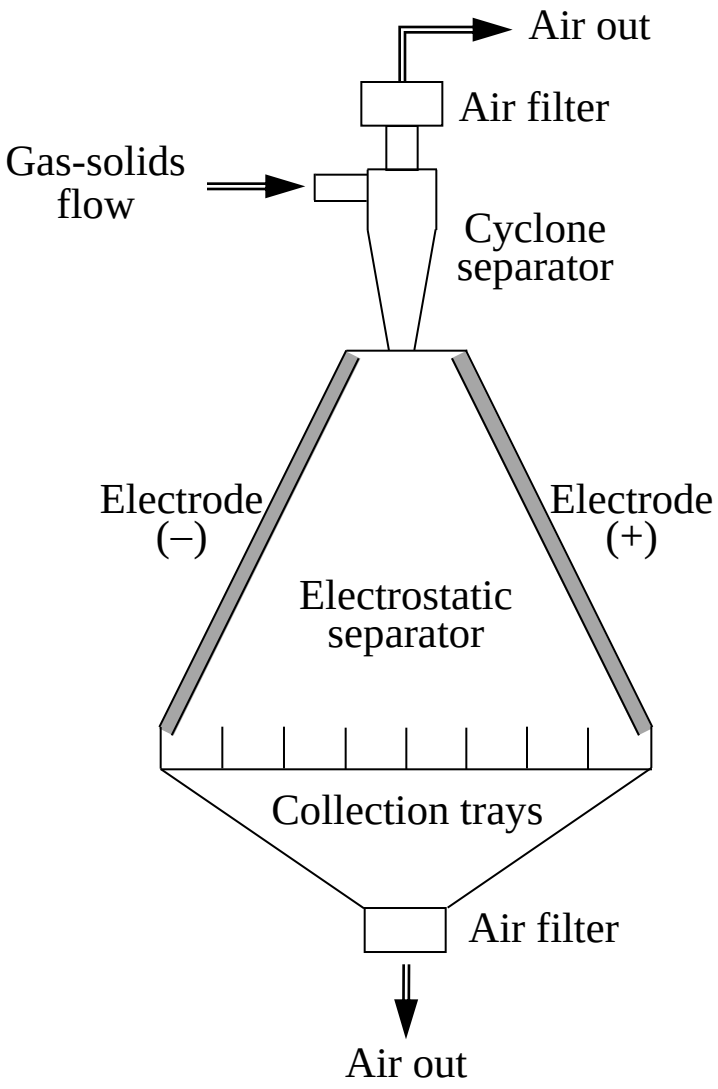

Fig. 54. Typical electrostatic separator.

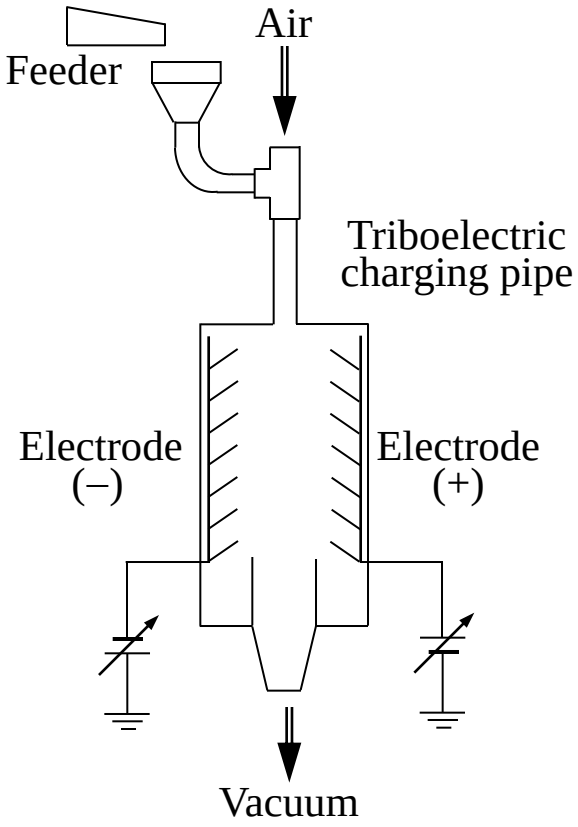

Fig. 55. Electrostatic separator with louvered plates.

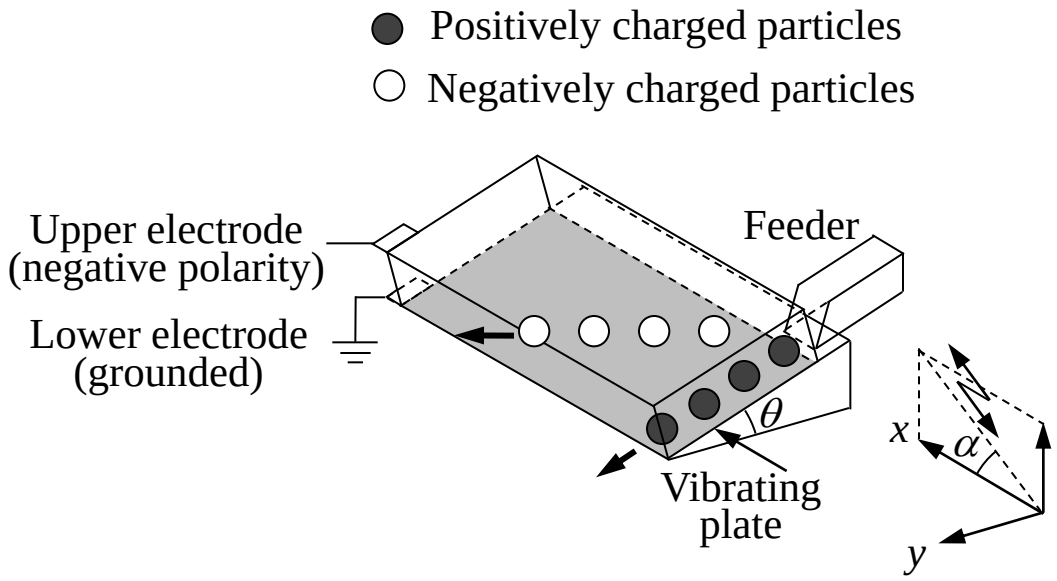

Fig. 56. Electrostatic separator using vibration.

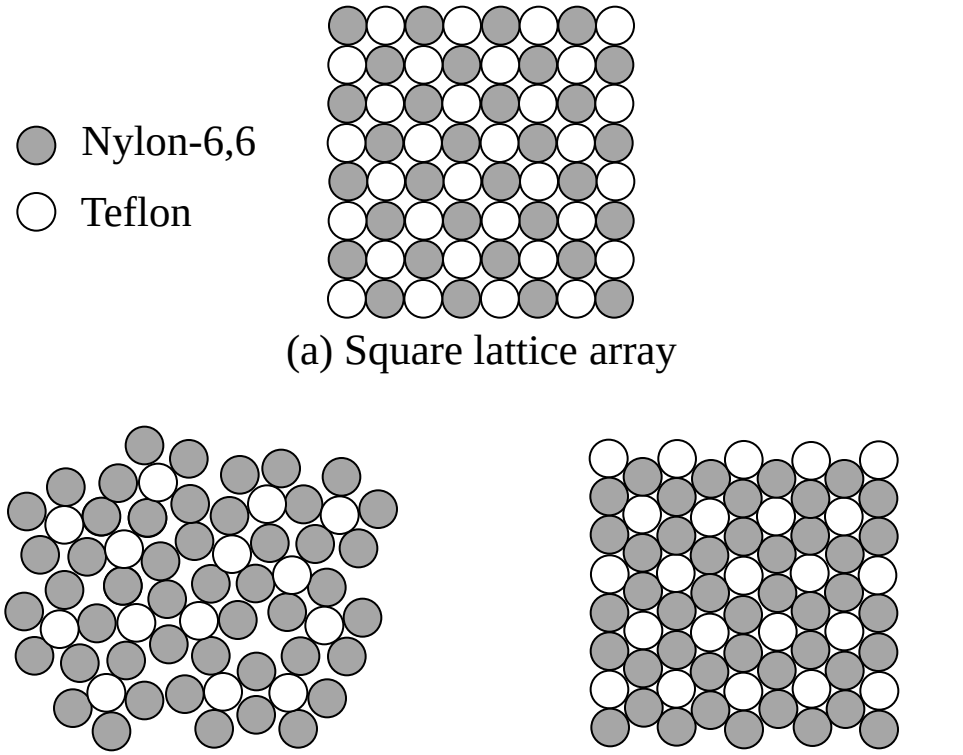

Fig. 57. Electrostatic self-assembly.

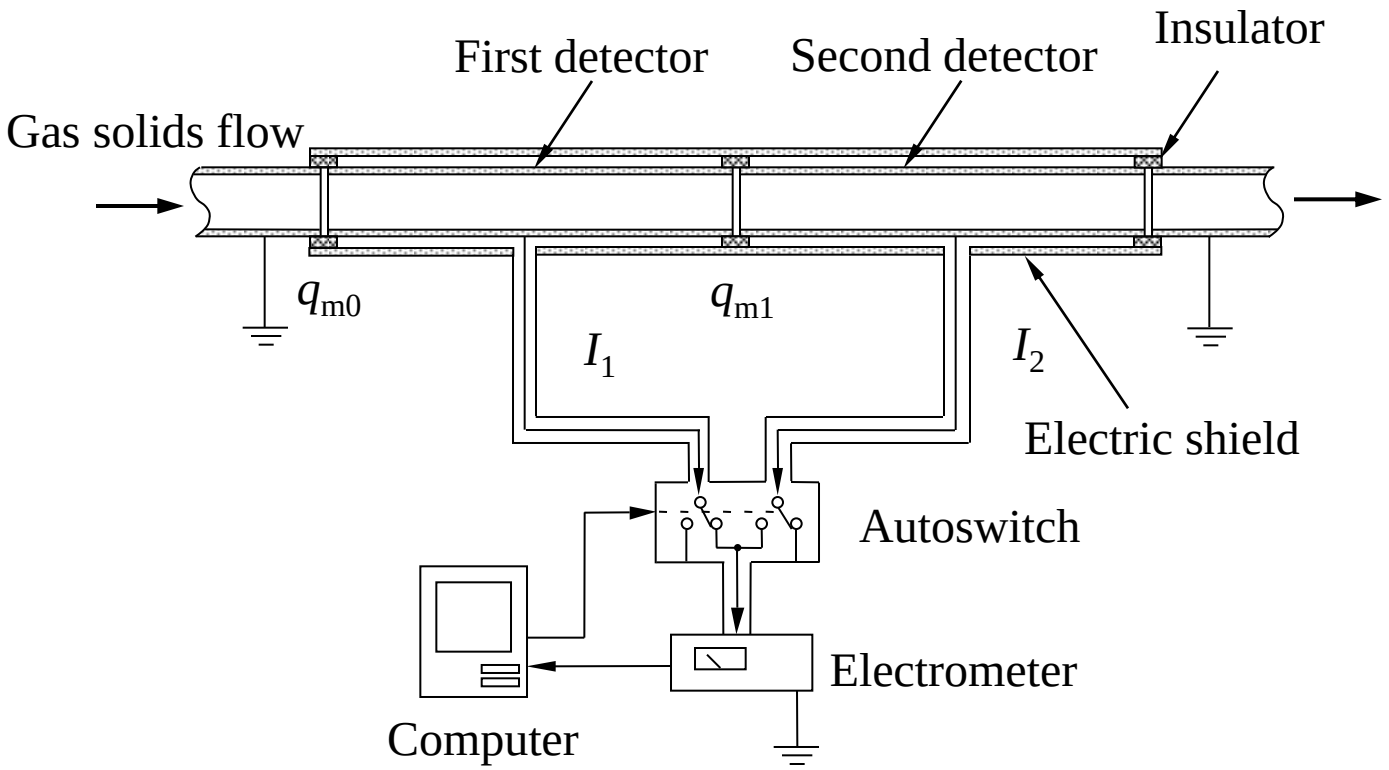

Fig. 58 Current detection system for measuring particle flow rate and specific charge.

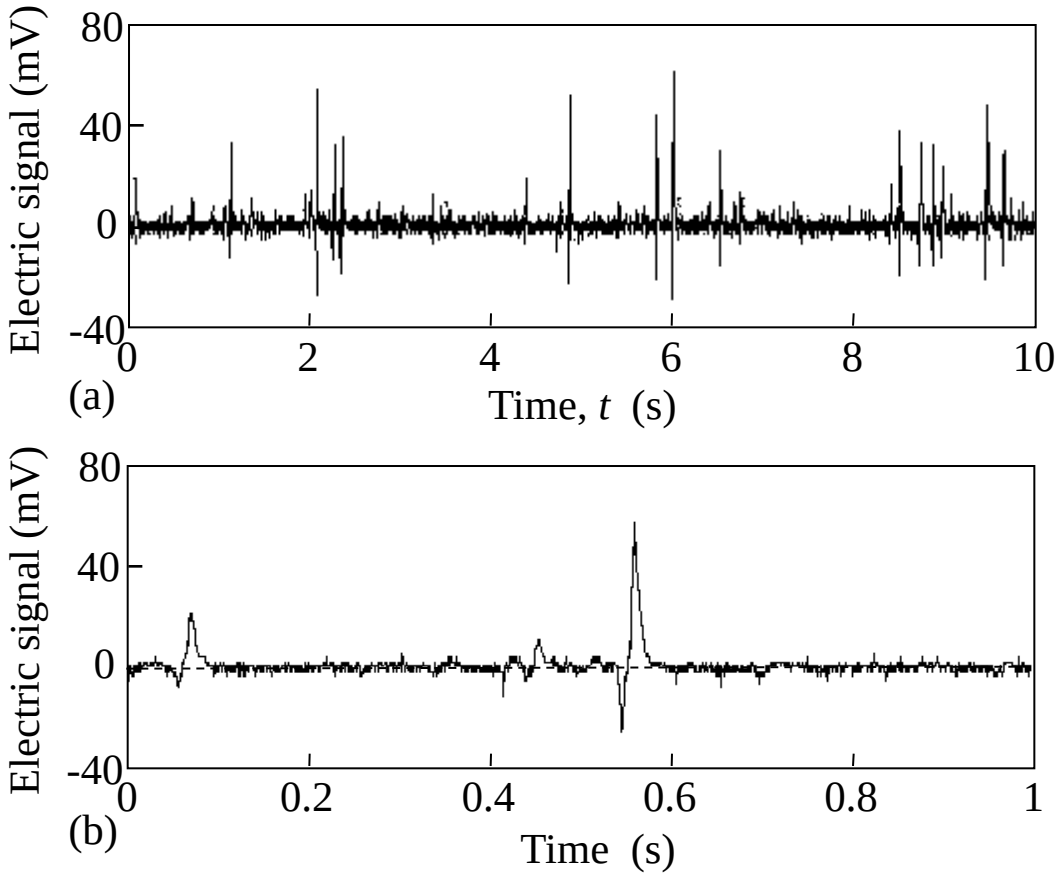

Fig. 59. (a) Signals detected with a digital oscilloscope and (b) signals on a magnified time scale (Matsusaka et al., 2008a).

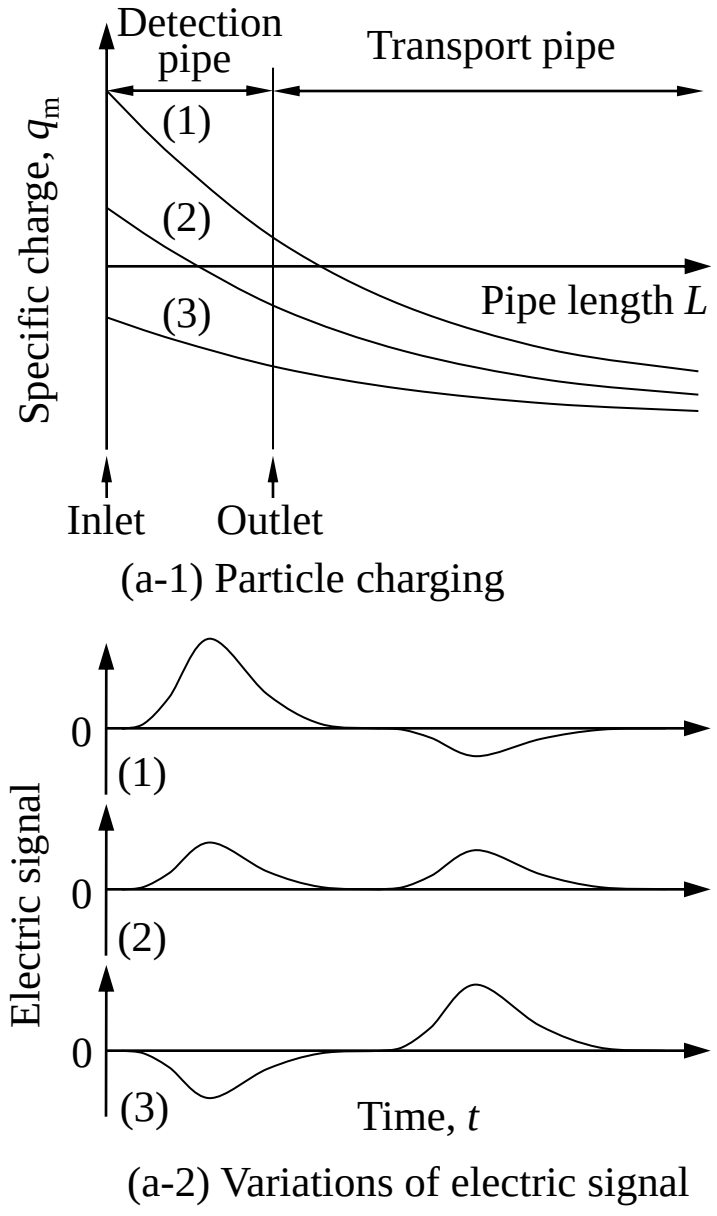

Fig. 60. Effect of particle charging on the shape of electric signal.

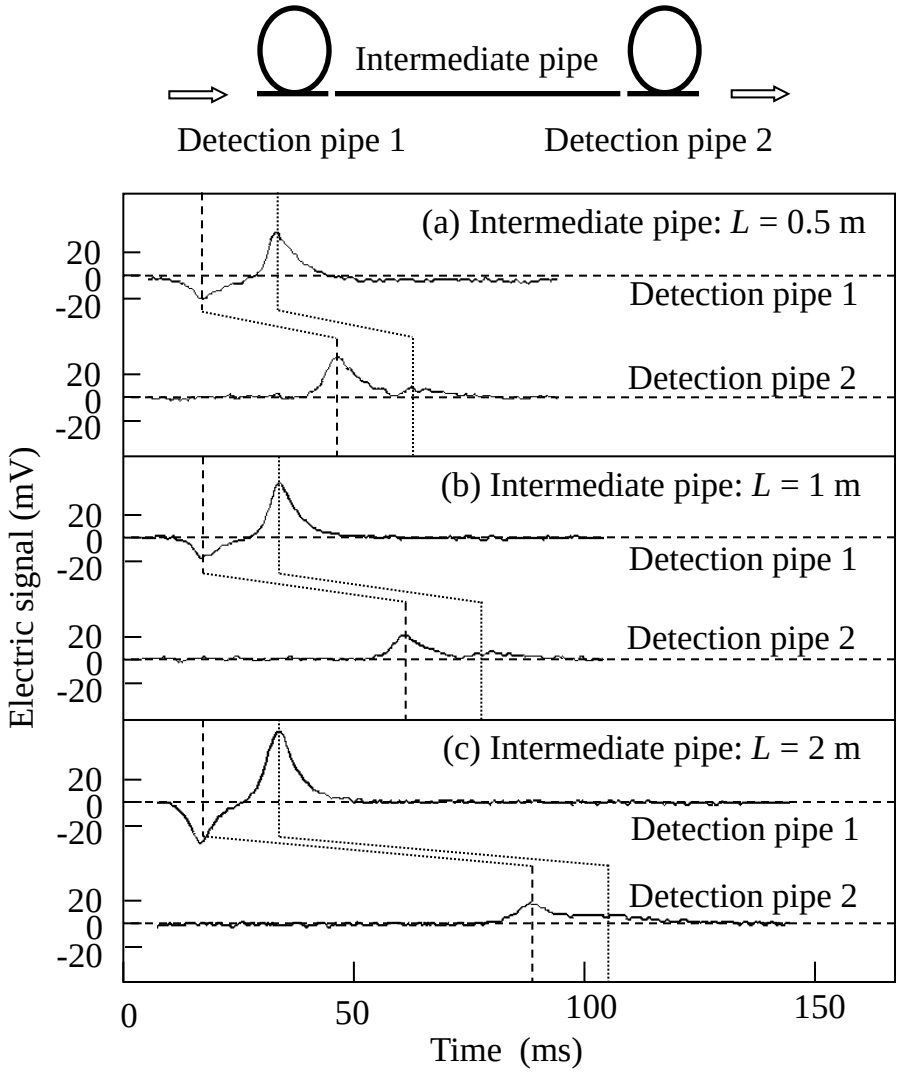

Fig. 61. Measurement of particle velocity by the correlation method (Matsusaka et al., 2008a).

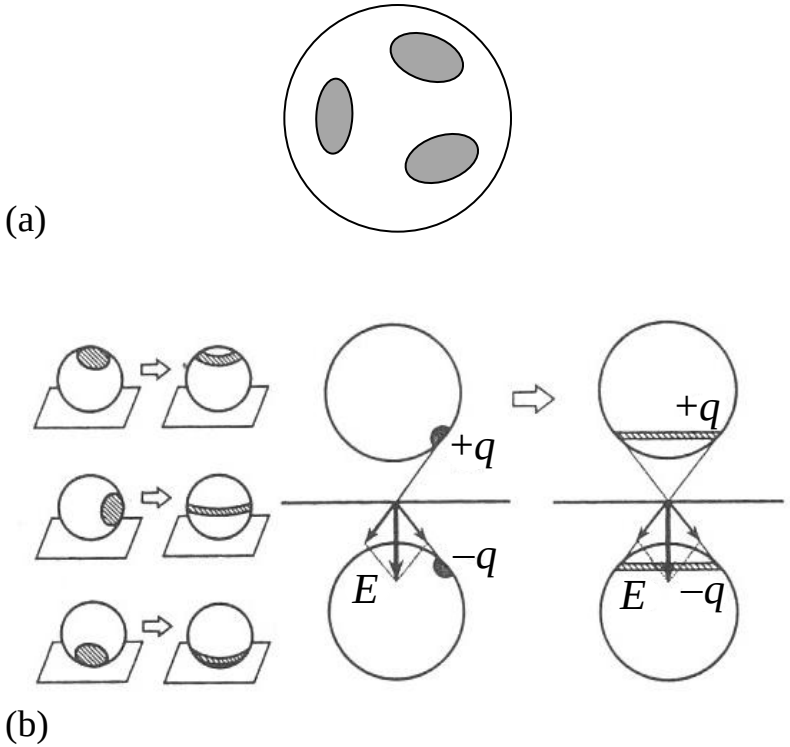

Fig. 62. (a) Schematic illustration of randomly given patch-like charge and (b) Schematic illustration of charge redistribution for axisymmetric calculation (Matsuyama and Yamamoto, 2006 b).

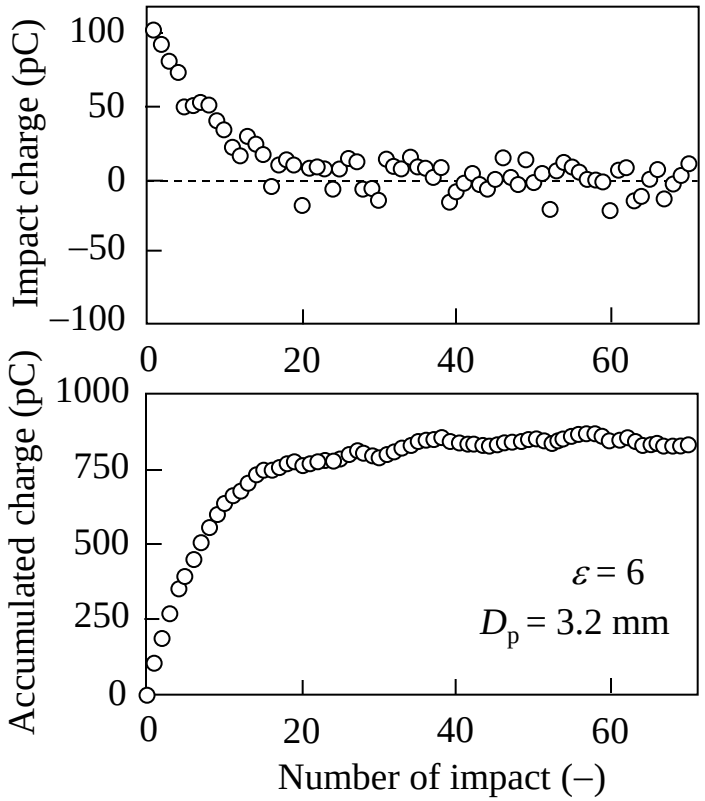

Fig. 63. Calculated results by a Monte Carlo simulation: (a) impact charge and (b) accumulated charge (Matsuyama and Yamamoto, 2006 b).

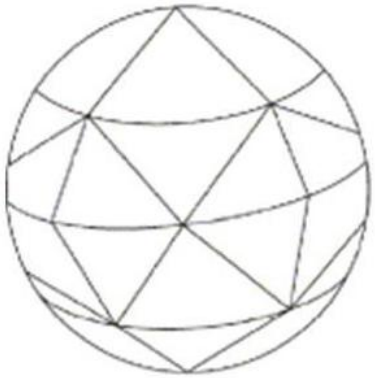

(a) 32-charging-sites

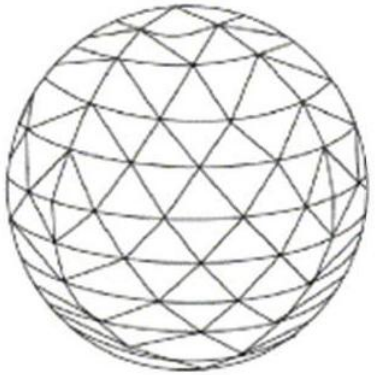

(b) 200-charging-sites

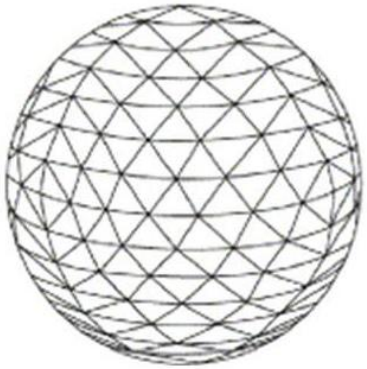

(c) 392-charging-sites

Fig. 64. Model particles used in the DEM simulation (the number of charging sites is (a) 32, (b) 200, and (c) 392) (Yoshida et al., 2003).

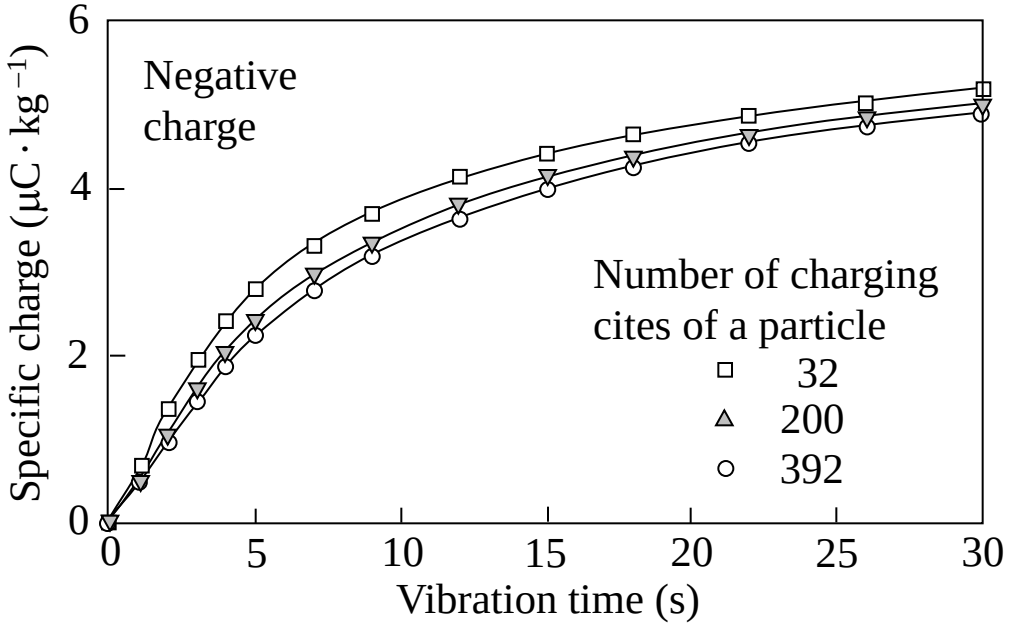

Fig. 65. Specific charge of particles in vibrating vessel (Yoshida et al., 2003).

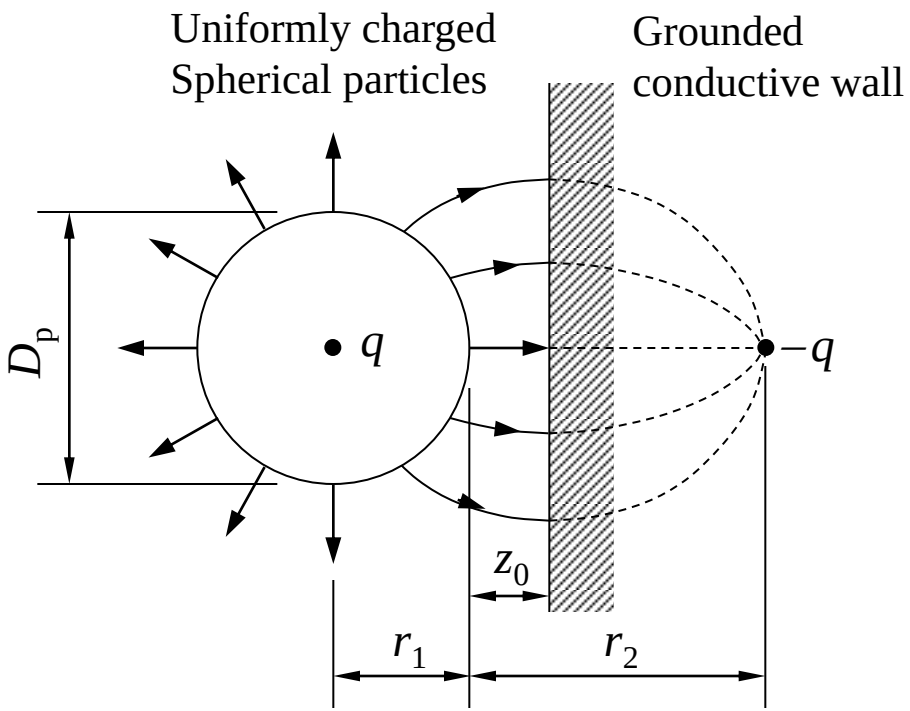

Fig. A-1. Potential difference caused by image charge.

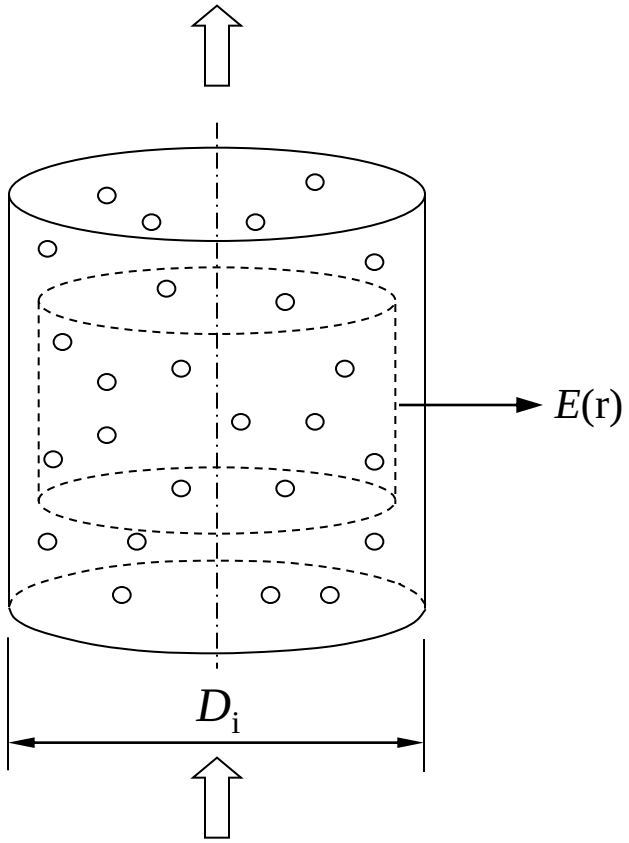

Fig. B-1. Electric field generated by space charge.